

CFAST Verification and Validation for Nuclear Power Plant Applications Volume 2

Draft Report for Comment

**U.S. Nuclear Regulatory Commission
Office of Nuclear Regulatory Research
Washington, DC 20555-0001**



**CFAST Verification and
Validation for Nuclear
Power Plant Applications**
Volume 2

Draft Report for Comment

Manuscript Completed: December 2004
Date Published: January 2005

Prepared by
M. Dey, K. Hill

Prepared for
Division of Risk Analysis & Applications
Office of Nuclear Regulatory Research
U.S. Nuclear Regulatory Commission
Washington, DC 20555-0001



Abstract

Consolidated Fire and Smoke Transport (CFAST) Model is a two-zone fire model capable of predicting the environment in a multi-compartment structure subjected to a fire. CFAST was developed by the Fire Research Division of the National Institute of Standards and Technology (NIST). It calculates the time evolving distribution of smoke and fire gases and the temperature throughout a building during a user-prescribed fire. This report describes the equations which constitute the model, the physical basis for these equations, and an evaluation of the sensitivity and predictive capability of the model.

This report is an assessment of the model following the outline set forth in ASTM E1355, "Standard Guide for Evaluating the Predictive Capability of Deterministic Fire Models."

DRAFT
FOR
FORMAT
REVIEW
ONLY

Table of Contents

Abstract	4
Table of Contents	6
List of Figures	12
List of Tables	16
Executive Summary	19
Acknowledgments	22
List of Symbols	23
Abbreviations	24
Chapter 1 Introduction	26
1.1 History	26
1.2 Model Evaluation	27
Chapter 2 Model and Scenario Definition	29
2.1.1 Name and Version of the Model	29
2.1.2 Type of Model	29
2.1.3 Model Developers	29
2.1.4 Relevant Publications	30
2.1.5 Governing Equations and Assumptions	30
2.1.6 Input Data Required to Run the Model	30
2.1.7 Property Data	31
2.1.8 Model Results	31
Chapter 3 Theoretical Basis for CFAST	34
3.1 Derivation of Equations for a Two-Layer Model	34
3.2 Equation Set Used in CFAST	38
3.3 Limitations of the Zone Model Assumptions	38
3.4 Source Terms for the Model	39
3.4.1 The Fire	39
3.4.1.1 Unconstrained Fire	39
3.4.1.2 Constrained Fire	40
3.4.1.3 Limiting Combustion by Available Oxygen	40
3.4.1.4 Limitation of the Algorithm for Fires and Mass Balance	42
3.4.2 Plumes	44
3.4.2.1 Limitation of the Plume Algorithm	46
3.4.3 Vent Flow	47
3.4.3.1 Horizontal Flow Through Vertical Vents	47

3.4.3.2	Vertical Flow Through Horizontal Vents	50
3.4.3.3	Forced Flow	51
	Resistance of Ducts:	59
3.4.4	Corridor Flow	61
3.4.5	Heat Transfer	66
3.4.5.1	Radiation	66
3.4.5.2	Computing Target Heat Flux and Temperature	72
3.4.5.3	Convection	75
3.4.5.4	Conduction	76
3.4.5.5	Inter-compartment Heat Transfer	77
3.4.6	Ceiling Jet	77
3.5	Heat Detection	80
3.6	Sprinkler Activation and Fire Attenuation	81
3.7	Species Concentration and Deposition	82
3.7.1	Species Transport	83
3.7.2	HCl Deposition	83
3.8	Flame Spread	85
3.9	Single Zone Approximation	86
3.10	Review of the Theoretical Development of the Model	87
3.10.1	Assessment of the Completeness of Documentation	88
3.10.2	Assessment of Justification of Approaches and Assumptions	88
3.10.3	Assessment of Constants and Default Values	88
Chapter 4	Mathematical and Numerical Robustness	91
4.1	Introduction	91
4.2	Structure of the Numerical Routines	91
4.2.1	Subroutine Structure	91
4.3	Code Checking	92
4.4	Numerical Tests	93
4.5	Comparison with Analytic Solutions	94
Chapter	5 Model Sensitivity	96
5.1	Parametric Analysis	96
5.1.1	International Benchmarking and Validation Exercise # 1	96
5.2	Probabilistic Sensitivity Analysis	99
5.2.1	VTT Sensitivity Analysis with Probabilistic Fire Simulator	99
5.2.2	Sensitivity Analysis	100
5.2.2.1	Factorial Design Studies	100
5.2.2.1.1	Model Inputs and Outputs	101
5.2.2.1.3	Sensitivity to Larger Changes in Model Inputs	105
5.2.2.2	Response Surface Studies	107
5.2.2.3	Latin Hypercube Sampling Studies	110
5.2.2.4	Summary	110
Chapter 6	Model Validation	112
6.1	Summary of Validation Studies	112
6.1.1	International Benchmarking and Validation Exercise # 2	112
6.1.2	International Benchmarking and Validation Exercise # 3	113
6.1.3	International Benchmarking and Validation Exercise # 4	115

6.1.4	International Benchmarking and Validation Exercise # 5	116
6.1.5	HDR T51 and T52 Tests	118
6.1.6	NIST Multi-Compartment Tests	121
6.2	Applicability of Validation Studies to NPP Scenarios	123
6.3	Comparison of Predictive Capability with Actual Events	130
6.3.1	Comparisons with Full-Scale Tests Conducted Specifically for the Chosen Evaluation	130
6.3.2	Comparisons with Previously Published Test Data	131
6.3.2.1	Experimental Data Selected for Comparison	132
6.3.2.2	Layer Temperature and Interface Position	133
6.3.2.3	Gas Species	139
6.3.2.4	Heat Release and Fuel Pyrolysis Rate	142
6.3.2.5	Pressure	144
6.3.2.6	Flow Through Openings	147
6.3.2.7	Plume Model	148
6.3.2.8	Other Comparisons with Previously Published Test Data	148
6.3.3	Prediction of Flashover	149
6.3.4	Comparison with Documented Fire Experience	152
6.3.5	Comparison with Experiments Which Cover Special Situations	152
6.3.5.1	Nuclear Facilities	152
6.3.5.2	Small Scale Testing	153
6.3.5.3	Unusual Geometry and Specific Algorithms	153
6.3.5.3.1	Railway and Vehicle Tunnels	154
6.3.5.3.2	Non-Uniform Compartments	154
6.3.5.3.3	Long Corridors	154
6.3.5.3.4	Mechanical Ventilation	154
6.3.5.3.5	Sprinkler Activation	155
6.3.5.3.6	t^2 Fires	155
6.3.6	Summary	155
Chapter 7	Bibliography and References	158

List of Figures

Figure 1-1	Zone model terms	26
Figure 3-1	Schematic of control volumes in a two-layer zone model	35
Figure 3-2	Schematic of entrainment and burning regions	41
Figure 3-3	Notation conventions for two-layer model in two compartments with a connecting vent	48
Figure 3-4	Flow pattern and layer numbering convention	49
Figure 3-5	Some simple fan-duct systems	52
Figure 3-6	Network representation of a residential system	53
Figure 3-7	Typical fan performance at constant speed	56
Figure 3-8	Some approaches to approximation of fan performance for computer simulation	57

Figure 3-9. \log_{10} of the relative temperature excess downstream in a corridor using an adiabatic temperature boundary condition for several inlet depths and inlet temperature boundary condition. The inlet velocity, V_o , is given by equation (70).	65
Figure 3-10. Radiation exchange in a two-zone fire model.	68
Figure 3-11. An example of the calculated two-wall (RAD2) and four-wall (RAD4) contributions to radiation exchange on a ceiling and wall surface.	69
Figure 3-12. Setup for a configuration factor calculation between two arbitrarily oriented finite areas	70
Figure 3-13. Radiative heat transfer from a point source fire to a target.	73
Figure 3-14. Radiative heat transfer from the upper and lower layer gas layers to a target in the lower layer.	74
Figure 3-15. Convective heat transfer to ceiling and wall surfaces via the ceiling jet.	78
Figure 3-16. Schematic of hydrogen chloride deposition region.	84
Figure 4-1. Subroutine structure for the CFAST Model.	93
Figure 5-2 Characterization of heat release rate of growing fires as t^2 fires.	103
Figure 5-1. Building geometry for base case scenario.	103
Figure 5-3. An example of time dependent sensitivity of fire model outputs to a 10% change in room volume for a single room fire scenario	104
Figure 5-4. Layer temperatures and volumes in several rooms resulting from variation in heat release rate for a four-room growing fire scenario.	106
Figure 5-6. Sensitivity of temperature to heat release rate for a four-room growing fire scenario.	107
Figure 5-5. Comparison of the time dependent heat release rate and layer temperatures in several rooms for a four-room growing fire scenario.	107
Figure 5-7. Comparison of heat release rate and upper layer volume in several rooms for a four-room growing fire scenario.	108
Figure 5-8. Effect of both heat release rate and vent opening size on upper layer temperature for a four-room growing fire scenario.	109
Figure 6-2 Compartment Isometric with thermocouple trees	114
Figure 6-3 3-D View of Fire Compartment	116
Figure 6-4 Three dimensional view of fire compartment	117
Figure 6-4 Layout of HDR T52 Test Facility	120
Figure 6-5 Three-room gas burner tests with a corridor.	121
Figure 6-6 Four Room Gas Burner with a corridor	122
Figure 6-7. Comparison of measured and predicted upper layer temperatures for several tests.	137
Figure 6-8. Comparison of measured and predicted lower layer temperatures for several tests.	138
Figure 6-9. Comparison of measured and predicted layer interface position for several tests	138
Figure 6-10. Comparison of measured and predicted gas species concentrations for several tests.	140
Figure 6-11. Comparison of measured and prescribed heat release rates for two selected tests.	143
Figure 6-12. Comparison of measured and predicted pressures for several tests.	145

Figure 6-13: Effect of leakage in an arbitrary single-room fire. 146
 Figure 6-14: Comparison of measured and predicted mass flow through vents for several tests.
 (Numbers indicate comparable rooms in the test structure.) 148
 Figure 6-15: Comparison of correlations, CFAST predictions, and experimental data for the
 prediction of flashover in a compartment fire. 151

DRAFT
 FOR
 FORMAT
 REVIEW
 ONLY

List of Tables

Table 3-1 Conservative zone model equations 37
 Table 3-1 Conservative zone model equations 37
 Table 3-2 Recommended compartment dimension limits 39
 Table 3-3: Absolute roughness values for common duct materials 61
 Table 3.4 Transfer coefficients for HCl deposition from reference [69] 85
 Table 5-1: Summary of Cases for Part I 97
 Table 5-2: Typical Inputs for a Two-Zone Fire Model. 101
 Table 5-3: Typical Outputs for a Two-Zone Fire Model. 102

Table 6-1 Summary of Cases	113
Table 6-2: T51 Fire Compartment Dimensions	119
Table 6-3: T51 Experimental Data	119
Table 6-4: T52 fire Compartment Dimensions	120
Table 6.5 Attributes of NPP Fire Scenarios	125
Table 6.6 Attributes of Benchmark Exercises and Other Tests	126
Table 6.7 NPP Scenario to Benchmark Exercise/Other Tests Correlation Matrix	128
Table 6.8 Comparison of experimental measurements and model predictions of upper layer temperature (°C) for several tests	135
Table 6.9 Comparison of experimental measurements and model predictions of lower layer temperature (°C) for several tests	136
Table 6.10 Comparison of experimental measurements and model predictions of layer interface position (m) for several tests	136
Table 6.11 Comparison of experimental measurements and model predictions of oxygen concentration for several tests	141
Table 6.12 Comparison of measured and prescribed heat release rate for several tests .	143
Table 6.13 Comparison of experimental measurements and model predictions of room pressure for several tests	146
Table 6.14 Comparison of experimental measurements and model predictions of mass flow through openings for several tests	147

DRAFT
 FORMAT
 REVIEW
 ONLY

DRAFT

FOR
Executive Summary

CFAST is a two-zone fire model used to calculate the evolving distribution of smoke, fire gases and temperature throughout compartments of a constructed facility during a fire. In CFAST, each compartment is divided into two gas layers, the upper hot gas layer and the lower cool gas layer.

The modeling equations used in CFAST take the mathematical form of an initial value problem for a system of ordinary differential equations (ODEs). These equations are derived using the conservation of mass, the conservation of energy (equivalently the first law of thermodynamics), the ideal gas law and relations for density and internal energy. These equations predict as functions of time quantities such as pressure, layer height and temperatures given the accumulation of mass and enthalpy in the two layers. The CFAST model then consists of a set of ODEs to compute the environment in each compartment and a collection of algorithms to compute the mass and enthalpy source terms required by the ODEs.

In general, this document provides the technical documentation for CFAST along with significant information on validation of the model. It follows the ASTM E1355 guide for model assessment. The guide provides several areas of evaluation:

- **Model and scenarios definition:** CFAST is designed primarily to predict the environment within compartmented structures which results from unwanted fires. These can range from very small containment vessels, on the order of 1 m³ to large spaces on the order of 1000 m³. The appropriate size fire for a given application depends on the size of the compartment being modeled. A range of such validation exercises is discussed in Chapter 6.
- **Theoretical basis for the model:** Details of the underlying theory, governing equations, correlations, and organization used in the model are presented. The process of development of the model is discussed with reference to a range of NIST memorandums,

published reports, and peer-reviewed journal articles on the model. In addition to overall limitations of zone-fire modeling, limitations of the individual sub-models are discussed.

- **Mathematical and numerical robustness:** CFAST has been subjected to extensive use and review both internal to NIST and by users worldwide in a broad range of applications. In addition to review within NIST independent of the model developers, the model has been published in international peer-reviewed journals worldwide, and in industry-standard handbooks referenced in specific consensus standards. Besides formal internal and peer review, CFAST is subjected to continuous scrutiny because it is available to the general public and is used internationally by those involved in fire safety design and post-fire reconstruction.
- **Model sensitivity:** Many of the outputs from the CFAST model are relatively insensitive to uncertainty in the inputs for a broad range of scenarios. Not surprisingly, the heat release rate is the most important variable because it provides the driving force for fire-driven flows. For CFAST, the heat release rate is prescribed by the user. Thus, careful selection of the fire size is necessary for accurate predictions. Other variables related to compartment geometry such as compartment height or vent sizes, while deemed important for the model outputs, are typically more easily defined for specific design scenarios than fire related inputs.
- **Model validation:**

Summarize NPP validation results - TBD

The CFAST model has been subjected to extensive validation studies by NIST and others. Although some differences between the model and the experiments were evident in these studies, they are typically explained by limitations of the model and uncertainty of the experiments. Most prominent in the studies reviewed was the over-prediction of gas temperature often attributed to uncertainty in soot production and radiative fraction. Still, studies typically show predictions accurate within 10 % to 25 % of measurements for a range of scenarios. Like all predictive models, the best predictions come with a clear understanding of the limitations of the model and of the inputs provided to the calculations.

DRAFT
FOR

Acknowledgments

This verification and validation(V&V) study for CFAST has been conducted by the U.S. Nuclear Regulatory Commission (NRC) in collaboration with the National Institute of Standards and Technology (NIST), U.S. Department of Commerce. Since the inception of this project in 1999, the NRC has collaborated with NIST through an inter-agency memorandum of understanding and conducted research to provide the necessary technical data and tools to support the use of fire models in nuclear power plant fire safety analysis. The NRC specifically appreciates the efforts of NIST staff, Dr. Anthony Hamins, Mr. Richard Peacock, and Dr. Walter Jones who have collaborated in research reported in this document and specifically contributed material presented here. The NRC also appreciates the efforts of organizations participating in the International Collaborative Fire Model Project (ICFMP) for providing experimental data, problem specifications, and insights and peer comment for the international fire model benchmarking and validation exercises, and for jointly preparing the ICFMP panel reports used and referred to in this study.

DRAFT
FOR
List of Symbols
FORMAT
REVIEW
ONLY

DRAFT FOR

Abbreviations

ANSI	American National Standards Institute
ASTM	American Society for Testing Materials
CAST	Consolidated Fire Growth and Smoke Transport Model
CFD	Computational Fluid Dynamics
CFR	Center for Fire Research
CSR	Cable Spreading Room
DAE	Differential Algebraic
FDS	Fire Dynamic Simulation Model
EPRI	Electric Power Research Institute
HCl	Hydrogen Chloride
HDR	Heiss-Dampf Reaktor
HGL	Hot Gas Layer
HRR	Heat Release Rate
iBMB	Institut für Baustoffe, Massivbau und Brandschutz
ICFMP	International Collaborative Fire Model project
LES	Large Eddy Simulation Model
NFPA	National Fire Protection Association
NIST	National Institute of Standards and Technology
NPP	Nuclear Power Plant
NRC	U.S. Nuclear Regulatory Commission
ODE	Ordinary Differential Equations
PFS	Probabilistic Fire Simulator
PWR	Pressurized Water Reactor
RCC	Rank-order Correlation Coefficients
SWGR	Switchgear Room
TUHC	Total Unburned Hydrocarbons

DRAFT FOR FORMAT REVIEW

Chapter 1 Introduction

ONLY

Connect to main report - TBD

1.1 History

Analytical models for predicting fire behavior have been evolving since the 1960's. Over the past decade, the completeness of the models has grown considerably. In the beginning, the focus of these efforts was to describe in mathematical language the various phenomena which were observed in fire growth and spread. These separate representations have typically described only a small part of a fire. However, when combined they can create a complex computational model that can predict the expected course of a fire.

Once a mathematical representation of the underlying physics has been developed, the conservation equations can be re-cast into predictive equations for temperature, smoke and gas concentration and other parameters of interest, and solved numerically.

The equations are usually in the form of *differential equations*. A complete set of equations can describe the conditions produced by the fire at a given time in a specified volume of air. Referred to as a *control volume*, the model assumes that the predicted conditions within this volume are uniform at any time. Thus, the control volume has one temperature, smoke density, gas concentration, etc. Different models divide the building into different numbers of control volumes depending on the desired level of detail. The most common fire model, known as a *zone model*, generally uses two control volumes to describe a compartment – an upper layer and a lower layer. In the compartment with the fire, additional control volumes for the fire plume or the ceiling jet may be included to improve the accuracy of the prediction (see Figure 1-1).

This two-layer approach has evolved from observation of such layering in real-scale fire experiments. Hot gases collect at the ceiling and fill the compartment from the top. While these experiments show some variation in conditions within the layer, these are small compared to the differences between the layers. Thus, the zone model can produce a fairly realistic simulation under many common and important conditions.

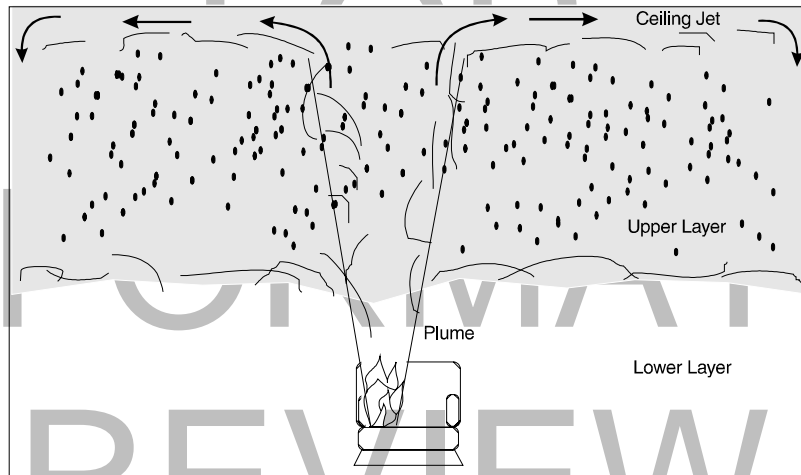


Figure 1-1 Zone model terms.

Other types of models include *network models* and *field models*. Network models use one control volume per compartment and are used to predict conditions in spaces far removed from the fire compartment where temperatures are near ambient and layering does not occur. The field model goes to the other extreme, dividing the compartment into thousands or millions of control volumes. Such models can predict the variation in conditions within the layers, but typically require far longer run times than zone models. They are used when a highly detailed prediction of the flow itself is of interest.

1.2 Model Evaluation

The process of model evaluation is critical to establishing both the acceptable uses and limitations of fire models. It is not possible to evaluate a model in total; instead, available guides such as ASTM¹ E 1355 are intended to provide a methodology for evaluating the predictive capabilities for a specific use [1]. Validation for one application or scenario does not imply validation for different scenarios. Several alternatives are

¹ ASTM International - formerly the American Society for Testing and Materials

provided for performing the evaluation process including comparison of predictions against standard fire tests, full-scale fire experiments, field experience, published literature, or previously evaluated models.

The use of fire models currently extends beyond the fire research laboratory and into the engineering, fire service and legal communities. Sufficient evaluation of fire models is necessary to ensure that those using the models can judge the adequacy of the scientific and technical basis for the models, select models appropriate for a desired use, and understand the level of confidence which can be placed on the results predicted by the models. Adequate evaluation will help prevent the unintentional misuse of fire models. *Verification* is a process to check the correctness of the solution of the governing equations. Verification does not imply that the governing equations are appropriate; only that the equations are being implemented and solved correctly. *Validation* is a process to determine the appropriateness of the governing equations as a mathematical model of the physical phenomena of interest. Typically, validation involves comparing model results with experimental measurement. Differences that cannot be explained by numerical errors in the model or uncertainty in the experiments are attributed to the assumptions and simplifications of the physical model. These terms are used together to perform a model assessment. The more general term, "model assessment," encompasses both verification and validation of a computer model.

In general, this document follows the ASTM E1355 guide for model assessment and provides a model assessment for the zone fire model CFAST. The guide provides four areas of evaluation for predictive fire models:

- Defining the model and scenarios for which the evaluation is to be conducted (Chapter 2),
- Assessing the appropriateness of the theoretical basis and assumptions used in the model (Chapter 3),
- Assessing the mathematical and numerical robustness of the model (Chapter 4), and
- Quantifying the uncertainty and accuracy of the model results in predicting the course of events in similar fire scenarios (Chapters 5 and 6).

Chapter 2 Model and Scenario Definition

Sufficient documentation of calculation models is necessary to assess the adequacy of the scientific and technical basis of the model and the accuracy of the computational procedures for scenarios of interest. In addition, adequate documentation will help prevent the unintentional misuse of the model. The documentation in this document follows the guidelines in ASTM E1355-04 [1]

2.1 Model Documentation

2.1.1 Name and Version of the Model

The name of the model is the Consolidated Fire Growth and Smoke Transport Model or CFAST. The first public release was version 1.0 in June of 1990. This version was restructured from FAST [2] to incorporate the "lessons learned" from the zone model CCFM developed by Cooper and Forney [3], namely that modification is easier and more robust if the components such as the physical routines are separated from the solver. Chapter 4 (Mathematical and Numerical Robustness) discusses this in more detail. Version 2 was released as a component of Hazard 1.2 in 1994 [4]. The first of the 3.x series was released in 1995 and included a vertical flame spread algorithm, ceiling jets and nonuniform heat loss to the ceiling, spot targets, and heating and burning of multiple objects (ignition by flux, temperature or time) in addition to multiple prescribed fires. As it evolved over the next five years, version 3 included smoke and heat detectors, suppression through heat release reduction, better characterization of flow through doors and windows, vertical heat conduction through ceiling/floor boundaries, and non-rectangular compartments. In 2000, version 4 was released and included horizontal heat conduction through walls, and horizontal smoke flow in corridors. Version 5 improved the combustion chemistry. The current version is 5.1.

Most of the code is written in FORTRAN 90, though some of the input/output routines as well as those for handling objects, are written in ANSI² C.

2.1.2 Type of Model

CFAST is a model that predicts the environment within compartmented structures resulting from a fire prescribed by the user. It is an example of the class of models called finite element. This particular implementation is called a zone model, and essentially the space to be modeled is broken down to a few elements. The physics of the compartment fire phenomena is driven by fluid flow, primarily buoyancy. The usual set of elements or zones are the upper and lower gas layers, partitioning of the wall/ceiling/floor to an element each, one or more plumes and objects such as fires, targets, and detectors. One feature of this implementation of a finite element model is that the interface between the elements (in this case, the upper and lower gas layers) can move, with its position defined by the governing equations.

2.1.3 Model Developers

CFAST was developed and is maintained primarily by the Fire Research Division of the National Institute of Standards and Technology. The developers are Walter Jones, Richard Peacock, Glenn Forney, Rebecca Portier, Paul Reneke, John Hoover³, and John Klote.

There have been contributions through research and published papers at Worcester Polytechnic Institute, University of California at Berkeley, VTT of Finland and CITCM of France. An important guide to development of the model has been from many people around the world who have provided ideas, suggestions, comments, detailed questions, opinions on what should happen in particular scenarios, what physics and chemistry are needed and what types of problems must be addressed by such a model in order to be useful for real world applications.

2.1.4 Relevant Publications

² ANSI - American National Standards Institute - The governing national standards body for the United States. FORTRAN and C are two programming languages which are standardized through the ANSI consensus process.

³Naval Research Laboratory, Washington, DC 20375.

CFAST is documented by two publications, this Technical Reference Manual and the User's Guide [5]. The user's guide describes how to use the model and this technical reference manual describes the underlying physical principles, provides a comparison with other models and includes a description of the limitations of this zone model. This technical reference guide applies to version 5 and later and the user's guide to versions 3 and later. Version 5 of CFAST does not include a graphical user interface, so that portion of the user's guide [5] is not applicable. The remainder of the material on use of key words and data files is applicable.

There are documents available (<http://cfast.nist.gov>) that are applicable to versions 2, 3, 4 and 5 of both the model and user interface.

2.1.5 Governing Equations and Assumptions

For CFAST, as for most zone fire models, the equations solved are for conservation of mass and energy. The momentum equation is not solved explicitly, except for use of the Bernoulli equation for the flow velocity at vents. Based on an integration over the volume of an element, these equations are solved as ordinary differential equations.

There are two assumptions which reduce the computation time dramatically. The first is that relatively few zones or elements per compartment is sufficient to model the physical situation. The second assumption is to close the set of equations without using the momentum equation in the compartment interiors. This simplification eliminates acoustic waves. Though this prevents one from calculating gravity waves in compartments (or between compartments), coupled with only a few elements per compartment allows for a prediction in a large and complex space very quickly.

The equations themselves and the algorithms and sub-models used are discussed in detail in chapter 3.

2.1.6 Input Data Required to Run the Model

All of the data to run the model is contained in a primary data file, together with databases for objects, thermophysical properties of boundaries, and sample prescribed fire descriptions [6]. These files contain information about the building geometry (compartment sizes, materials of construction, and material properties), connections between compartments (horizontal flow openings such as doors, windows), vertical flow openings in floors and ceilings, and mechanical ventilation connections), fire properties (fire size and species production rates as a function of time), and specifications for detectors, sprinklers, and targets (position, size, heat transfer characteristics, and flow characteristics for sprinklers). Materials are defined by their thermal conductivity, specific heat, density, thickness, and burning behavior.

Sample data files are provided which encompass many of the validation exercises described in chapter 6 and in the various articles and reports referenced in chapter 6. These examples range from simple one-compartment simulations to a large multi-story hotel scenario that includes an elevator shaft and stairwell pressurization. A complete description of the input parameters required by CFAST can be found in the CFAST User's Guide [5].

2.1.7 Property Data

Any simulation of a real fire scenario involves prescribing material properties for the walls, floor, ceiling, and furnishings. CFAST treats all of these materials as homogeneous solids, thus the physical parameters for

many real objects can only be viewed as approximations to the actual properties. Describing these materials in the input data file is a challenging task for the model user. Thermal properties for the most common barrier materials used in construction, e.g. gypsum wall board, are included in a database, thermal.df, included with the model. These properties come directly from handbook values for typical materials [7].

2.1.8 Model Results

The output of CFAST are the sensible variables that are needed for assessing the environment in a building subjected to a fire. These include the average temperatures of the upper and lower gas layers within each compartment, the ceiling/wall/floor temperatures within each compartment, the visible smoke and gas species concentrations within each layer, target temperatures and sprinkler activation time. There is more extensive discussion of the output in Chapter 6 of this technical reference manual and the user's guide. The output is always in the metric system of units.

2.1.9 Uses and Limitations of the Model

CFAST has been developed for solving practical fire problems in fire protection engineering, while at the same time providing a tool to study fundamental fire dynamics and smoke spread. It is intended for system modeling of building and building components. It is not intended for detailed study of flow within a compartment such as is needed for smoke detector siting. It includes the activation of sprinklers, and fire suppression by water droplets.

The most extensive use of the model is in fire and smoke spread in complex buildings. The efficiency and computational speed are inherent in the few computation cells needed for a zone model implementation. Most of the use is for reconstruction of time-lines for fire and smoke spread in residential, commercial and industrial fire reconstructions. Some applications of the model have been for design of smoke control systems.

- **Compartments:** CFAST is generally limited to situations where the compartment volumes are strongly stratified. However, in order to facilitate the use of the model for preliminary estimates when a more sophisticated calculation is ultimately needed, there are algorithms for corridor flow, smoke detector activation and detailed heat conduction through solid boundaries. This model does provide for non-rectangular compartments, though the application is intended to be limited to relatively simple spaces such as attics and ship corridors. There is no intent to include complex geometries where a complex flow field is a driving force. For these applications, computational fluid dynamics (CFD) models are appropriate.
- There are also limitations inherent in the assumption of stratification of the gas layers. The zone model concept, by definition, implies a sharp boundary between the upper and lower layers, whereas in reality, the transition is typically over about 10 % of the height of the compartment and can be larger in weakly stratified flow. For example, a burning cigarette in a normal room is not within the purview of a zone model. While it is possible to make predictions within 5 % of the actual temperatures of the gas layers, this is not the optimum use of the model. It is more properly used to make estimates of fire spread (not flame spread), smoke detection and contamination, and life safety calculations.
- **Heat Release Rate:** There are limitations inherent in the assumptions used in application of the empirical models. As a general guideline, the heat release should not exceed about 1 MW per cubic meter. This is a limitation on the numerical routines due to the coupling between gas flow and heat transfer through boundaries (conduction, convection and radiation). The inherent two-layer assumption is likely to break down well before this limit is reached.

- **Flame Spread:** While there is a flame spread model included, it should only be used for estimating such effects since it is a simplified empirical model developed to simulate vertical flame spread in a wall-corner configuration.
- **Radiation:** Since the model includes a sophisticated radiation model and ventilation algorithms it has further use for studying building contamination through the ventilation system, as well as the stack effect and the effect of wind on air circulation in buildings.
- **Ventilation and Leakage:** In a single compartment, the ratio of the area of vents connecting one compartment to another to the volume of the compartment should not exceed roughly 2 m^{-1} . This is a limitation on the plug flow assumption for vents. An important limitation arises from the uncertainty in the scenario specification. For example, leakage in buildings is significant, and this affects flow calculations especially when wind is present and for tall buildings. These effects can overwhelm limitations on accuracy of the implementation of the model. The overall accuracy of the model is closely tied to the specificity, care, and completeness with which the data are provided.
- **Thermal Properties:** The accuracy of the model predictions is limited by how well the user can specify the thermophysical properties. For example, the fraction of fuel which ends up as soot has an important effect on the radiation absorption of the gas layer and therefore the relative convective versus radiative heating of the layers and walls, which in turn affects the buoyancy and flow. There is a higher level of uncertainty of the predictions if the properties of real materials and real fuels are unknown or difficult to obtain, or the physical processes of combustion, radiation and heat transfer are more complicated than their mathematical representations in CFAST.

User feedback indicates that using CFAST to predict the transport of heat and combustion products from a prescribed fire is straightforward, easily and quickly accomplished, and the results are within expectations. Any user of a computer based (numerical) model must be aware of the assumptions and approximations being employed. Except for those few materials supplied in the property databases, the user must supply the thermal properties of the materials, and then assess the performance of the model compared with experiments to ensure that the model is valid for a specific application. Only then can the model be expected to predict the outcome of fire scenarios that are similar to those that have actually been tested.

In addition, there are specific limitations and assumptions made in the development of the algorithms. These are detailed in the discussion of each of these sub-models:

- section ? on zone model assumptions,
- section 3.4.1 on prescribed fires,
- section 3.4.1.3 on the relationship between fires and mass balance,
- section ? on the plume entrainment model,
- section 3.4.3.1 on doorway flows and entrainment at vents,
- section ? on the assumptions made for corridor flow correlations,
- section ? on the assumptions made for radiation heat transfer,
- section 3.6 on the suppression model, and
- section 3.7.2 on HCl deposition.

DRAFT
FOR
FORMAT
REVIEW
ONLY

Chapter 3 Theoretical Basis

for CFAST

Adequately detailed documentation of the theoretical basis of the model allows the model user to understand the underlying theory behind the model implementation and thus be able to assess the appropriateness of the model to specific problems. This chapter presents a derivation of the predictive equations for zone fire models and explains in detail the ones used in CFAST [7], [9].

The modeling equations used in CFAST take the mathematical form of an initial value problem for a system of ordinary differential equations. These equations are derived using the conservation of mass, the conservation of energy (equivalently the first law of thermodynamics), the ideal gas law. These equations predict as functions of time quantities such as pressure, layer height and temperatures given the accumulation of mass and enthalpy in the two layers. The assumption of a zone model is that properties such as temperature can be approximated throughout a control volume by an average value.

Many formulations based upon these assumptions can be derived. One formulation can be converted into another using the definitions of density, internal energy and the ideal gas law. Though equivalent analytically, these formulations differ in their numerical properties. Each formulation can be expressed in terms of mass and enthalpy flow. These rates represent the exchange of mass and enthalpy between zones due to physical phenomena such as plumes, natural and forced ventilation, convective and radiative heat transfer, and so on. For example, a vent exchanges mass and enthalpy between zones in connected rooms, a fire plume typically adds heat to the upper layer and transfers entrained mass and enthalpy from the lower to the upper layer, and convection transfers enthalpy from the gas layers to the surrounding walls.

As discussed in references [10] and [8], the zone fire modeling ordinary differential equations (ODE's) are stiff. The term stiff means that large variations in time scales are present in the ODE solution. In our problem, pressures adjust to changing conditions more quickly than other quantities such as layer temperatures or interface heights. Special solvers are required in general to solve zone fire modeling ODE's because of this stiffness. Runge-Kutta methods or predictor-corrector methods such as Adams-Bashforth require prohibitively small time steps in order to track the short-time scale phenomena (pressure in our case). Methods that calculate the Jacobian (or at least approximate it) have a much larger stability region for stiff problems and are thus more successful at their solution.

3.1 Derivation of Equations for a Two-Layer Model

A compartment is divided into two control volumes, a relatively hot upper layer and a relatively cool lower layer, as illustrated in Figure 3-1. The gas in each layer has attributes of mass, internal energy, density, temperature, and volume denoted respectively by m_i , E_i , ρ_i , T_i , and V_i where $i=L$ for the lower layer and $i=U$ for the upper layer. The compartment as a whole has the attribute of pressure P . These 11 variables are related by means of the following seven constraints (counting density, internal energy and the ideal gas law twice, once for each layer).

$$\rho_i = \frac{m_i}{V_i} \quad (\text{density}) \quad (1)$$

$$E_i = c_v m_i T_i \quad (\text{internal energy}) \quad (2)$$

$$P = R\rho_i T_i \quad (\text{ideal gas law}) \quad (3)$$

$$V = V_L + V_U \quad (\text{total volume}) \quad (4)$$

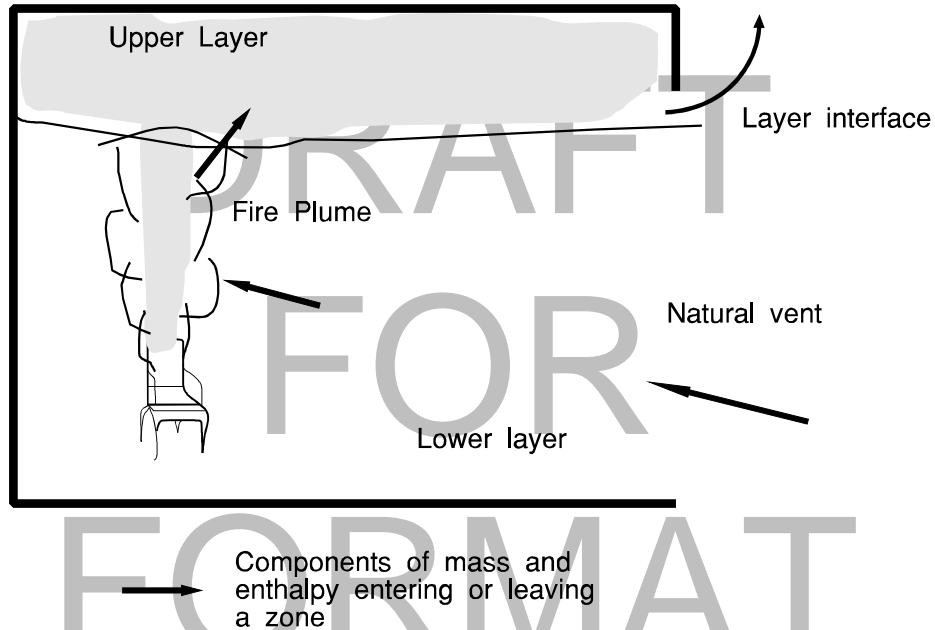


Figure 3-1. Schematic of control volumes in a two-layer zone model.

The specific heat at constant volume and at constant pressure c_v and c_p , the universal gas constant, R , and the ratio of specific heats, γ , are related by $\gamma = c_p / c_v$ and $R = c_p - c_v$. For ambient air, $c_p \approx 1$ kJ/kg/K and $\gamma = 1.4$. Four additional equations obtained from conservation of mass and energy for each layer are required to complete the equation set. The differential equations for mass in each layer are

$$\begin{aligned} \frac{dm_L}{dt} &= \dot{m}_L \\ \frac{dm_U}{dt} &= \dot{m}_U \end{aligned} \quad (5)$$

The first law of thermodynamics states that the rate of increase of internal energy plus the rate at which the layer does work by expansion is equal to the rate at which enthalpy is added to the gas. In differential form this is

$$\underbrace{\text{internal energy}} + \underbrace{\text{work}} = \underbrace{\text{enthalpy}} \quad (6)$$

$$\frac{dE_i}{dt} + P \frac{dV_i}{dt} = \dot{h}_i$$

where c_p is taken as constant in the enthalpy term,

$$\dot{h} = c_p \dot{m}_u T_u + \dot{E}_u + c_p \dot{m}_L T_L + \dot{E}_L \quad (7).$$

A differential equation for pressure can be derived by adding the upper and lower layer versions of eq (6), noting that $dV_U/dt = -dV_L/dt$, and substituting the differential form of eq (2) to yield

$$\frac{dP}{dt} = \frac{\gamma - 1}{V} (\dot{h}_L + \dot{h}_U). \quad (8)$$

Differential equations for the layer volumes can be obtained by substituting the differential form of eq (2) into eq (6) to obtain

$$\frac{dV_i}{dt} = \frac{1}{P\gamma} \left((\gamma - 1) \dot{h}_i - V_i \frac{dP}{dt} \right). \quad (9)$$

Equation (6) can be rewritten using eq (9) to eliminate dV/dt to obtain

$$\frac{dE_i}{dt} = \frac{1}{\gamma} \left(\dot{h}_i + V_i \frac{dP}{dt} \right). \quad (10)$$

A differential equation for density can be derived by applying the quotient rule to $\frac{d\rho_i}{dt} = \frac{d}{dt} \left(\frac{m_i}{V_i} \right)$ and using eq (9) to eliminate dV/dt to obtain

$$\frac{d\rho_i}{dt} = -\frac{1}{c_p T_i V_i} \left((\dot{h}_i - c_p \dot{m}_i T_i) - \frac{V_i}{\gamma - 1} \frac{dP}{dt} \right). \quad (11)$$

Temperature differential equations can be obtained from the equation of state by applying the quotient rule to $\frac{dT_i}{dt} = \frac{d}{dt} \left(\frac{P}{R\rho_i} \right)$ and using eq. (11) to eliminate $d\rho/dt$ to obtain

$$\frac{dT_i}{dt} = \frac{1}{c_p \rho_i V_i} \left((\dot{h}_i - c_p \dot{m}_i T_i) + V_i \frac{dP}{dt} \right). \quad (12)$$

These equations for each of the eleven variables are summarized in table 1. The time evolution of these solution variables can be computed by solving the corresponding differential equations together with appropriate initial conditions. The remaining seven variables can be determined from the four solution variables using eqs (1) to (4).

There are, however, many possible differential equation formulations. Indeed, there are 330 different ways to select four variables from eleven. Many of these systems are incomplete due to the relationships that exist between the variables given in eqs (1) to (4). For example the variables, ρ_U , V_U , m_U , and P form a dependent set since $\rho_U = m_U / V_U$.

The number of differential equation formulations can be considerably reduced by not mixing variable types between layers; that is, if upper layer mass is chosen as a solution variable, then lower layer mass must also be chosen. For example, for two of the solution variables choose m_L and m_U , or ρ_L and ρ_U , or T_L and T_U . For the other two solution variables pick E_L and E_U or P and V_L or P and V_U . This reduces the number of distinct formulations to nine. Since the numerical properties of the upper layer volume equation are the same as a lower layer one, the number of distinct formulations can be reduced to six.

Table 3-1 Conservative zone model equations

Equation Type	Differential Equation
i'th layer mass	$\frac{dm_i}{dt} = \dot{m}_i$
pressure	$\frac{dP}{dt} = \frac{\gamma-1}{V} (\dot{h}_L + \dot{h}_U)$
i'th layer energy	$\frac{dE_i}{dt} = \frac{1}{\gamma} \left(\dot{h}_i + V_i \frac{dP}{dt} \right)$
i'th layer volume	$\frac{dV_i}{dt} = \frac{1}{\gamma P} \left((\gamma - 1) \dot{h}_i - V_i \frac{dP}{dt} \right)$
i'th layer density	$\frac{d\rho_i}{dt} = -\frac{1}{c_p T_i V_i} \left(\dot{h}_i - c_p \dot{m}_i T_i \right) - \frac{V_i}{\gamma-1} \frac{dP}{dt}$
i'th layer temperature	$\frac{dT_i}{dt} = \frac{1}{c_p \rho_i V_i} \left(\dot{h}_i - c_p \dot{m}_i T_i \right) + V_i \frac{dP}{dt}$

3.2 Equation Set Used in CFAST

The current version of CFAST is set up to use the equation set for layer temperature, layer volume, and pressure as shown below.

$$\frac{dP}{dt} = \frac{\gamma-1}{V}(\dot{h}_L + \dot{h}_U) \quad (13)$$

$$\frac{dV_U}{dt} = \frac{1}{\gamma P} \left((\gamma - 1)\dot{h}_U - V_U \frac{dP}{dt} \right) \quad (14)$$

$$\frac{dT_U}{dt} = \frac{1}{c_p \rho_U V_U} \left((\dot{h}_U - c_p \dot{m}_U T_U) + V_U \frac{dP}{dt} \right) \quad (15)$$

$$\frac{dT_L}{dt} = \frac{1}{c_p \rho_L V_L} \left((\dot{h}_L - c_p \dot{m}_L T_L) + V_L \frac{dP}{dt} \right) \quad (16)$$

In these equations, the pressure is actually modeled with the pressure difference relative to an ambient reference pressure to minimize numerical instability.

3.3 Limitations of the Zone Model Assumptions

The basic assumption of all zone fire models is that each compartment can be divided into a small number of control volumes, each of which is uniform in temperature and composition. In CFAST all compartments have two zones except for the fire room which has an additional zone for the plume. Since a real upper/lower interface is not as sharp as this, one has a spatial error of about 10 % in determining the height of the layer [9],[28].

The zone model concept best applies for an enclosure in which the width and length are not too different. If the horizontal dimensions of the room differ too much (i.e. the room looks like a corridor), the flow pattern in the room may become asymmetrical. If the enclosure is too shallow, the temperature may have significant radial differences. The width of the plume may at some height become equal to the width of the room and the model assumptions may fail in a tall and narrow enclosure. Therefore, the user should recognize approximate limits on the ratio of the length (L), width (W), and height (H) of the compartment.

If the aspect ratio (length/width) is over about 10, the corridor flow algorithm should be used. This provides the appropriate filling time. Similarly, for tall shafts (elevators and stairways), a single zone approximation is more appropriate. It was found experimentally [10] that the mixing between a plume and lower layer due to the interaction with the walls of the shaft, caused complete mixing. This is the flip side of the corridor problem and occurs at a ratio of the height to characteristic floor length of about 10. The following quantitative limits are recommended:

Table 3-2 Recommended compartment dimension limits

Group	Acceptable	Special consideration required	Corridor flow algorithm
$(L/W)_{max}$	$L/W < 3$	$3 < L/W < 5$	$L/W > 5$
$(L/H)_{max}$	$L/H < 3$	$3 < L/H < 6$	$L/H > 6$
$(W/H)_{min}$	$W/H > 0.4$	$0.2 < W/H < 0.4$	$W/H < 0.2$

3.4 Source Terms for the Model

This section discusses each of the sub-models in CFAST. In general, the sections are similar to the way the model itself is structured. The sub-sections which follow discuss the way the actual phenomena are implemented numerically. For each of the phenomena discussed below, the physical basis for the model is discussed first, followed by a brief presentation of the implementation within CFAST. For all of the phenomena, there are basically two parts to the implementation: the physical interface routine (which is the interface between the CFAST model and the algorithm) and the actual physical routine(s) which implement the physics. This implementation allows the physics to remain independent of the structure of CFAST and allows easier insertion of new phenomena.

3.4.1 The Fire

A fire in CFAST is implemented as a source of fuel mass which is released at a prescribed rate (the pyrolysis rate). Energy is released by the fuel and combustion products are created as it burns. The model incorporates two distinct types of fires: unconstrained and constrained. In the unconstrained fire, the fire simply releases mass and energy at a rate prescribed by the user; no calculation or tracking of products of combustion is included. In the constrained fire, species production is calculated based on production yields prescribed by the user. In addition, for the constrained fire, the pyrolysis rate and resulting energy and species generation may be limited by the oxygen available for combustion. When sufficient oxygen is available for combustion, heat release rate for the constrained fire is the same as for the unconstrained fire.

The model can simulate multiple fires in one or more compartments of the building. These fires are treated as totally separate entities, with no interaction of the plumes. These fires are generally referred to as “objects” and can be ignited at a prescribed time, temperature or heat flux.

CFAST does not include a pyrolysis model to predict fire growth. Rather, pyrolysis rates for each fire are prescribed by the user. While this approach does not directly account for increased pyrolysis due to radiative feedback from the flame or compartment, in theory these effects could be prescribed by the user. In an actual fire, this is an important consideration, and the specification used should consider the experimental conditions as closely as possible.

3.4.1.1 Unconstrained Fire

An unconstrained fire releases energy based on the pyrolysis rate of the fuel. This type of fire is applicable to fuels for which there is always sufficient oxygen in the fuel for combustion to take place and when the concentrations of products of combustion are not of interest.

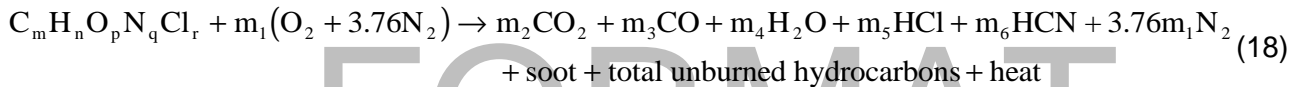
The pyrolysis rate is specified as \dot{m}_p , the burning rate as \dot{m}_b and the heat of combustion as H_c so that the heat release rate, Q_f , is (total heat release less the energy necessary to heat the fuel)

$$Q_f = H_c \dot{m}_b - c_p (T_v - T_a) \dot{m}_b \quad (17)$$

where T_v and T_a are the fuel volatilization and ambient temperatures, respectively and H_c is the heat of combustion of the fuel. In CFAST, T_v is assumed to be the upper layer temperature in the compartment with a fire. For the unconstrained fire, $\dot{m}_b = \dot{m}_p$.

3.4.1.2 Constrained Fire

A constrained fire releases energy based on the pyrolysis of fuel, but may be constrained by the oxygen available for combustion depending on the compartment conditions. Complete burning will take place only where there is sufficient oxygen. When insufficient oxygen is entrained into the fire plume, unburned fuel will be transported from zone to zone until there is sufficient oxygen and a high enough temperature to support combustion. In general, CFAST uses a simple definition of a combustion reaction that includes major products of combustion for hydrocarbon fuels:



where the coefficients m_1, m_2 , etc. represent appropriate molar ratios for a stoichiometric balance of the equation. For complete combustion of the simplest hydrocarbon fuel, methane reacts with oxygen to form carbon dioxide and water. The only input required is the pyrolysis rate and the heat of combustion. For fuels that contain oxygen, nitrogen, or chlorine, the reaction becomes more complex. In this case, production yields for the species are prescribed by the user. Stoichiometry is used to insure conservation of mass and elements in the reaction. The species which are calculated are oxygen, carbon dioxide, carbon monoxide, water, total unburned hydrocarbons (tuhc), and soot. Gaseous nitrogen is included, but only acts as a diluent. Production of hydrogen cyanide and hydrogen chloride are tracked solely based on user prescribed yields.

The heat release rate for a constrained fire may be reduced below its prescribed value based upon the oxygen available for combustion. For the constrained fire, the burning rate may be less than the pyrolysis rate and eq. (17) cannot be simplified as in the case of the unconstrained fire.

As fuel and oxygen are consumed, heat is released and various products of combustion are formed. The heat is released as radiation and convected enthalpy:

$$\begin{aligned} Q_{f,r} &= \chi_R Q_f \\ Q_{f,c} &= (1 - \chi_R) Q_f \end{aligned} \quad (19)$$

where, χ_R , is the fraction of the fire's heat release rate given off as radiation. The convective enthalpy, $Q_{f,c}$ then becomes the driving term in the plume flow. For a constrained fire there is radiation to both the upper and lower layers, whereas the convective part contributes only to the upper layer.

3.4.1.3 Limiting Combustion by Available Oxygen

For a constrained fire, the heat release rate is limited by available oxygen. This limit is applied in three places, which are shown schematically in Figure 3-2. The first is burning in the portion of the plume which is in the lower layer of the room of fire origin (region #1). The second is the portion of the plume in the upper layer, also in the room of origin (region #2). The third is in the vent flow which entrains air from a lower layer into an upper layer in an adjacent compartment (region #3). The unburned hydrocarbons are tracked in this model. Further combustion of CO to CO₂ is not included in the model.

or $\dot{m}_f = \dot{m}_{tuhc}$ from a previous region (kg/s) (region #2 and #3).

and $\dot{m}_{tuhc} = \dot{m}_f - \dot{m}_b$

where *tuhc* stands for total un-burned hydrocarbons.

The first step is to limit the actual burning which takes place in the combustion zone. In each combustion zone, there is a quantity of fuel available. At the source this results from the pyrolysis of the material, \dot{m}_f . In other situations such as a plume or door jet, it is the net unburned fuel available, \dot{m}_{tuhc} . In each case, the fuel which is available but not burned is then deposited into the “ \dot{m}_{tuhc} ” category. This provides a consistent notation. In the discussion below, \dot{m}_f is the amount of fuel burned. This value is initially specified as to the available fuel, and then reduced if there is insufficient oxygen to support complete combustion. Subsequently, the available fuel, \dot{m}_{tuhc} , is reduced by the final value of \dot{m}_f . Thus we have a consistent description in each burning region, with an algorithm that is invoked independent of the region being analyzed.

$$Q = \dot{m}_f \times H_c, \tag{20}$$

with the mass of oxygen required to achieve this energy release rate of

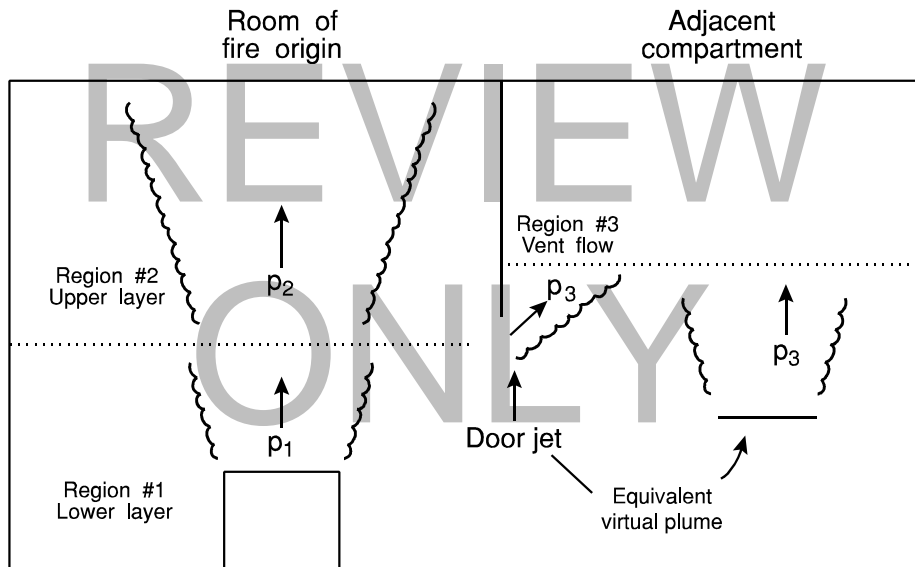


Figure 3-2 Schematic of entrainment and burning regions.

$$\dot{m}_O = \frac{Q}{E} = \dot{m}_f \times \frac{H_c}{E}. \tag{21}$$

where E is the heat release per mass unit of oxygen consumed, taken to be 1.31×10^7 J/kg (based on oxygen consumption calorimetry [11],[12], [13]⁴ for typical fuels). If the fuel contains oxygen (available for combustion), the oxygen needed to achieve full combustion is less:

$$\dot{m}_{O,needed} = \dot{m}_O - \dot{m}_{O,in\ the\ fuel} \quad (22)$$

If sufficient oxygen is available, then it is fully burned. However, if the oxygen concentration is low enough, it will constrain the burning and impose a limit on the amount of fuel actually burned, as opposed to the amount pyrolyzed. The actual limitation is discussed below and is:

$$\dot{m}_{O,actual} = \text{minimum of } \left\{ \dot{m}_{O,available}, \dot{m}_{O,needed} \right\}, \quad (23)$$

$$\dot{m}_{f,actual} = \dot{m}_{O,actual} \times \frac{E}{H} \quad (24)$$

The relationship between oxygen and fuel concentration defines a range in which burning will take place. In the CFAST model, a limit is incorporated by limiting the burning rate as the oxygen level decreases until a “lower oxygen limit” (LOL) is reached. The lower oxygen limit is incorporated through a smooth decrease in the burning rate near the limit:

$$\dot{m}_{o,available} = \dot{m}_e Y_{O_2} C_{LOL} \quad (25)$$

where \dot{m}_e is the mass entrainment flow rate, Y_{O_2} is the mass fraction of oxygen, and the lower oxygen limit coefficient, C_{LOL} , is the fraction of the available fuel which can be burned with the available oxygen and varies from 0 at the limit to 1 above the limit. The functional form that utilizes the hyperbolic tangent was determined empirically to provide a smooth cutoff of the burning over a *narrow* range above the limit.

$$C_{LOL} = \frac{\tanh\left(800(Y_{O_2} - Y_{LOL}) - 4\right) + 1}{2} \quad (26)$$

A temperature criterion is also imposed so that no burning will take place when the temperature is below a user prescribed temperature.

In summary, it is possible to follow the formation of the major products of combustion (carbon dioxide, carbon monoxide, soot, water, hydrogen cyanide, and hydrogen chloride) using appropriate measured product yields (e.g., [14]) to define product yields for eq. (18). Actual combustion chemistry is not considered in CFAST due to the complexities associated with detailed kinetics and transport.

3.4.1.4 Limitation of the Algorithm for Fires and Mass Balance

⁴ The units for oxygen consumption calorimetry are Joules/kg. The value 1.31×10^7 J/kg is representative of typical fuels such as furniture (see reference [13]) and implies these units. The variation or uncertainty (2σ) associated with this value is on the order of $\pm 5\%$. This is a fixed parameter in CFAST version 5 and earlier.

CFAST depends on pyrolysis data for the source term for a fire. The usual way to obtain this data is a large-scale calorimeter, e.g. [15]. Generally, a product (e.g., chair, table, bookcase) is placed under a large collection hood and ignited by a burner (~50 kW simulating a wastebasket) placed adjacent to the item. The combustion process then proceeds under assumed “free-burning” conditions, and the heat release rate is measured. Potential sources of uncertainty include measurement errors related to the instrumentation and the degree to which “free-burning” conditions are not achieved (e.g., radiation from the gases under the hood or from the hood itself, and restrictions in the air entrained by the object causing locally reduced oxygen concentrations affecting the combustion chemistry). There are limited experimental data for upholstered furniture which suggest that prior to the onset of flashover in a compartment, the influence of the compartment on the burning behavior of the item is small. The differences obtained from the use of different types or locations of ignition sources have not been explored. These factors are discussed in reference [16].

Where small-scale calorimeter data are used, procedures are available to extrapolate to the behavior of a full-size item. These procedures are based on empirical correlations of data which exhibit significant scatter, thus limiting their accuracy. For example, for upholstered furniture, the peak heat release rates estimated by the “triangular approximation” method averaged 91 % (range 46 % to 103 %) of values measured for a group of 26 chairs with noncombustible frames, but only 63 % (range 46 % to 83 %) of values measured for a group of 11 chairs with combustible frames [17]. Also, the triangle neglects the “tails” of the curve; these are the initial time from ignition to significant burning of the item, and the region of burning of the combustible frame, after the fabric and filler are consumed.

The provided data and procedures only relate directly to burning of items initiated by relatively large flaming sources. Little data are currently available for release rates under smoldering combustion, or for the high external flux and low oxygen conditions characteristic of post-flashover burning. While the model allows multiple items burning simultaneously, it does not account for the synergy of such multiple fires. Thus, for other ignition scenarios, multiple items burning simultaneously (which exchange energy by radiation and convection), combustible interior finish, and post-flashover conditions, the model can give estimates which are often nonconservative (the actual release rates would be *greater* than estimated). At present, the only sure way to account for all of these complex phenomena is to conduct a full-scale compartment burn and use the pyrolysis rates directly.

Burning can be constrained by the available oxygen. However, this “constrained fire” is not subject to the influences of radiation to enhance its burning rate, but is influenced by the oxygen available in the compartment. If a large mass loss rate is entered, the model will follow this input until there is insufficient oxygen available for that quantity of fuel to burn in the compartment. The unburned fuel (sometimes called excess pyrolysate) is tracked as it flows out in the door jet, where it can entrain more oxygen. If this mixture is within the user-constrained flammable range, it burns in the door plume. If not, it will be tracked throughout the building until it eventually collects as unburned fuel or burns in a vent. The enthalpy released in the fire compartment and in each vent, as well as the total enthalpy released, is detailed in the output of the model. Since mass and enthalpy are conserved, the total will be correct. However, since combustion did not take place adjacent to the burning object, the actual mass burned could be lower than that specified by the user. The difference will be the unburned fuel.

An oxygen combustion chemistry scheme is employed only in constrained fires. Here user-constrained hydrocarbon ratios and species yields are used by the model to predict concentrations. A balance among hydrogen, carbon, and oxygen molecules is maintained. Under some conditions, low oxygen can change the combustion chemistry, with a resulting increase in the yields of products of incomplete combustion such as carbon monoxide. However, not enough is known about these chemical processes to build this relationship into the model at the present time. Some data exist in reports of full-scale experiments (e.g., reference [18]) which can assist in making such determinations.

3.4.2 Plumes

A plume is formed above any burning object. It acts as a pump transferring mass and enthalpy from the lower layer into the upper layer. A correlation is used to predict the amount of mass and enthalpy that is transferred. A more complete plume model would predict plume entrainment by creating a separate zone and solving the appropriate equations.

Two sources exist for moving enthalpy and mass between the layers within and between compartments. Within the compartment, the fire plume provides one source. The other source of mixing between the layers occurs at vents such as doors or windows. Here, there is mixing at the boundary of the opposing flows moving into and out of the compartment. The degree of mixing is based on an empirically-derived mixing relation. Both the outflow and inflow entrain air from the surrounding layers. The flow at vents is also modeled as a plume (called the door plume or jet), and uses the same equations as the fire plume, with two differences. First, an offset is calculated to account for entrainment within the doorway and second, the equations are modified to account for the rectangular geometry of vents compared to the round geometry of fire plumes. All plumes within the simulation entrain air from their surroundings according to an empirically-derived entrainment relation. Entrainment of relatively cool, non-smoke laden air adds oxygen to the plume and allows burning of the fuel. It also causes it to expand as the plume moves upward in the shape of an inverted cone. The entrainment in a vent is caused by bi-directional flow and results from vortices formed near a shear layer. This phenomenon is called the Kelvin-Helmholtz instability [19]. It is not exactly the same as a normal plume, so some error (not measured) arises when this entrainment is approximated by a normal plume entrainment algorithm.

While experiments show that there is very little mixing between the layers at their interface, sources of convection such as radiators or diffusers of heating and air conditioning systems, and the downward flows of gases caused by cooling at walls, will cause such mixing. These are examples of phenomena which are inconsistent with the two-zone approximation. Also, the plumes are *assumed* not to be affected by other flows which may occur. For example, if the burning object is near the door the strong inflow of air will cause the plume axis to lean away from the door and affect entrainment of gases into the plume. Such effects are not included in the model.

As discussed above, each compartment is divided into an upper and lower layer. At the start of the simulation, the layers in each compartment are initialized at ambient conditions and by default, the upper layer volume set to 0.001 of the compartment volume (an arbitrary, small value set to avoid the potential mathematical problems associated with dividing by zero). Other values can be set. As enthalpy and mass are pumped into the upper layer by the fire plume, the upper layer expands in volume causing the lower layer to decrease in volume and the interface to move downward. If the door to the next compartment has a soffit, there can be no flow through the vent from the upper layer until the interface reaches the bottom of that soffit. Thus in the early stages the expanding upper layer will push down on the lower layer air and force it into the next compartment through the vent by expansion.

Once the interface reaches the soffit level, a door plume forms and flow from the fire compartment to the next compartment is initiated. As smoke flow from the fire compartment fills the second compartment, the lower layer of air in the second compartment is pushed down. As a result, some of this air flows into the fire compartment through the lower part of the connecting doorway (or vent). Thus, a vent between the fire compartment and connecting compartments can have simultaneous, opposing flows of air. All flows are driven by pressure and density differences that result from temperature differences and layer depths. The key to getting the correct flow is to distribute correctly the fire and plume's mass and enthalpy between the layers.

Buoyancy generated by the combustion processes in a fire causes the formation of a plume. Such a plume can transport mass and enthalpy from the fire into the lower or upper layer of a compartment. In the present implementation, we assume that both mass and enthalpy from the fire are deposited only into the upper layer. In addition the plume entrains mass from the lower layer and transports it into the upper layer. This yields a net enthalpy transfer between the two layers.

A fire generates energy at a rate \dot{Q}_f . Some fraction, χ_R , will exit the fire as radiation. The remainder, χ_C , will then be deposited in the layers as convective energy or heat additional fuel which may then pyrolyze. McCaffrey [20] estimated the mass entrained by the fire/plume from the lower into the upper layer. This correlation divides the flame/plume into three regions as given in eq(28). This prescription agrees with the work of Cetegen *et al.* [21] in the intermittent regions but yields greater entrainment in the other two regions. This difference is particularly important for the initial fire since the upper layer is far removed from the fire.

$$\begin{aligned} \frac{\dot{m}_e}{Q_f} &= 0.011 \left(\frac{Z}{Q_f^{2/5}} \right)^{0.566} & 0.00 \leq Z < 0.08 \\ \frac{\dot{m}_e}{Q_f} &= 0.026 \left(\frac{Z}{Q_f^{2/5}} \right)^{0.909} & 0.08 \leq Z < 0.20 \\ \frac{\dot{m}_e}{Q_f} &= 0.124 \left(\frac{Z}{Q_f^{2/5}} \right)^{1.895} & 0.20 \leq Z \end{aligned} \quad (28)$$

McCaffrey's correlation is an extension of the common point source plume model, with a different set of coefficients for each region. These coefficients are experimental correlations.

Within CFAST, the radiative fraction defaults to 0.30 [22]; i.e., 30 % of the fire's energy is released via radiation. For other fuels, the work of Tewarson [23], McCaffrey [24], or Koseki [25] is available for reference. The typical range for the radiative fraction is from about 0.05 to 0.4.

In CFAST, there is a constraint on the quantity of gas which can be entrained by a plume arising from a fire. The constraint arises from the physical fact that a plume can rise only so high for a given size of a heat source. Early in a fire, when the energy flux is very small, the plume may not have sufficient energy to reach the compartment ceiling. The correct sequence of events is for a small fire to generate a plume which does not reach the ceiling or upper layer initially. The plume entrains enough cool gas to decrease the buoyancy to the point where it no longer rises. When there is sufficient energy present in the plume, it will penetrate the upper layer. To this end the following prescription has been incorporated: for a given size fire, a limit is placed on the amount of mass which can be entrained, such that no more is entrained than would allow the plume to reach the layer interface. The result is that the interface falls at about the correct rate, although it starts a little too soon, and the upper layer temperature is over predicted, but follows experimental data after the initial phase.

For the plume to be able to penetrate the inversion formed by a hot gas layer over a cooler gas layer, the density of the gas in the plume at the point of intersection must be less than the density of the gas in the upper layer. In practice, this places a maximum on the air entrained into the plume. From conservation of mass and enthalpy

$$\dot{m}_p = \dot{m}_f + \dot{m}_e \quad (29)$$

where the subscripts p , f , e , and l refer to the plume, fire, entrained air, and lower layer, respectively.

$$\dot{m}_p c_p T_p = \dot{m}_f c_p T_f + \dot{m}_e c_p T_l \quad (30)$$

The criterion that the density in the plume region be lower than the upper layer implies that $T_u < T_p$. Solving eq (30) for T_p and eliminating \dot{m}_p using eq (29) yields

$$T_p = \frac{T_f \dot{m}_f + T_l \dot{m}_e}{\dot{m}_f + \dot{m}_e} > T_u \quad (31)$$

or

$$\dot{m}_e < \left(\frac{T_f - T_u}{T_u - T_l} \right) \dot{m}_f < \frac{T_f}{T_u - T_l} \dot{m}_f \quad (32)$$

Substituting the convective energy released by the fire,

$$Q_{f,c} = \dot{m}_f c_p T_f, \quad (33)$$

into eq (32) yields the final form of the entrainment limit used in the CFAST model:

$$\dot{m}_e < \frac{Q_{f,c}}{c_p (T_u - T_l)} \quad (34)$$

which is incorporated into the model. It should be noted that both the plume and layers are assumed to be well mixed with negligible mixing and transport time for the plume and layers.

3.4.2.1 Limitation of the Plume Algorithm

The entrainment coefficients are empirically determined values from the work of McCaffrey [25]. Small errors in these values will have a small effect on the fire plume or the flow in the plume of gases exiting the door of that compartment. In a multi-compartment model such as CFAST, however, small errors in each door plume are multiplicative as the flow proceeds through many compartments, possibly resulting in a significant error in the furthest compartments. The data available from validation experiments [26] indicate that the values for entrainment coefficients currently used in most zone models produce good agreement for a three-compartment configuration. More data are needed for larger numbers of compartments to study this further.

In real fires, smoke and gases are introduced into the lower layer of each compartment primarily due to mixing at connections between compartments and from the downward flows along walls (where contact with the wall cools the gas and reduces its buoyancy). Doorway mixing has been included in CFAST, using the same empirically derived mixing coefficients as used for calculating fire plume entrainment. Downward wall flow has not been included. This could result in underestimates of lower layer temperatures and species concentration.

Entrainment at a vent (doors, windows, ...) yields mixing into the lower and upper layers. The latter has been studied more extensively than the former. The door jets are not symmetric for these mixing phenomena, however. We have constrained the phenomenon for CFAST to be in the range as predicted by Zukoski *et al.* [27].

3.4.3 Vent Flow

Flow through vents is a dominant component of any fire model because it is sensitive to small changes in pressure and transfers the greatest amount of enthalpy on an instantaneous basis of all the source terms (except of course for the fire and plume). Its sensitivity to environmental changes arises through its dependence on the pressure difference between compartments which can change rapidly.

CFAST models two types of vent flow, vertical flow through horizontal vents (ceiling holes, hatches *etc.*) and horizontal flow through vertical vents (doors, windows *etc.*). Horizontal flow is the flow which is normally thought of when discussing fires. Vertical flow is particularly important in two disparate situations: a ship, and the role of fire fighters doing roof venting.

Horizontal vent flow is determined using the pressure difference across a vent. Flow at a given elevation may be computed using Bernoulli's law by first computing the pressure difference at that elevation. The pressure on each side of the vent is computed using the pressure at the floor, the height of the floor and the density.

Atmospheric pressure is about 100 000 Pa. Fires produce pressure changes from 1 Pa to 1000 Pa and mechanical ventilation systems typically involve pressure differentials of about 1 Pa to 100 Pa. The pressure variables are solved to a higher accuracy than other solution variables because of the subtraction (with resulting loss of precision) needed to calculate vent flows from pressure differences.

Mass flow (in the remainder of this section, the term "flow" will be used to mean mass flow) is the dominant source term for the predictive equations because it fluctuates most rapidly and transfers the greatest amount of enthalpy on an instantaneous basis of all the source terms (except of course the fire). Also, it is most sensitive to changes in the environment. Horizontal flow encompasses flow through doors, windows and so on. Horizontal flow is discussed in section ?. Vertical flow occurs in ceiling vents. It is important in two separate situations: on a ship with open hatches and in house fires with roof venting. Vertical flow is discussed in section ?.

Flow through vents can be forced (mechanical) or natural (convective). Force flow can occur through either vertical or horizontal vents. The differences are primarily the selection rules for the source of the gases or whether the resultant plume enters the lower or upper layer of each compartment.

There is a special case of horizontal flow for long corridors. A corridor flow algorithm is incorporated to calculate the time delay from when a plume enters a compartment to when the effluent is available for flow into adjacent compartments.

3.4.3.1 Horizontal Flow Through Vertical Vents

Flow through normal vents such as windows and doors is governed by the pressure difference across a vent. A momentum equation for the zone boundaries is not solved directly. Instead momentum transfer at the zone boundaries is included by using an integrated form of Euler's equation, namely Bernoulli's solution for the velocity equation. This solution is augmented for restricted openings by using flow coefficients [28] to allow for constriction from finite size doors. The flow (or orifice) coefficient is an empirical term which addresses the problem of constriction of velocity streamlines at an orifice.

Bernoulli's equation is the integral of the Euler equation and applies to general initial and final velocities and pressures. The implication of using this equation for a zone model is that the initial velocity in the doorway is the quantity sought, and the final velocity in the target compartment vanishes. That is, the flow velocity vanishes where the final pressure is measured. Thus, the pressure at a stagnation point is used. This is consistent with the concept of uniform zones which are completely mixed and have no internal flow. The general form for the velocity of the mass flow is given by

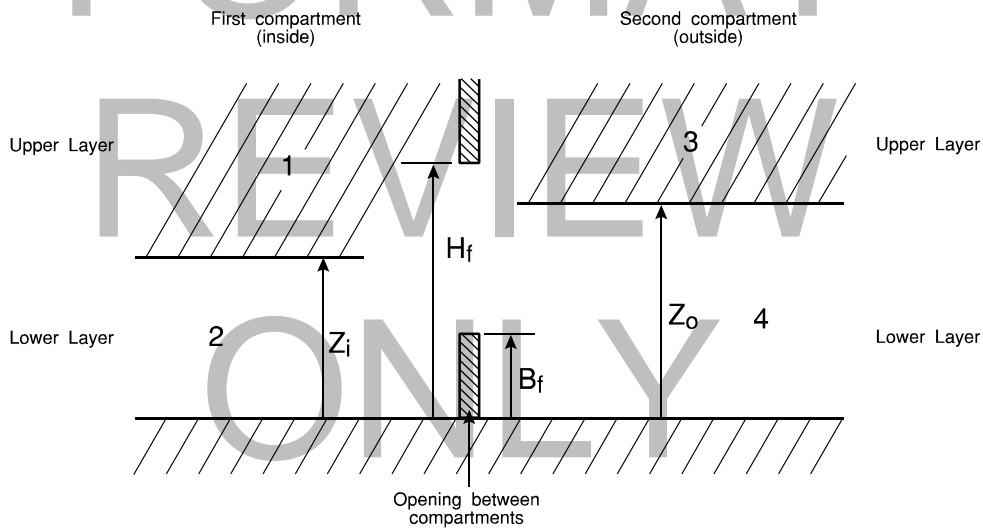
$$v = C \left(\frac{2\Delta P}{\rho} \right)^{1/2} \quad (35)$$

where C is the constriction (or flow) coefficient (≈ 0.7), ρ is the gas density on the source side, and DP is the pressure across the interface. (Note: at present we use a constant C for all gas temperatures)

The simplest means to define the limits of integration is with neutral planes, that is the height at which flow reversal occurs, and physical boundaries such as sills and soffits. By breaking the integral into intervals defined by flow reversal, a soffit, a sill, or a zone interface, the flow equation can be integrated piecewise analytically and then summed.

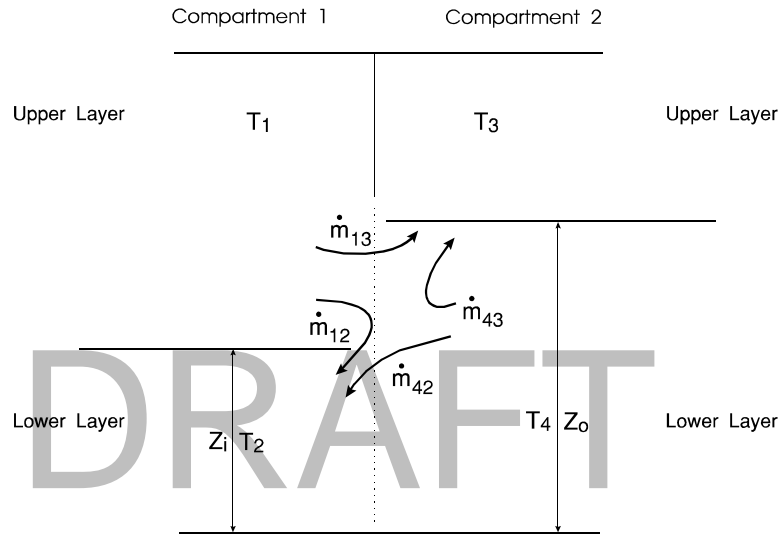
The approach to calculating the flow field is of some interest. The flow calculations are performed as follows. The vent opening is partitioned into at most six slabs where each slab is bounded by a layer height, neutral plane, or vent boundary such as a soffit or sill. The most general case is illustrated in Figure **Figure 6**.

The mass flow for each slab can be determined from



Z = height of layer interface
 H_f = height of soffit
 B_f = height of sill
 Layer numbers refer to nomenclature used in text

Figure 3-3 Notation conventions for two-layer model in two compartments with a connecting vent.



\dot{m}_{ij} mass flow from zone i to zone j

Figure 3-4 Flow pattern and layer numbering convention.

$$\dot{m}_{io} = \frac{1}{3} C (8\rho) A_{slab} \left(\frac{x^2 + xy + y^2}{x+y} \right) \quad (36)$$

where $x = |P_t|^{1/2}$, and $y = |P_b|^{1/2}$. P_t and P_b are the cross-vent pressure differential at the top and bottom of the slab respectively and A_{slab} is the cross-sectional area of the slab. The value of the density, ρ , is taken from the source compartment.

A mixing phenomenon occurs at vents which is similar to entrainment in plumes. As hot gases from one compartment leave that compartment and flow into an adjacent compartment a door jet can exist which is analogous to a normal plume. Mixing of this type occurs for $\dot{m}_{13} > 0$ as shown in Figure 3-4. To calculate the entrainment (\dot{m}_{43} in this example), once again we use a plume description consistent with the work of McCaffrey, but with an extended point source. The estimate for the point source extension is given by Cetegen *et al.* [21]. This virtual point source is chosen so that the flow at the door opening would correspond to a plume with the heating for a equivalent doorway fire source (with respect to the lower layer) given by

$$Q_{f,eq} = c_p (T_l - T_4) \dot{m}_{13} \quad (37)$$

where $Q_{f,eq}$ is the heat release rate of the doorway fire. The concept of the virtual source is that the enthalpy flux from the virtual point source should equal the actual enthalpy flux in the door jet at the point of exit from the vent using the same prescription. Thus the entrainment is calculated the same way as was done for a normal plume. The reduced height of the plume, z_p , is [20]

where v_p , the virtual point source, is defined by inverting the entrainment process to yield

$$z_p = \frac{z_{13}}{Q_{eq}^{2/5}} + v_p \quad (38)$$

$$v_p = \left(\frac{90.9\dot{m}}{Q_{eq}} \right)^{1.76} \quad \text{if } 0.00 < v_p \leq 0.08$$

$$v_p = \left(\frac{38.5\dot{m}}{Q_{eq}} \right)^{1.001} \quad \text{if } 0.08 < v_p \leq 0.20$$

$$v_p = \left(\frac{8.10\dot{m}}{Q_{eq}} \right)^{0.528} \quad \text{if } 0.20 < v_p$$
(39)

Although outside of the normal range of validity of the plume model, a level of agreement with experiment is apparent (section 6 includes discussion of validation experiments for the plume model). Since a door jet forms a flat plume whereas a normal fire plume will be approximately circular, strong agreement is not expected.

The other type of mixing is much like an inverse plume and causes contamination of the lower layer. It occurs when there is flow of the type $\dot{m}_{42} > 0$. The shear flow causes vortex shedding into the lower layer and thus some of the particulates end up in the lower layer. The actual amount of mass or energy transferred is usually not large, but its effect can be large. For example, even minute amounts of carbon can change the radiative properties of the gas layer, from negligible to something finite. It changes the rate of radiation absorption significantly and invalidates the simplification of an ambient temperature lower layer. This term is predicated on the Kelvin-Helmholz flow instability and requires shear flow between two separate fluids. The mixing is enhanced for greater density differences between the two layers. However, the amount of mixing has never been well characterized. Quintiere *et al.* [28] discuss this phenomena for the case of crib fires in a single room, but their correlation does not yield good agreement with experimental data in the general case [29]. In the CFAST model, it is assumed that the incoming cold plume behaves like the inverse of the usual door jet between adjacent hot layers; thus we have a descending plume. It is possible that the entrainment is overestimated in this case, since buoyancy, which is the driving force, is not nearly as strong as for the usually upright plume.

3.4.3.2 Vertical Flow Through Horizontal Vents

Flow through a ceiling or floor vent can be somewhat more complicated than through door or window vents. The simplest form is uni-directional flow, driven solely by a pressure difference. This is analogous to flow in the horizontal direction driven by a piston effect of expanding gases. Once again, it can be calculated based on the Bernoulli equation, and presents little difficulty. However, in general we must deal with more complex situations that must be modeled in order to have a proper understanding of smoke movement. The first is an occurrence of puffing. When a fire exists in a compartment in which there is only one hole in the ceiling, the fire will burn until the oxygen has been depleted, pushing gas out the hole. Eventually the fire will die down. At

this point ambient air will rush back in, enable combustion to increase, and the process will be repeated. Combustion is thus tightly coupled to the flow. The other case is exchange flow which occurs when the fluid configuration across the vent is unstable (such as a hotter gas layer underneath a cooler gas layer). Both of these pressure regimes require a calculation of the onset of the flow reversal mechanism.

Normally a non-zero cross vent pressure difference tends to drive unidirectional flow from the higher to the lower pressure side. An unstable fluid density configuration occurs when the pressure alone would dictate stable stratification, but the fluid densities are reversed. That is, the hotter gas is underneath the cooler gas. Flow induced by such an unstable fluid density configuration tends to lead to bi-directional flow, with the fluid in the lower compartment rising into the upper compartment. This situation might arise in a real fire if the room of origin suddenly had a hole punched in the ceiling. No pretense is made of being able to do this instability calculation analytically. Cooper's algorithm [30] is used for computing mass flow through ceiling and floor vents. It is based on correlations to model the unsteady component of the flow. What is surprising is that we can find a correlation at all for such a complex phenomenon. There are two components to the flow. The first is a net flow dictated by a pressure difference. The second is an exchange flow based on the relative densities of the gases. The overall flow is given by [30]

$$\dot{m} = C f(\gamma, \varepsilon) \left(\frac{\Delta P}{\rho} \right)^{1/2} A_v \quad (40)$$

where $\gamma = c_p/c_v$ is the ratio of specific heats and

$$C = 0.68 + 0.17\varepsilon, \quad (41)$$

$$\varepsilon = \frac{\Delta P}{P}, \quad (42)$$

and f is a weak function of both γ and ε [30]. In the situation where we have an instability, we use Cooper's correlations for the function f . The resulting exchange flow is given by

$$\dot{m}_{ex} = 0.1 \left(\frac{g \Delta \rho A_v^{5/2}}{\rho_{av}} \right) \left(1.0 - \frac{2 A_v^2 \Delta P}{S^2 g \Delta \rho D^5} \right) \quad (43)$$

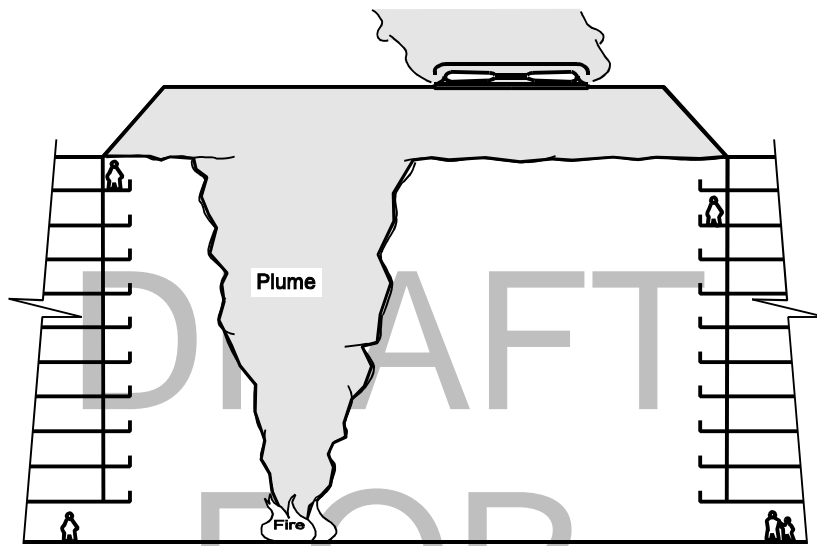
where

$$D = 2 \sqrt{\frac{A_v}{\pi}} \quad (44)$$

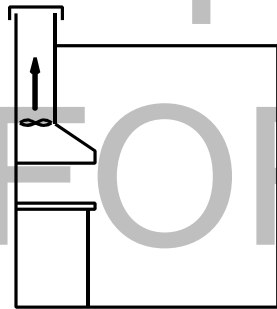
and S is 0.754 or 0.942 for round or square openings, respectively [30].

3.4.3.3 Forced Flow

Fan-duct systems are commonly used in buildings for heating, ventilation, air conditioning, pressurization, and exhaust. Figure 3-5(a) shows smoke management by an exhaust fan at the top of an atrium, and Figure 3-5(b) illustrates a kitchen exhaust. Cross ventilation, shown in Figure 3-5(c), is occasionally used without heating or cooling. Generally systems that maintain comfort conditions have either one or two fans. Residences often have a system with a single fan as shown in Figure 3-5 and 3-6(a). In this system return air from the living quarters is drawn in at one location, flows through filter, fan and coils, and is distributed back to the residence. This system does not have the capability of providing fresh outside air. These systems are intended for



(a) Atrium Smoke Management



(b) Kitchen Exhaust



(c) Space With Cross Ventilation

Figure 3-5 Some simple fan-duct systems.

applications where there is sufficient natural air leakage through cracks in walls and around windows and doors for odor control. Further information about these systems is presented in Klote and Milke [31] and the American Society of Heating, Refrigerating and Air Conditioning Engineers [32].

The model for mechanical ventilation used in CFAST is based on the theory of networks and is based on the model developed by Klote [33]. This is a simplified form of Kirchoff's law which says that flow into a node must be balanced by flow out of the node. Adapting Ohm's law,

$$\text{voltage} = \text{current} \times \text{resistance},$$

to HVAC flow, we have

pressure change = mass flow \times resistance

which can then be written equivalently

$$\text{mass flow} = \text{conductance} \times (\text{pressure drop across a resistance})^{1/2}.$$

For each node, this flow must sum to zero. There are several assumptions which are made in computing this flow in ducts, fans, elbow, etc. First, we assume unidirectional flow. Given the usual size of ducts, and the nominal presence of fans, this is quite reasonable. Also, the particular implementation used here [33] does not allow for reverse flow in the fans. The difficulty lies in describing how a fan behaves in such a case.

Each fan-duct system is represented as a network of nodes, each at a specific temperature and pressure. The

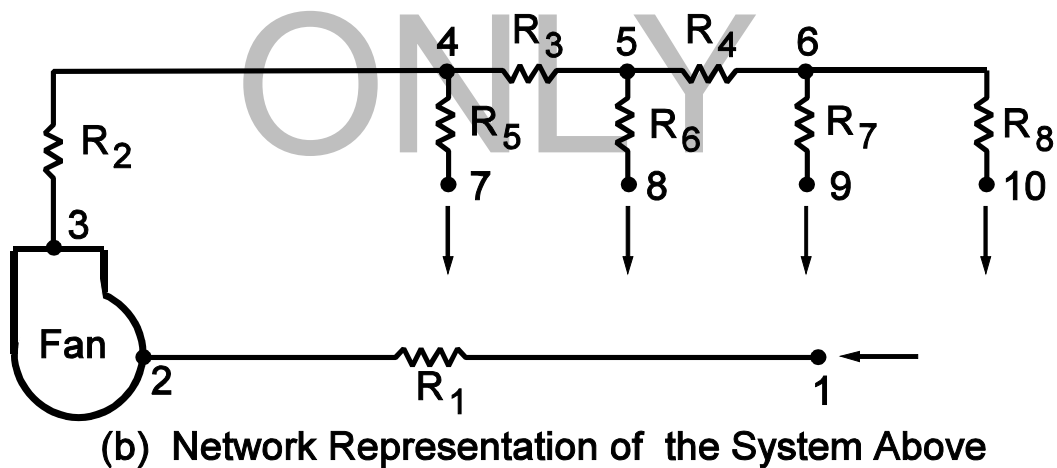
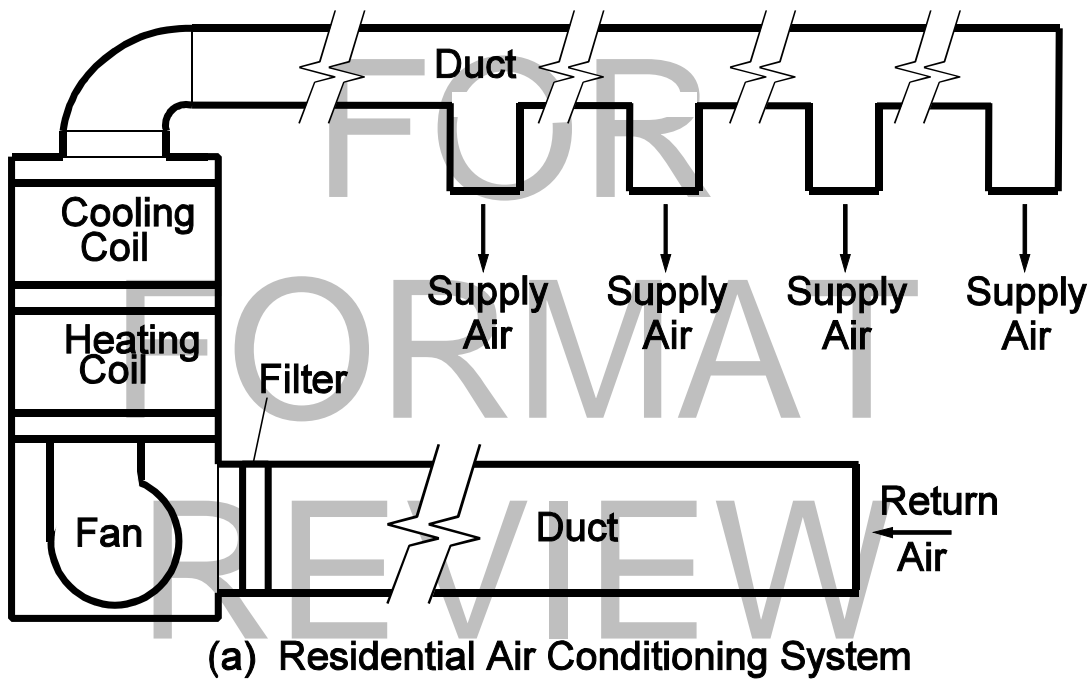


Figure 3-6 Network representation of a residential system

nodes may be connected by fans, ducts, fittings and other components. Except for fans, air flows through these components from nodes of higher pressure to nodes of lower pressure. For example, the residential system illustrated in 3-6(a) is represented in 3-6(b) as a network of a fan, eight resistances and ten nodes. These resistances incorporate all the resistance to flow between nodes. For instance, the equivalent resistance, R_1 , between nodes 1 and 2 accounts for resistances of the inlet, duct, filter and connection to the fan.

Given that we can describe mass flow in terms of pressure differences and conductance, the conservation equation for each node is

$$g_i(P_1, P_2, \dots) = \sum_j \dot{m}_{ij} = 0. \quad (45)$$

The index “ j ” is a summation over connections to a node, and there is an equation “ i ” for each node. The remaining problem is to specify the boundary conditions. At each connection to a compartment, the pressure is specified. Then, given that flow at each connection is unidirectional (at a given instant of time, the flow is either all into or all out of a given connection), the mass and enthalpy flow into or out of a room can be calculated explicitly. Thus we end up with a set of equations of the form

$$\begin{aligned} g_1(P_1, P_2, \dots) &= 0 \\ &\vdots \\ g_i(P_1, P_2, \dots) &= 0 \\ &\vdots \\ g_n(P_1, P_2, \dots) &= 0. \end{aligned} \quad (46)$$

This is an algebraic set of equations that is solved simultaneously with the equations for flow in the compartments.

The equations describe the relationship between the pressure drop across a duct, the resistance of a duct, and the mass flow. The pressure can be changed by conditions in a compartment, or a fan in line in the duct system. Resistance arises from the finite size of ducts, roughness on surfaces, bends and joints. To carry the electrical analog a little further, fans act like constant voltage sources. The analogy breaks down in this case because the pressure (voltage) is proportional to the square of the velocity (current) rather than linearly related as in the electrical case. Since we are using the current form of the conservation equation to balance the system, the flow can be recast in terms of a conductance

$$\dot{m} = G\sqrt{\Delta P}. \quad (47)$$

The conductance can be expressed generally as

$$G = \sqrt{\frac{2\rho}{C_0}} A_0 \quad (48)$$

where C_0 is the flow coefficient, and A_0 is the area of the inlet, outlet, duct, contraction or expansion joint, coil, damper, bend, filter, and so on. Their values for the most common of these items are tabulated in the ASHRAE Handbook [34].

The mechanical ventilation system is partitioned into one or more independent systems. Differential equations for species for each of these systems are derived by lumping all ducts in a system into one pseudo tank. This set of equations is then solved at each time step. Previously the mechanical ventilation computations in CFAST were performed as a side calculation using time splitting. This could cause problems since time-splitting methods require that the split phenomenon (the pressures and temperatures in this case) change slowly compared to other phenomenon such as room pressures, layer heights *etc.* The pressures at each internal node and the temperatures in each branch (duct, fan) are now determined explicitly by the solver, once again using conservation of mass and energy discussed in this section.

Ducts

Ducts are long pipes through which gases can flow. They have been studied much more extensively than other types of connections. For this reason, eq (48) can be put into a form which allows one to characterize the conductance in more detail, depending on the type of duct (e.g., oval, round, or square) and is given by

$$G = \sqrt{\frac{FL}{2\rho D_e A_0^2}}, \quad (49)$$

where F is the friction factor, L and D_e are the length and effective diameter of the duct respectively. The temperature for each duct d is determined using the following differential equation:

accumulated heat = (heat in - heat out) - convective losses through duct walls

$$V_d \frac{dT_d}{dt} = c_p m_d (T_{in} - T_{out}) - h_d A_d (T_d - T_{amb}) \quad (50)$$

where c_v , c_p are the constant volume/pressure specific heats; V_d is the duct volume, ρ_d is the duct gas density, dT_d/dt is the time rate of change of the duct gas temperature, m_d is the mass flow rate, T_{in} and T_{out} are the gas temperatures going into and out of the duct, h_d , A_d are the convective heat transfer coefficient and surface area for duct d and T_{amb} is the ambient temperature. The first term on the right hand side of eq (50) represents the net gain of energy due to gas transported into or out of the duct. The second term represents heat transferred to the duct walls due to convection. Heat loss through the duct walls is assumed to be zero. The differential and algebraic (DAE) solver used by CFAST solves eq (50) exactly as written. A normal ordinary differential equation solver would require that this equation be solved for dT/dt . By writing it this way, the duct volumes can be zero which is the case for fans.

Fans

This section provides background information about fan performance. For more information about fans, readers are referred to Jorgensen [35] and ASHRAE [32]. Normal fan operating range is represented by the line segment AB in Figure 3-7. In this figure, ΔP_f is the static pressure of the fan, and \dot{V}_f is the volumetric flow of the fan. The point B represents a margin of safety selected by the fan manufacturer in order to avoid unstable flow.

Fans operating in the positively sloping portion (CD of Figure 3-7) of the fan curve exhibit unstable behavior called surging or pulsing. Unstable flow consists of violent flow reversals accompanied by significant changes in pressure, power and noise. There is little information about how long a fan can operate in the unstable region before it is destroyed.

Backward flow through a fan occurs when the static pressure is greater than that at point D . This is also called second quadrant flow. Quadrant terminology is customarily used in description of fan performance. The horizontal axis and the vertical axis divide a plane into four quadrants which for convenience are labeled Q I, Q II, Q III and Q IV on Figure 3-7. Backward flow can be exhibited by all types of fans. The wind blowing into the outlet of a propeller fan can result in backflow, and pressures produced by fires could also produce backflow. Fourth quadrant flow is probably representative of all fans. As Δp_f becomes negative, the flow increases with decreasing Δp_f until a choking condition develops at point E .

It is common practice in the engineering community and fan industry to represent fan performance with Δp_f on the vertical axis and \dot{V}_f on the horizontal axis. Probably the reason is that \dot{V}_f can be thought of as a single valued function of Δp_f for flow in the first and second quadrants. Fan manufacturers generally supply flow-pressure data for the normal operating range, and they often supply data for the rest of the fan curve in the first quadrant. Specific data is not available for either second or fourth quadrant flow. No approach has been developed for simulation of unstable fan operation, and numerical modeling of unstable flow would be a complicated effort requiring research.

Numerical Approximation of Fan Performance: Figure 3-8 illustrates four approaches that can be used to approximate fan performance without simulation of unstable flow. For all of these approaches, the fan curve is used for the normal operating range of AB . Also for all of the approaches, flows above the normal operating range are approximated by a straight line tangent to the fan curve at point A . This results in fourth quadrant flow that is similar to the expected flow provided that Δp_f is not overly far below the horizontal axis. In Figure 3-

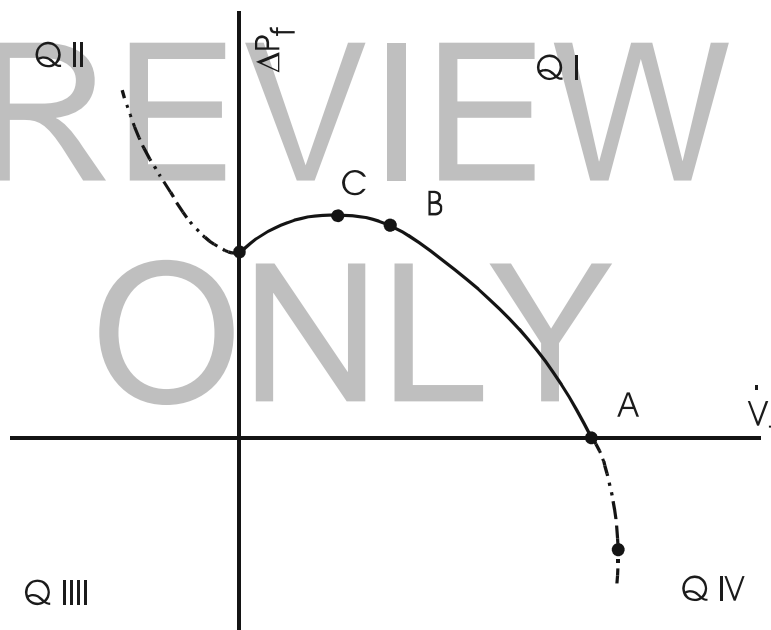


Figure 3-7 Typical fan performance at constant speed.

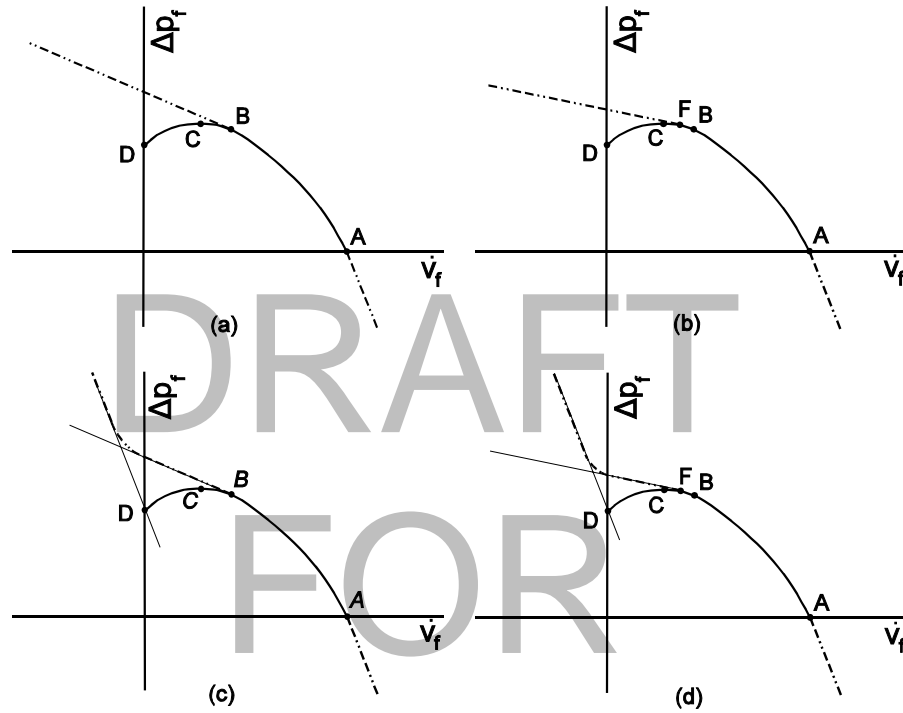


Figure 3-8 Some approaches to approximation of fan performance for computer simulation

8(a), flows below the normal range are approximated by a linear curve tangent to the fan curve at point *B*. This avoids simulation of unstable flows, but the approximated flow is higher than expected in the first quadrant and lower than expected for much of the fourth quadrant.

The approach of Figure 3-8(b) reduces the approximated flow in the first quadrant. In this approach, the fan curve is also used for the range *BF*, and flows above the normal operating range are approximated by a straight line tangent to the fan curve at point *F*. To increase the flow in the second quadrant, Figure 3-8(c) uses a line passing through point *D* with the slope of the fan curve at point *A*. Both of the modifications of Figure 3-8(b) and Figure 3-8(c) are combined in the approach of Figure 3-8(d).

Fan manufacturer data is routinely either in tabular or graphical form. As indicated by Jorgensen [35], the use of a polynomial form of fan curve is common within the industry.

$$\dot{V}_f = B_1 + B_2 \Delta p_f + B_3 (\Delta p_f)^2 + \dots + B_n (\Delta p_f)^{n-1} \quad (51)$$

The units for \dot{V}_f and Δp_f in CFAST are m^3/s and Pa respectively. Therefore the units for the coefficients B_i ($i=1, \dots, 5$) are $\text{m}^3/(\text{s Pa}^i)$. The coefficients can be entered as data or calculated by least squares regression from flow and pressure data. For constant volumetric flow applications, the only non-zero coefficient in eq (51) is B_1 .

($n = 1$). For incompressible fluids, eq (51) is independent of temperature and pressure. For fan data at 20 °C, compressibility effects amount to an error of about 6 % at a temperature of 200 °C.

DRAFT
FOR
FORMAT
REVIEW
ONLY

Effective Resistance: The resistance, R , of a flow element can be defined as

$$R = \frac{\sqrt{\Delta p}}{\dot{m}} \quad (52)$$

where Δp is the pressure loss through the element corresponding to a mass flow rate, \dot{m} . The effective resistance between two nodes is always positive, however, sometimes one of the resistances between nodes can be negative as will be explained later. To account for this, $R = K'^{1/2}$ can be substituted into eq (52) to give

$$\Delta p = K \dot{m}^2 \quad (53)$$

The total pressure loss, Δp_t , from one node to the next is the sum of the losses, Δp_i , through each flow element, i , between the nodes.

$$\Delta p_t = \sum_i \Delta p_i \quad (54)$$

The effective value, K_e , relates the total pressure loss to the mass flow rate as $\Delta p_t = K_e \dot{m}^2$, and K_i relates the pressure loss through element i as $\Delta p_i = K_i \dot{m}^2$. These pressure losses can be substituted into eq (54), and canceling like terms yields

$$K_e = \sum_i K_i \quad (55)$$

Values of K_i can be calculated for each element using equations developed later, and K_e can be calculated by eq (55).

Resistance of Ducts: For a straight section of duct with constant cross sectional area, the Bernoulli equation incorporating pressure loss, Δp_{fr} , due to friction is commonly written

$$p_1 - p_2 = \Delta p_{fr} + \rho g(Z_1 - Z_2) \quad (56)$$

where the subscripts 1 and 2 refer to the duct inlet and outlet respectively, p is pressure, Z is elevation, g is the acceleration due to gravity, and ρ is the density of the gas. The pressure loss due to friction is expressed by the Darcy equation in most elementary treatments of flow in pipes and ducts [34], [36], [37].

$$\Delta p_{fr} = f \frac{L}{D_e} \frac{\rho U^2}{2} \quad (57)$$

where f is the friction factor, L is the duct length, D_e is the effective diameter of the duct and U is the average velocity in the duct ($\dot{m} = \rho UA$ where A is the cross-sectional area of the duct). For a circular duct, the effective diameter is the duct diameter. For rectangular duct, Huebscher [38] developed the relationship

$$D_e = 1.30 \frac{(ab)^{0.625}}{(a + b)^{0.250}} \quad (58)$$

where a is the length of one side of the duct, and b is the length of the adjacent side. For flat oval duct, Heyt and Diaz [39] developed the relationship

$$D_e = \frac{1.55A^{0.625}}{P^{0.200}} \quad (59)$$

where A and P are the cross-sectional area and the perimeter of the flat oval duct. The area of a flat oval duct is

$$A = (\pi b^2/4) + b(a - b) \quad (60)$$

and the perimeter of a flat oval duct is

$$P = \pi b + 2(a - b) \quad (61)$$

where a is the major dimension of the flat oval duct, and b is the minor dimension of the duct. Combining eqs 52 and 56 results in

$$\dot{m}_{ij} = \frac{1}{R} \sqrt{p_j - p_i + \rho g(Z_j - Z_i)} \quad (62)$$

Combining eqs 53 and 57 results in

$$K = \frac{fL}{2D_e \rho A^2} \quad (63)$$

where A is the cross sectional area of the duct. Colebrook developed the following equation for the friction factor [40].

$$\frac{1}{\sqrt{f}} = -2 \text{Log}_{10} \left(\frac{\varepsilon}{3.7 D_e} + \frac{2.51}{R_e \sqrt{f}} \right) \quad (64)$$

where R_e is the Reynolds number (UD_e/ν where ν is the kinematic viscosity) and ϵ is the roughness of the inside surface of the duct. Data on roughness of duct materials are listed in Table 3. A graphical presentation of the Colebrook equation developed by Moody [41] was used for decades to calculate friction factors. However, today it is practical to solve the Colebrook equation with computers.

Table 3-3: Absolute roughness values for common duct materials

Duct Material	Roughness Category	Absolute Roughness, ϵ	
		mm	ft
Uncoated Carbon Steel, Clean. PVC Plastic Pipe. Aluminum.	Smooth	0.03	0.0001
Galvanized Steel, Longitudinal Seams, 1200 mm Joints. Galvanized Steel, Continuously Rolled, Spiral Seams, 3000 mm Joints. Galvanized Steel, Spiral Seam with 1, 2 and 3 Ribs, 3600 mm Joints.	Medium Smooth	0.09	0.0003
Galvanized Steel, Longitudinal Seams, 760 mm Joints.	Average	0.15	0.0005
Fibrous Glass Duct, Rigid. Fibrous Glass Duct Liner, Air Side With Facing Material.	Medium Rough	0.9	0.003
Fibrous Glass Duct Liner, Air Side Spray Coated. Flexible Duct, Metallic. Flexible Duct, All Types of Fabric and Wire. Concrete.	Rough	3.0	0.01

Local Loss Resistances: The pressure loss, Δp , through many other elements can be expressed as

$$\Delta p = C_o \frac{\rho U_o^2}{2} \quad (65)$$

where U_o is the average velocity at cross section o within the element, and C_o is a local loss coefficient. This equation is commonly used for inlets, outlets, duct contractions and expansions, heating and cooling coils, dampers, bends and many filters. For a large number of these elements, values of C_o have been empirically determined and are tabulated frequently as functions of geometry in handbooks [32],[42]. Manufacturers' literature also contains some values of C_o . The value of K for these resistances is

$$K = \frac{C_o}{2\rho A_o^2} \quad (66)$$

where A_o is the area at cross section o .

3.4.4 Corridor Flow

A standard assumption in zone fire modeling is that once hot smoke enters a compartment, a well defined upper layer forms instantly throughout the compartment. This assumption breaks down in large compartments and long corridors due to the time required to fill these spaces. A simple procedure is described for accounting

for the formation delay of an upper layer in a long corridor by using correlations developed from numerical experiments generated with the NIST fire model Large Eddy Simulation Model (LES) [43], which is now the Fire Dynamic Simulation Model (FDS) [44]. FDS is a computational fluid dynamics model capable of simulating fire flow velocities and temperatures with high (~0.1 m) resolution. Two parameters related to corridor flow are then estimated: the time required for a ceiling jet to travel in a corridor and the temperature distribution down the corridor. These estimates are then used in CFAST by delaying flow into compartments connected to corridors until the ceiling jet has passed these compartments.

FDS was used to estimate ceiling jet characteristics by running a number of cases for various inlet layer depths and temperatures. The vent flow algorithm in CFAST then uses this information to compute mass and enthalpy flow between the corridor and adjacent compartments. This is accomplished by presenting the vent algorithm with a one layer environment (the lower layer) before the ceiling jet reaches the vent and a two layer environment afterwards. Estimated ceiling jet temperatures and depths are used to define upper layer properties.

The problem is to estimate the ceiling jet temperature and depth as a function of time until it reaches the end of the corridor. The approach used here is to run a field model as a pre-processing step and to summarize the results as correlations describing the ceiling jet's temperatures and velocities. The steps used in this process are as follows:

1. Model corridor flow for a range of inlet ceiling jet temperatures and depths. Inlet velocities are derived from the inlet temperatures and depths.
2. For each model run calculate average ceiling jet temperature and velocity as a function of distance down the corridor.
3. Correlate the temperature and velocity distribution down the hall.

The zone fire model then uses these correlations to estimate conditions in the corridor as follows:

1. Estimate the inlet temperature, depth and velocity of the ceiling jet. If the corridor is the fire room then use a standard correlation. If the source of the ceiling jet is another room then calculate the inlet ceiling jet flow using Bernoulli's law for the vent connecting the source room and the corridor.
2. Use correlations in 3. above to estimate the ceiling jet arrival time at each vent.
3. For each vent in the corridor use lower layer properties to compute vent flow before the ceiling jet arrives at the vent and lower/upper layer properties afterwards.

Assumptions: The assumptions made in order to develop the correlations are:

- The time scale of interest is the time required for a ceiling jet to traverse the length of the corridor. For example, for a 100 m corridor with 1 m/s flow, the characteristic time would be 100 s.
- Cooling of the ceiling jet due to mixing with adjacent cool air is large compared to cooling due to heat loss to walls. Equivalently, we assume that walls are adiabatic. This assumption is conservative. An adiabatic corridor model predicts more severe conditions downstream in a corridor than a model that accounts for heat transfer to walls, since cooler ceiling jets travel slower and not as far.

- We do not account for the fact that ceiling jets that are sufficiently cooled will stagnate. Similar to the previous assumption, this assumption is conservative and results in over predictions of conditions in compartments connected to corridors (since the model predicts that a ceiling jet may arrive at a compartment when in fact it may have stagnated before reaching it).
- Ceiling jet flow is buoyancy driven and behaves like a gravity current. The inlet velocity of the ceiling jet is related to its temperature and depth.
- Ceiling jet flow lost to compartments adjacent to the corridor is not considered when estimating ceiling jet temperatures and depths. Similarly, a ceiling jet in a corridor is assumed to have only one source.
- The temperature and velocity at the corridor inlet is constant in time.
- The corridor height and width do not effect a ceiling jet's characteristics. Two ceiling jets with the same inlet temperature, depth and velocity behave the same when flowing in corridors with different widths or heights as long as the ratio of inlet widths to corridor width are equal.
- Flow entering the corridor enters at or near the ceiling. The inlet ceiling jet velocity is reduced from the vent inlet velocity by a factor of w_{vent}/w_{room} where w_{vent} and w_{room} are the width of the vent and room, respectively.

Corridor Jet Flow Characteristics: Ceiling jet flow in a corridor can be characterized as a one dimensional gravity current. To a first approximation, the velocity of the current depends on the difference between the density of the gas located at the leading edge of the current and the gas in the adjacent ambient air. The velocity also depends on the depth of the current below the ceiling. A simple formula for the gravity current velocity may be derived by equating the potential energy of the current, $mgd_0/2$, measured at the half-height $d_0/2$ with its kinetic energy, $mV^2/2$ to obtain

$$V = \sqrt{gd_0} \quad (67)$$

where m is mass, g is the acceleration of gravity, d_0 is the height of the gravity current and U is the velocity. When the density difference, between the current and the ambient fluid is small, the velocity, V , is proportional to $\sqrt{gd_0\Delta\rho/\rho_{cj}} = \sqrt{gd_0\Delta T/T_{amb}}$ where ρ_{amb} and T_{amb} are the ambient density and temperature and ρ_{cj} and T_{cj} are the density and temperature of the ceiling jet and $\Delta T = T_{cj} - T_{amb}$ is the temperature difference. Here use has been made of the ideal gas law, $\rho_{amb}T_{amb} \approx \rho_{cj}T_{cj}$. This can be shown using an integrated form of Bernoulli's law noting that the pressure drop at the bottom of the ceiling jet is $P_b = 0$, the pressure drop at the top is $P_t = gd_0(\rho_{cj} - \rho_{amb})$ and using a vent coefficient c_{vent} of 0.74, to obtain

$$\begin{aligned}
V_0 &= c_{vent} \frac{\sqrt{8}}{3} \frac{1}{\sqrt{\rho_{cj}}} \frac{P_t + \sqrt{P_t P_b} + P_b}{\sqrt{P_t} + \sqrt{P_b}} \\
&= c_{vent} \frac{\sqrt{8}}{3} \sqrt{P_t / \rho_{cj}} \\
&= c_{vent} \frac{\sqrt{8}}{3} \sqrt{g d_0 \frac{\rho_{amb} - \rho_{cj}}{\rho_{cj}}} \\
&\approx 0.7 \sqrt{g d_0 \frac{\Delta T}{T_{amb}}}
\end{aligned}$$

(70)

Formulas of the form of the above equation lead one to conclude that a ceiling jet's characteristics in a corridor depend on its depth, d_0 , and relative temperature difference, $\Delta T/T_{amb}$. Therefore, as the jet cools, it slows down. If no heat transfer occurs between the ceiling jet and the surrounding walls, then the only mechanism for cooling is mixing with surrounding cool air.

Twenty numerical experiments were performed using FDS in order to better understand the effects of the inlet ceiling jet temperature and depth on ceiling jet characteristics downstream in a corridor. These cases were run with five different inlet depths and four different inlet temperatures. The inlet ceiling jet temperature rise, ΔT_0 , and depth, d_0 , were used to define an inlet velocity, U_0 using eq(70). The inlet ceiling jet depths, d_0 , used in the parameter study are 0.15 m, 0.30 m, 0.45 m, 0.60 m and 0.75 m. The inlet ceiling jet temperature rises, T_0 , used in the parameter study are 100 °C, 200 °C, 300 °C and 400 °C.

Correlations: Ceiling jet functions were plotted as a function of distance down a corridor for each of the twenty test cases. These results are shown in Figure 12. Note that all but the 0.15 m ceiling jet data lies on essentially the same line.

The best fit line is given in the form of

$$\log \frac{\Delta T}{\Delta T_0} = a + bx.$$

(72)

This is equivalent to

$$\frac{\Delta T}{\Delta T_0} = C_1 10^{bx} = C_1 \left(\frac{1}{2}\right)^{x/h_{1/2}} \quad (73)$$

where $C_1 = 10^a$ and $h_{1/2} = -\log(2)/b$. The parameter $h_{1/2}$ has a physical interpretation. It is the distance down the corridor where the temperature rise T , falls off to 50 per cent of its original value or equivalently, $T(x + h_{1/2}) = T(x)/2$.

The half-distance, $h_{1/2}$, can be approximated by $h_{1/2} = \log(2)/0.018 = 16.7$ m where $b = -0.018$ is given in Figure 12. Similarly, the coefficients C_1 is approximated by $C_1 = 10^a = 10^{-0.003} \approx 1$ where a can be determined from Figure 12. Therefore the temperature rise, ΔT , may be approximated by

$$\Delta T = \Delta T_0 \left(\frac{1}{2}\right)^{\frac{x}{16.7}} \quad (74)$$

The numerical experiments with FDS [44] demonstrated that for the cases simulated, ceiling jet characteristics depend on the relative inlet temperature rise and not the inlet depth. Flow in long corridors (greater than 10 m) need to be better characterized due to the flow stagnation which may occur because of the ceiling jet's temperature decay.

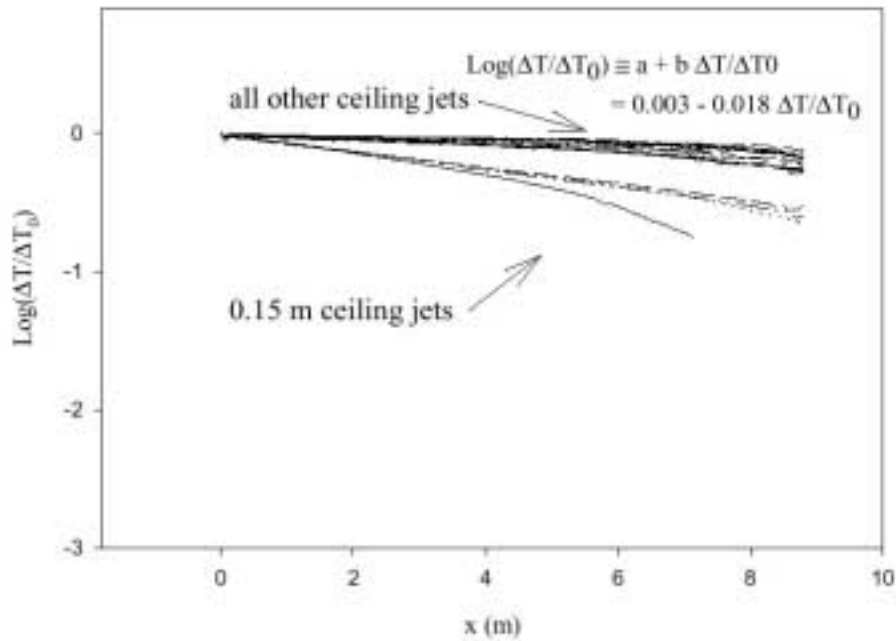


Figure3-9. Log_{10} of the relative temperature excess downstream in a corridor using an adiabatic temperature boundary condition for several inlet depths and inlet temperature boundary condition. The inlet velocity, V_0 , is given by equation (70).

3.4.5 Heat Transfer

This section discusses radiation, convection and conduction, the three mechanisms by which heat is transferred between the gas layers and the enclosing compartment walls. This section also discusses heat transfer algorithms for calculating target temperatures.

Gas layers exchange energy with their surroundings via convective and radiative heat transfer. Different material properties can be used for the ceiling, floor, and walls of each compartment (although all the walls of a compartment must be the same). Additionally, CFAST allows each surface to be composed of up to three distinct materials. This allows the user to deal naturally with the actual building construction. Material thermophysical properties are *assumed* to be constant, although we know that they actually vary with temperature. The user should also recognize that the mechanical properties of some materials may change with temperature, but these effects are not modeled.

Radiative transfer occurs among the fire(s), gas layers and compartment surfaces (ceiling, walls and floor). This transfer is a function of the temperature differences and the emissivity of the gas layers as well as the compartment surfaces. Typical surface emissivity values only vary over a small range. For the gas layers, however, the emissivity is a function of the concentration of species which are strong radiators, predominately smoke particulates, carbon dioxide, and water. Thus errors in the species concentrations can give rise to errors in the distribution of enthalpy among the layers, which results in errors in temperatures, resulting in errors in the flows. This illustrates just how tightly coupled the predictions made by CFAST can be.

3.4.5.1 Radiation

Radiation heat transfer forms a significant portion of the energy balance in a zone fire model, especially in the fire room. Radiative heat transfer is computed from wall and gas temperatures, emissivities and fire heat release rates. To calculate the radiation absorbed in a zone, a heat balance must be done accounting for all surfaces that radiate to and absorb radiation from a zone.

A radiation heat transfer calculation can easily dominate the computational requirements of any fire model. Approximations are then required to perform these calculations in a time consistent with other zone fire model sources terms. For example, it is assumed that all zones and surfaces radiate and absorb like a gray body, that the fires radiate as point sources and that the plume does not radiate at all. Radiative heat transfer is approximated using a limited number of radiating wall surfaces, four in the fire room and two everywhere else. The use of these and other approximations allows CFAST to perform the radiation computation in a reasonably efficient manner [45].

Modeling Assumptions: The following assumptions are made in order to simplify the radiation heat exchange model used in CFAST and to make its calculation tractable.

Iso-thermal - Each gas layer and each wall segment is assumed to be at a uniform temperature.

Equilibrium - The wall segments and gas layers are assumed to be in a quasi-steady state. In other words, the wall and gas layer temperatures are assumed to change slowly over the duration of the time step of the associated differential equation.

Point Source Fires - The fire is assumed to radiate uniformly in all directions giving off a fraction, χ_R , of the total energy release rate. This radiation is assumed to originate from a single point. Radiation feedback to the fire and radiation from the plume is not modeled in the radiation exchange algorithm.

Diffuse and gray surfaces - The radiation emitted is assumed to be diffuse and gray. In other words, the radiant fluxes emitted are independent of direction and wavelength. These assumptions allow us to infer that the emittance, ϵ , absorptance, α and reflectance, ρ , are related via $\epsilon=\alpha=1-\rho$.

Geometry - Rooms or compartments are assumed to be rectangular boxes. Each wall is either perpendicular or parallel to every other wall. Radiation transfer through vent openings, doors *etc.* is lost from the room.

4-Wall and 2-Wall Radiation Exchange: When computing wall temperatures, CFAST partitions a compartment into four parts; the ceiling, the floor, the wall segments above the layer interface and the wall segments below the layer interface. The radiation algorithm then computes a heat flux striking each wall segment using the surface temperature and emissivity.

The four wall algorithm used in CFAST for computing radiative heat exchange is based upon the equations developed in Siegel and Howell [46] which in turn is based on the work of Hottel [47]. Siegel and Howell model an enclosure with N wall segments and a homogeneous gas. A radiation algorithm for a two layer zone fire model requires treatment of an enclosure with two uniform gases. Hottel and Cohen [48] developed a method where the enclosure is divided into a number of wall and gas volume elements. An energy balance is written for each element. Each balance includes interactions with all other elements. Treatment of the fire and the interaction of the fire and gas layers with the walls is based upon the work of Yamada and Cooper [49]. They model fires as point heat sources radiating uniformly in all directions and use the Lambert-Beer law to model the interaction between heat emitting elements (fires, walls, gas layers) and the gas layers. By implementing a four wall rather than an N wall model, significant algorithmic speed increases are achieved. This is done by exploiting the simple structure and symmetry of the four wall problem.

The nomenclature used in this section follows that of Siegel and Howell [46]. The radiation exchange at the k'th surface is shown schematically in Figure 3-10. For each wall segment k from 1 to N, a net heat flux, $\Delta q_k''$, must be found such that the energy balance,

$$\sigma A_k \epsilon_k T_k^4 + (1 - \epsilon_k) q_k^{in} = q_k^{in} + A_k \Delta q_k'' \quad (75)$$

at each wall segment k is satisfied, where σ is the Stefan-Boltzman constant, A_k is the area of the k'th wall segment, ϵ_k is the emissivity of the k'th wall segment, T_k is the temperature of the k'th wall segment and q_k^{in} is the energy arriving at the k'th wall segment from all other wall segments and heat sources.

Radiation exchange at each wall segment considers the emitted, reflected, incoming and net radiation terms. The unknown net radiative fluxes, $\Delta q_k''$, are found by solving the modified net radiation equation

$$\Delta \hat{q}_k'' - \sum_{j=1}^N (1-\varepsilon_j) \Delta \hat{q}_j'' F_{k-j} \tau_{j-k} = \sigma T_k^4 - \sum_{j=1}^N \sigma T_j^4 F_{k-j} \tau_{j-k} - \frac{c_k}{A_k}, \quad (76)$$

where $\Delta \hat{q}_k = \Delta q_k / \varepsilon_k$, F_{k-j} is the configuration factor, τ is the transmittance and other terms are defined previously. The parameters c_k represent the various sources of heat, namely the fire itself and the gas layers.

The walls can be modeled using two surfaces or four. The four wall model is necessary for fire rooms because the temperatures of the ceiling and upper walls differ significantly. The two wall model is used for compartments that contain no fires.

To simplify the comparison between the two and four wall segment models, assume that the emissivities of all wall segments are one and that the gas absorptivities are zero. Let the room dimensions be 4 m x 4 m x 4 m, the temperature of the floor and the lower and upper walls be 300 K, and the ceiling temperature vary from 300 K to 600 K. Figure 3-11 shows a plot of the heat flux to the ceiling and upper wall as a function of the ceiling temperature [45], [50]. The two wall model predicts that the extended ceiling (a surface formed by combining the ceiling and upper wall into one wall segment) cools, while the four wall model predicts that the ceiling cools and the upper wall warms. The four-wall model moderates temperature differences that may exist between the ceiling and upper wall (or floor and lower wall) by allowing heat transfer to occur between the ceiling and upper wall. This problem does not arise when a fire is not present.

Reference [45] documents how to minimize the work required to compute the 16 configuration factors, F_{k-j} , required in a 4 wall model.

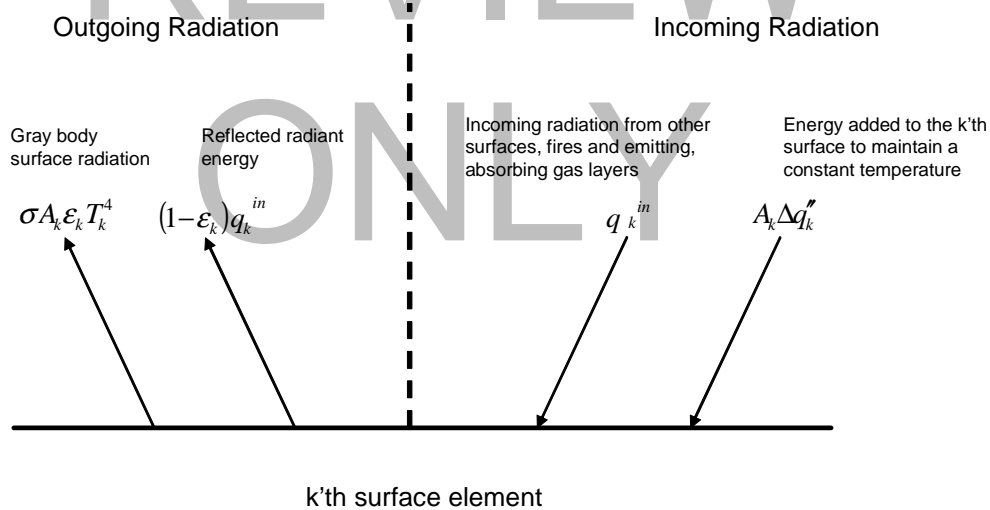


Figure 3-10. Radiation exchange in a two-zone fire model.

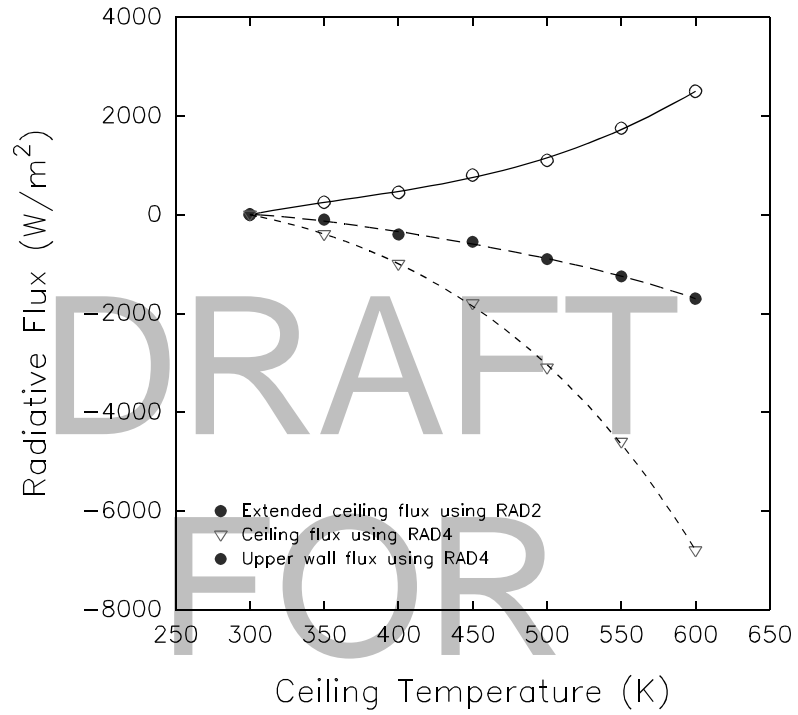


Figure 3-11. An example of the calculated two-wall (RAD2) and four-wall (RAD4) contributions to radiation exchange on a ceiling and wall surface.

DRAFT
 FOR
 REVIEW
 ONLY

Configuration Factors: A configuration factor between two finite areas denoted F_{1-2} is the fraction of radiant energy given off by surface 1 that is intercepted by surface 2 and is given by

$$F_{1-2} = \frac{1}{A_1} \int_{A_1} \int_{A_2} \frac{\cos(\theta_1) \cdot \cos(\theta_2)}{\pi L^2} dA_1 dA_2 \quad (77)$$

where L is the distance along the line of integration, θ_1 and θ_2 are the angles for surface 1 and 2 between the respective normal vectors and the line of integration, and A_1 and A_2 are the areas of the two surfaces. These terms are illustrated in Figure 3-12. When the surfaces A_1 and A_2 are far apart relative to their surface area, eq (77) can be approximated by assuming that θ_1 , θ_2 and L are constant over the region of integration to obtain

$$F_{1-2} \approx \frac{\cos(\theta_1) \cos(\theta_2)}{\pi L^2} A_2 \quad (78)$$

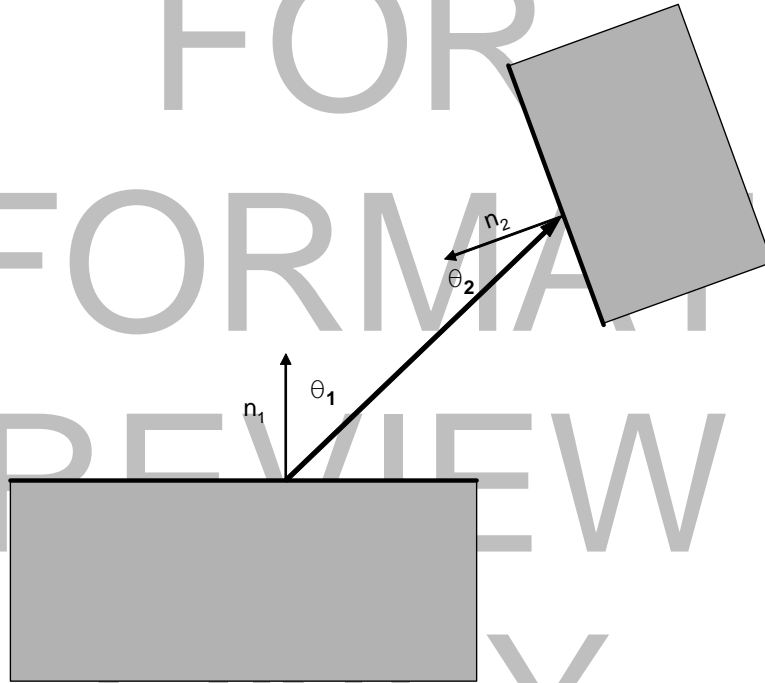


Figure 3-12. Setup for a configuration factor calculation between two arbitrarily oriented finite areas

Transmittance and Absorptance: The transmittance of a gas volume is the fraction of radiant energy that will pass through it unimpeded and is given by

$$\tau(L) = e^{-aL} \quad (79)$$

where a is the absorption coefficient of the gas volume and L is a characteristic path length.

The absorptance, α , of a gas volume is the fraction of radiant energy absorbed by that volume. For a gray gas, $\alpha + \tau = 1$.

Calculating absorption for broad band gas layer radiation: In general, the transmittance and absorptance are a function of wavelength. This is an important factor to consider for the major gaseous products (CO_2 and H_2O); however soot has a continuous absorption spectrum which allows the transmittance and absorptance to be approximated as “gray” [46] across the entire spectrum.

The gas absorptance, α_G , is due to the combination of the CO_2 and H_2O and is given by

$$\alpha_G = \alpha_{\text{H}_2\text{O}} + \alpha_{\text{CO}_2} - C \quad (80)$$

where C is a correction for band overlap. For typical fire conditions, the overlap amounts to about half of the CO_2 absorptance [51] so the gas transmittance is approximated by

$$\tau_G = 1 - \alpha_{\text{H}_2\text{O}} - 0.5\alpha_{\text{CO}_2} \quad (81)$$

The total transmittance of a gas-soot mixture is the product of the gas and soot transmittances

$$\tau_T = \tau_S \tau_G \quad (82)$$

Substitution of eqs. (79) and (81) into eq. (82) yields

$$\tau_T = e^{-aL} [1 - \alpha_{\text{H}_2\text{O}} - 0.5\alpha_{\text{CO}_2}] \quad (83)$$

In the optically thin limit the absorption coefficient, a , may be replaced by the Planck mean absorption coefficient and in the optically thick limit, it may be replaced by the Rosseland mean absorption coefficient. For the entire range of optical thicknesses, Tien *et al.* [51] report that a reasonable approximation is

$$a = k f_v T \quad (84)$$

where k is a constant which depends on the optical properties of the soot particles, f_v is the soot volume fraction and T is the soot temperature in Kelvin. Values of a , have been found to be about constant for a wide range of fuels [52]. The soot volume fraction, f_v , is calculated from the soot mass, soot density and layer volume. The soot is assumed to be in thermal equilibrium with the gas layer.

Edwards' absorptance data for H_2O and CO_2 are reported [53] as $\log(\text{emissivity})$ versus $\log(\text{pressure-pathlength})$, with $\log(\text{gas concentration})$ as a parameter. For each gas, these data were incorporated into a look-up table, implemented as a two-dimensional array of $\log(\text{emissivity})$ values, with indices based on

temperature and gas concentration. It is assumed that absorptance and emittance are equivalent for the gaseous species as well as for soot.

An effective path length (mean beam length, L) treats an emitting volume as if it were a hemisphere of a radius such that the flux impinging on the center of the circular base is equal to the average boundary flux produced by the real volume. The value of this radius is approximated as [51],[54]

$$L = c \sqrt[4]{V / A} \quad (85)$$

where L is the mean beam length in meters, c is a constant (approximately 0.9, for typical geometries), V is the emitting gas volume (m^3) and A is the surface area (m^2) of the gas volume. The volume and surface area are calculated from the dimensions of the layer.

For each gas, the $\log(\text{absorptance})$ is estimated from the look-up table for that gas by interpolating both the $\log(\text{temperature})$ and $\log(\text{concentration})$ domains. In the event that the required absorptance lies outside the temperature or concentration range of the look-up table, the nearest acceptable value is returned. Error flags are also returned, indicating whether each parameter was in or out of range and, in the latter case, whether it was high or low. This entire process is carried out for both CO_2 and H_2O .

3.4.5.2 Computing Target Heat Flux and Temperature

The calculation of the radiative heat flux to a target is similar to the radiative heat transfer calculation discussed previously. The main difference is that CFAST does not compute feedback from the target to the wall surfaces or gas layers. The target is simply a probe or sensor not interacting with the modeled environment.

The net flux striking a target can be used as a boundary condition in order to compute the temperature of the target. If the target is thin, then its temperature quickly rises to a level where the heat flux to and from the target are in equilibrium.

There are four components of heat flux to a target: fires, walls (including the ceiling and floor), gas layer radiation and gas layer convection.

Heat Flux from a Fire to a Target: Figure 3-13 illustrates terms used to compute heat flux from a fire to a target. Let n_t be a unit vector perpendicular to the target and θ_t be the angle between the vectors $-\bar{L}$ and n_t .

Using the definition that $q_{f,r}$ is the radiative portion of the energy release rate of the fire, then the heat flux on a sphere of radius L due to this fire is $q_{f,r} / (4\pi L^2)$. Correcting for the orientation of the target and accounting for heat transfer through the gas layers, the heat flux to the target is

$$q_{f,t}'' = \frac{q_{f,r}}{4\pi L^2} \cos(\theta_t) \tau_U(L_U) \tau_L(L_L) = -q_{f,r} \frac{n_t \cdot \bar{L}}{4\pi L^3} \tau_U(L_U) \tau_L(L_L) \quad (86)$$

Radiative Heat Flux from a Wall Segment to a Target: Figure 3-14 illustrates terms used to compute heat flux from a wall segment to a target. The flux, $q''_{w,t}$ from a wall segment to a target can then be computed using

$$q_{w,t}'' = \frac{A_w q_{w,out}'' F_{w-t}}{A_t} \tau_U(L_U) \tau_L(L_L) \quad (87)$$

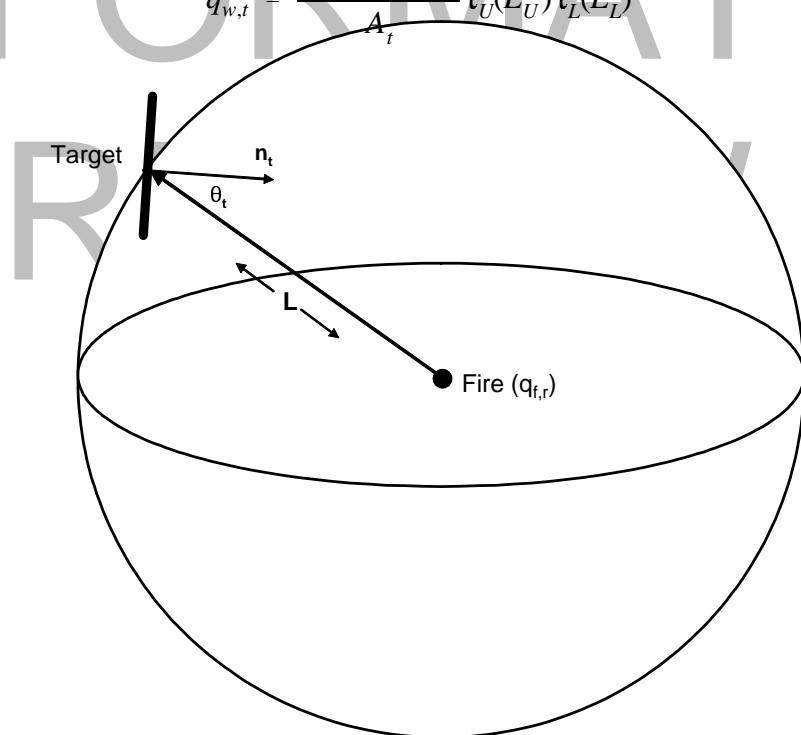


Figure 3-13. Radiative heat transfer from a point source fire to a target.

where $q''_{w,out}$ is the flux leaving the wall segment, A_w , A_t are the areas of the wall segment and target respectively, F_{w-t} is the fraction of radiant energy given off by the wall segment that is intercepted by the target (i.e. a configuration factor) and $\tau_U(L_U)$ and $\tau_L(L_L)$ are defined as before. Equation (87) can be simplified using the symmetry relation $A_w F_{w-t} = A_t F_{t-w}$ to obtain

$$q''_{w,t} = q''_{w,out} F_{t-w} \tau_U(L_U) \tau_L(L_L) \quad (88)$$

where

$$q''_{w,out} = \sigma T_w^4 - (1 - \epsilon_w) \frac{\Delta q_w''}{\epsilon_w} \quad (89)$$

T_w is the temperature of the wall segment, ϵ_w is the emissivity of the wall segment and $\Delta q_w''$ is the net flux striking the wall segment.

Radiation from the Gas Layer to the Target: Figure 3-14 illustrates the setup for calculating the heat flux from the gas layers to the target. The upper and lower gas layers in a room contribute to the heat flux striking the target if the layer absorptances are non-zero.

Let $q''_{w,t,gas}$ denote the flux striking the target due to the gas g in the direction of wall segment w . Then

$$q''_{w,t,gas} = \begin{cases} \sigma F_{t-w} (T_L^4 \alpha_L \tau_U + T_U^4 \alpha_U) & w \text{ is in the lower layer} \\ \sigma F_{t-w} (T_U^4 \alpha_U \tau_L + T_L^4 \alpha_L) & w \text{ is in the upper layer} \end{cases} \quad (90)$$

The total target flux due to the gas (upper or lower layer) is obtained by summing eq (90) over each wall segment or

$$q''_{g,t} = \sum_w q''_{w,t,gas} \quad (91)$$

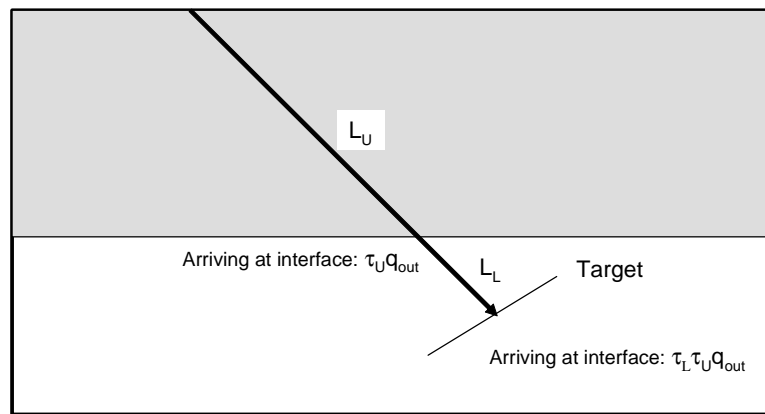


Figure 3-14. Radiative heat transfer from the upper and lower layer gas layers to a target in the lower layer.

Computing the Target Temperature The steady state target temperature, T_t can be found by solving an energy balance on the target; namely

$$\varepsilon_t \sigma T_t^4 = \varepsilon_t q_{r,in} + h(T_g - T_t) \quad (92)$$

Let $f(T_t)$ be the difference between the left and right hand side of equation (92). Then this equation may be solved using the Newton iteration

$$T_{new} = T_{old} - \frac{f(T_{old})}{f'(T_{old})} \quad (93)$$

Equation (93) is iterated until the difference $T_{new} - T_{old}$ is sufficiently small.

3.4.5.3 Convection

In general, convective heat transfer, q'' , across a surface of area A_s , is defined as

$$q'' = hA_s(T_g - T_s). \quad (94)$$

The convective heat transfer coefficient, h , is a function of the gas properties, temperature, and velocity. The Nusselt number is defined as $Nu_L = hL/k$, which for natural convection is related to the Rayleigh number,

$$Ra_L = \frac{g\beta(T_s - T_g)L^3}{\nu\alpha} \quad (96)$$

where L is a characteristic length of the geometry, g is the gravitational constant (m/s^2), k is the thermal conductivity (W/m^2K), β is a volumetric expansion coefficient (K^{-1}), T_s and T_g are the temperatures of the surface and gas, respectively (K), ν is the kinematic viscosity (m^2/s), and α is the thermal diffusivity (m^2/s). All properties are evaluated at the film temperature, $T_f \equiv (T_s + T_g)/2$. The typical correlations applicable to the problem at hand are available in the literature. The table below gives the correlations used in CFAST [55]:

Geometry	Correlation	Restrictions
Walls	$Nu_L = \left(0.825 + \frac{0.387Ra_L^{1/6}}{\left(1 + (0.492/Pr)^{9/16}\right)^{8/27}} \right)^2$ $\approx 0.12 Ra_L^{1/3}$	none
Ceilings and floors (hot surface up or cold surface down)	$Nu_L = 0.13 Ra_L^{1/3}$	$2 \cdot 10^8 \leq Ra_L \leq 10^{11}$
Ceilings and floors (cold surface up or hot surface down)	$Nu_L = 0.16 Ra_L^{1/3}$	$10^8 \leq Ra_L \leq 10^{10}$

The Prandtl number, Pr is the ratio of the kinematic viscosity and the thermal diffusivity. The thermal diffusivity, α , and thermal conductivity, k , of air are defined as a function of the film temperature from data in reference [55].

$$\alpha = 1.0 \times 10^{-9} T_f^{7/4}$$

$$k = \left(\frac{0.0209 + 2.33 \times 10^{-5} T_f}{1 - 0.000267 T_f} \right) \quad (97)$$

3.4.5.4 Conduction

Procedures for solving 1-d heat conduction problems are well known, (e.g., backward difference (fully implicit), forward difference (fully explicit) or Crank-Nicolson[56]). A finite difference approach [57] using a non-uniform spatial mesh is used to advance the wall temperature solution. The heat equation is discretized using a second order central difference for the spatial derivative and a backward differences for the time derivative. The resulting tri-diagonal system of equations is then solved to advance the temperature solution to time $t+DT$. This process is repeated, using the work of Moss and Forney [57], until the heat flux striking the wall (calculated from the convection and radiation algorithms) is consistent with the flux conducted into the wall calculated via Fourier's law

$$q'' = -k \frac{dT}{dx} \quad (98)$$

where k is the thermal conductivity. This solution strategy requires a differential algebraic (DAE) solver that can simultaneously solve both differential and algebraic equations. With this method, only one or two extra equations are required per wall segment (two if both the interior and exterior wall segment surface temperatures are computed). This solution strategy is more efficient than the method of lines since fewer equations need to be solved. Wall segment temperature profiles, however, still have to be stored so there is no decrease in storage requirements. Conduction is then coupled to the room conditions by temperatures

supplied at the interior boundary by the differential equation solver. The exterior boundary condition types (constant flux, insulated, or constant temperature) are specified in the configuration of CFAST.

A non-uniform mesh scheme was chosen to allow breakpoints to cluster near the interior and exterior wall segment surfaces. This is where the temperature gradients are the steepest. A breakpoint x_b was defined by $x_b = \text{MIN}(x_p, W/2)$, where $x_p = 2(\alpha t_{final})^{\frac{1}{2}} \text{erfc}^{-1}(.05)$ and erfc^{-1} denotes the inverse of the complementary error function. The value x_p is the location in a semi-infinite wall where the temperature rise is 5 % after t_{final} seconds and is sometimes called the penetration depth. Eighty percent of the breakpoints were placed on the interior side of x_b and the remaining 20 % were placed on the exterior side.

To illustrate the method, consider a one room case with one active wall. There are four gas equations (pressure, upper layer volume, upper layer temperature, and lower layer temperature) and one wall temperature equation. Implementation of the gradient matching method requires that storage be allocated for the temperature profile at the previous time, t , and at the next time, $t + \delta t$. Given the profile at time t and values for the five unknowns at time $t + \delta t$ (initial guess by the solver), the temperature profile is advanced from time t to time $t + \delta t$. The temperature profile gradient at $x = 0$ is computed followed by the residuals for the five equations. The DAE solver adjusts the solution variables and the time step until the residuals for all the equations are below an error tolerance. Once the solver has completed the step, the array storing the temperature profile for the previous time is updated, and the DAE solver is ready to take its next step.

3.4.5.5 Inter-compartment Heat Transfer

Heat transfer between vertically connected compartments is modeled by merging the connected surfaces for the ceiling and floor compartments or for the connected horizontal compartments. A heat conduction problem is solved for the merged walls using a temperature boundary condition for both the near and far wall. As before, temperatures are determined by the DAE solver so that the heat flux striking the wall surface (both interior and exterior) is consistent with the temperature gradient at that surface. This option is implemented with the CFCON (for vertical heat transfer) and the HHEAT (for horizontal heat transfer) keywords.

For horizontal heat transfer between compartments, the connections may be between partial wall surfaces, expressed as a fraction of the wall surface. CFAST first estimates conduction fractions analogous to radiative configuration factors. For example, if only one half of the rear wall in one compartment is adjacent to the front wall in a second compartment, the conduction fraction between the two compartments is 1/2. These fractions can be prescribed on the HHEAT keyword line. Once these fractions are determined, an average flux, q''_{avg} , is calculated using

$$q''_{avg} = \sum_{walls} F_{ij} q''_{wall_j} \quad (99)$$

where F_{ij} is the fraction of flux from wall i that contributes to wall j , q''_{wall_j} is the flux striking wall j .

3.4.6 Ceiling Jet

Relatively early in the development of a fire, fire-driven ceiling jets and gas-to-ceiling convective heat transfer can play a significant role in room-to-room smoke spread and in the response of near-ceiling mounted detection hardware. Cooper [58] details a model and computer algorithm to predict the instantaneous rate of convective heat transfer from fire plume gases to the overhead ceiling surface in a room of fire origin. The room is assumed to be a rectangular parallelepiped and, at times of interest, ceiling temperatures are simulated

as being uniform. Also presented is an estimate of the convective heat transfer due to ceiling-jet driven wall flows. The effect on the heat transfer of the location of the fire within the room is taken into account. This algorithm has been incorporated into the CFAST model. In this section, we provide an overview of the model. Complete details are available in reference [58].

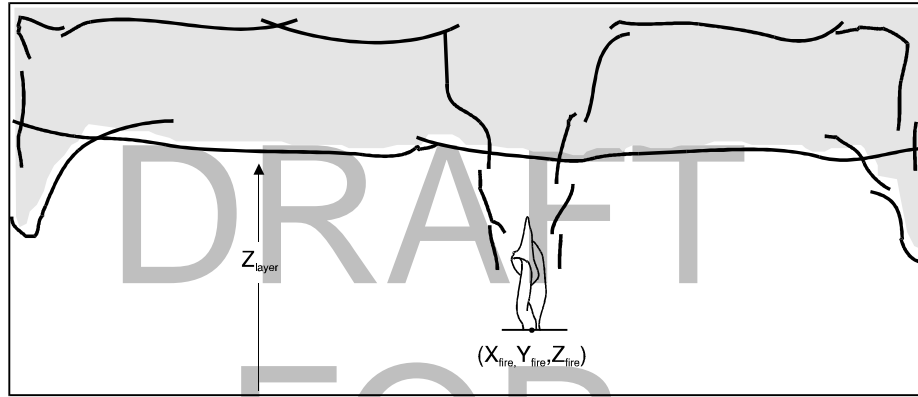


Figure 3-15. Convective heat transfer to ceiling and wall surfaces via the ceiling jet.

A schematic of a fire, fire plume, and ceiling jet is shown in Figure 3-15. The buoyant fire plume rises from the height Z_{fire} toward the ceiling. When the fire is below the layer interface, its mass and enthalpy flow are assumed to be deposited into the upper layer at height Z_{layer} . Having penetrated the interface, a portion of the plume typically continues to rise toward the ceiling. As it impinges on the ceiling surface, the plume gases turn and form a relatively high temperature, high velocity, turbulent ceiling jet which flows radially outward along the ceiling and transfers heat to the relatively cool ceiling surface. The convective heat transfer rate is a strong function of the radial distance from the point of impingement, reducing rapidly with increasing radius. Eventually, the relatively high temperature ceiling jet is blocked by the relatively cool wall surfaces [59]. The ceiling jet then turns downward and outward in a complicated flow along the vertical wall surfaces [60], [61]. The descent of the wall flows and the heat transfer from them are eventually stopped by upward buoyant forces. They are then buoyed back upward and mix with the upper layer.

The average convective heat transfer from the ceiling jet gases to the ceiling surface, Q_{ceil} , can be expressed in integral form as

$$Q_{ceil} = \int_0^{X_{wall}} \int_0^{Y_{wall}} q''_{ceil}(x,y) dx dy \quad (100)$$

The instantaneous convective heat flux, $q''_{ceil}(X,Y)$ can be determined as derived by Cooper [58]:

$$q''_{ceil}(x,y) = h_l (T_{ad} - T_{ceil}) \quad (101)$$

where T_{ad} , a characteristic ceiling jet temperature, is the temperature that would be measured adjacent to an adiabatic lower ceiling surface, and h is a heat transfer coefficient. h and T_{ad} are given by

$$\frac{h}{\tilde{h}} = \begin{cases} 8.82 Re_H^{-1/2} Pr^{-2/3} \left(1 - \left(5 - 0.284 Re_H^{2/5} \right) \frac{r}{H} \right) & 0 \leq \frac{r}{H} < 0.2 \\ 0.283 Re_H^{0.3} Pr^{-2/3} \left(\frac{r}{H} \right)^{-1.2} \frac{\frac{r}{H} - 0.0771}{\frac{r}{H} + 0.279} & 0.2 \leq \frac{r}{H} \end{cases} \quad (102)$$

$$\frac{T_{ad} - T_u}{T_u Q_H^{*2/3}} = \begin{cases} 10.22 - 14.9 \frac{r}{H} & 0 \leq \frac{r}{H} < 0.2 \\ 8.39 f\left(\frac{r}{H}\right) & 0.2 \leq \frac{r}{H} \end{cases} \quad (103)$$

where

$$f\left(\frac{r}{H}\right) = \frac{1 - 1.10 \left(\frac{r}{H}\right)^{0.8} + 0.808 \left(\frac{r}{H}\right)^{1.6}}{1 - 1.10 \left(\frac{r}{H}\right)^{0.8} + 2.20 \left(\frac{r}{H}\right)^{1.6} + 0.690 \left(\frac{r}{H}\right)^{2.4}} \quad (104)$$

$$r = \left((X - X_{fire})^2 + (Y - Y_{fire})^2 \right)^{1/2} \quad (105)$$

$$\tilde{h} = \rho_u c_p g^{1/2} H^{1/2} Q_H^{*1/3}; \quad Re_H = \frac{g^{1/2} H^{3/2} Q_H^{*1/3}}{v_u}; \quad Q_H^* = \frac{Q}{\rho_u c_p T_u (gH)^{1/2} H^2} \quad (106)$$

$$Q = \begin{cases} Q_{fc} \frac{\sigma \dot{M}^*}{1 + \sigma} & Z_{fire} < Z_{layer} < Z_{ceiling} \\ Q_{fc} & Z_{fire} \geq Z_{layer} \\ & Z_{layer} = Z_{ceiling} \end{cases} \quad \dot{M}^* = \begin{cases} 0 & -1 < \sigma \leq 0 \\ \frac{1.04599\sigma + 0.360391\sigma^2}{1 + 1.37748\sigma + 0.360391\sigma^2} & \sigma > 0 \end{cases} \quad (107)$$

$$\sigma = \frac{1 - \frac{T_u}{T_l} + C_T Q_{EQ}^{*2/3}}{\frac{T_u}{T_l}}; \quad C_T = 9.115 \quad (108)$$

$$Q_{EQ}^* = \left(\frac{0.21 Q_{fc}}{c_p T_l \dot{m}_p} \right)^{3/2} \quad (109)$$

In the above, H is the distance from the (presumed) point source fire and the ceiling, X_{fire} and Y_{fire} are the position of the fire in the room, Pr is the Prandtl number (taken to be 0.7) and ν_u is the kinematic viscosity of the upper layer gas which is assumed to have the properties of air and can be estimated from $\nu_u = 0.04128(10^7) T_u^{5/2} / (T_u + 110.4)$. Q_H^* and Q_{EQ}^* are dimensionless numbers and are measures of the strength of the plume at the ceiling and the layer interface, respectively.

When the ceiling jet is blocked by the wall surfaces, the rate of heat transfer to the surface increases. Reference [58] provides details of the calculation of wall surface area and convective heat flux for the wall surfaces.

3.5 Heat Detection

Heat detection is modeled using temperatures obtained from the ceiling jet [62]. Rooms without fires do not have ceiling jets. Sensors in these types of rooms use gas layer temperatures instead of ceiling jet temperatures. The characteristic detector temperature is simply the temperature of the ceiling jet (at the location of the detector). The characteristic heat detector temperature is modeled using the differential equation [63]

$$\frac{dT_L}{dt} = \frac{\sqrt{V(t)}}{RTI} (T_g(t) - T_L(t)) \quad (110)$$

$$T_L(0) = T_g(0) \quad (111)$$

where T_L , T_g are the link and gas temperatures, V is the gas velocity, and RTI (response time index) is a measure of the sensor's sensitivity to temperature change (thermal inertia). The heat detector differential eq (110) may be rewritten to

$$\frac{dT(t)}{dt} = a(t) - b(t)T(t) \quad (112)$$

$$T(t_0) = T_0$$

where

$$a(t) = \frac{\sqrt{V(t)}T(t)}{RTI}, \quad b(t) = \frac{\sqrt{V(t)}}{RTI} \quad (114)$$

Equation (112) may be solved using the trapezoidal rule to obtain

$$\frac{T_{i+1} - T_i}{\Delta t} = \frac{1}{2} \left((a_i - b_i T_i) + (a_{i+1} - b_{i+1} T_{i+1}) \right) \quad (115)$$

where the subscript i denotes time at t_i . Equation (115) may be simplified to

$$T_{i+1} = A_{i+1} - b_{i+1} T_{i+1} \quad (116)$$

$$A_{i+1} = T_i + \frac{\Delta t}{2} (a_i - b_i T_i + a_{i+1}) \quad (117)$$

$$B_{i+1} = \frac{\Delta t}{2} b_{i+1} \quad (118)$$

which has a solution

$$T_{i+1} = \frac{A_{i+1}}{1 + B_{i+1}} = \frac{1 - \frac{\Delta t}{2} b_i}{1 + \frac{\Delta t}{2} b_{i+1}} T_i + \frac{\Delta t}{1 + \frac{\Delta t}{2} b_{i+1}} \left(\frac{a_i + a_{i+1}}{2} \right) \quad (119)$$

Equation (119) reduces to the trapezoidal rule for integration when $b(t) = 0$. When $a(t)$ and $b(t)$ are constant (the gas temperature, T_g , and gas velocity, V are not changing), eq (110) has the solution

$$T(t) = \frac{a}{b} + \frac{e^{-b(t-t_0)} (bT_0 - a)}{b} = T_g + e^{-\sqrt{V(t)}(t-t_0)/RTI} (T_0 - T_g) \quad (120)$$

3.6 Sprinkler Activation and Fire Attenuation

For suppression, the sprinkler is modeled using a simple model [64] generalized for varying sprinkler spray densities [65]. It is then modeled by attenuating all fires in the room where the sensor activated by a term of the form $e^{-(t-t_{act})/t_{rate}}$ where t_{act} is the time when the sensor activated and t_{rate} is a constant determining how quickly the fire attenuates. The term t_{rate} can be related to spray density of a sprinkler using a correlation developed in [65]. The suppression correlation was developed by modifying the heat release rate of a fire. For $t > t_{act}$ the heat release is given by

$$Q_f(t) = e^{-(t-t_{act})/3.0Q_{spray}^{-1.8}} Q(t_{act}) \quad (121)$$

where Q_{spray} is the spray density of a sprinkler. Note that decay rate can be formulated in terms of either the attenuation rate or the spray density. Both options are available. t_{rate} can be expressed in terms of Q_{spray} as

$$t_{rate} = 3.0Q_{spray}^{-1.8} \quad (122)$$

DRAFT

$$t_{50\%} = 3\ln(2)Q_{spray}^{-1.8} \quad (123)$$

and the decay time (time to 50% attenuation) as the input line allows the specification of either the spray density of the sprinkler or the time required to reduce the fire heat release rate by 50%, $t_{50\%}$. A calculation is done to make sure that the fuel burned is consistent with the available oxygen. Once detection has occurred, then the mass and energy release rates are attenuated by the term $e^{-(t-t_{act})/t_{rate}}$ to obtain

$$\dot{m}_{pyrolys}(t) = e^{-(t-t_{act})/t_{rate}} \dot{m}_{pyrolys}(t_{act}) \quad (124)$$

$$\dot{m}_{pyrolys}(t) = e^{-(t-t_{act})/t_{rate}} \dot{m}_{pyrolys}(t_{act}). \quad (125)$$

There are assumptions and limitations in this approach. Its main deficiency is that it assumes that sufficient water is applied to the fire to cause a decrease in the rate of heat release. This suppression model cannot handle the case when the fire overwhelms the sprinkler. The suppression model as implemented does not include the effect of a second sprinkler. Detection of all sprinklers are noted but their activation does not make the fire go out any faster. Further, multiple fires in a room imply multiple ceiling jets. It is not clear how this should be handled, *i.e.*, how two ceiling jets should interact. When there is more than one fire, the detection algorithm uses the fire that results in the worst conditions (usually the closest fire) in order to calculate the fire sensor temperatures. Finally, the ceiling jet algorithm that we use results in temperature predictions that are warmer (for a given heat release rate) than those used in the correlation developed by Madrzykowski [66], which will cause activation sooner than expected.

3.7 Species Concentration and Deposition

CFAST uses a combustion chemistry scheme based on a carbon-hydrogen-oxygen balance. The scheme is applied in three places. The first is burning in the portion of the plume which is in the lower layer of the compartment of fire origin. The second is the portion in the upper layer, also in the compartment of origin. The third is in the vent flow which entrains air from a lower layer into an upper layer in an adjacent compartment. This is equivalent to solving the conservation equations for each species independently.

3.7.1 Species Transport

The species transport in CFAST is primarily a matter of bookkeeping to track individual species mass as it is generated by a fire, transported through vents, or mixed between layers in a compartment. When the layers are initialized at the start of the simulation, they are set to ambient conditions. These are the initial temperature prescribed by the user, and 23 % by mass (21 % by volume) oxygen, 77 % by mass (79 % by volume) nitrogen, a mass concentration of water prescribed by the user as a relative humidity, and a zero concentration of all other species. As fuel is burned, the various species are produced in direct relation to the mass of fuel burned (this relation is the species yield prescribed by the user for the fuel burning). Since oxygen is consumed rather than produced by the burning, the “yield” of oxygen is negative, and is set internally to correspond to the amount of oxygen used to burn the fuel (within the constraint of available oxygen limits discussed in sec. ?).

Each unit mass of a species produced is carried in the flow to the various rooms and accumulates in the layers. The model keeps track of the mass of each species in each layer, and knows the volume of each layer as a function of time. The mass divided by the volume is the mass concentration, which along with the molecular weight gives the concentration in volume % or ppm as appropriate.

For soot, the input for C/CO₂ is used to calculate a “soot” yield from the fire (assuming all the carbon goes to soot). This soot generation is then transported as a species to yield a soot mass concentration to use in the optical density calculation based on the work of Seader and Einhorn [67].

3.7.2 HCl Deposition

Hydrogen chloride produced in a fire can produce a strong irritant reaction that can impair escape from the fire. It has been shown [68] that significant amounts of the substance can be removed by adsorption by surfaces which contact smoke. In our model, HCl production is treated in a manner similar to other species. However, an additional term is required to allow for deposition on, and subsequent absorption into, material surfaces.

The physical configuration that we are modeling is a gas layer adjacent to a surface (Figure **Figure 19**). The gas layer is at some temperature T_g with a concomitant density of hydrogen chloride, ρ_{HCl} . The mass transport coefficient is calculated based on the Reynolds analogy with mass and heat transfer; that is, hydrogen chloride is mass being moved convectively in the boundary layer, and some of it simply sticks to the wall surface rather than completing the journey during the convective roll-up associated with eddy diffusion in the boundary layer. The boundary layer at the wall is then in equilibrium with the wall. The latter is a statistical process and is determined by evaporation from the wall and stickiness of the wall for HCl molecules. This latter is greatly influenced by the concentration of water in the gas, in the boundary layer and on the wall itself.

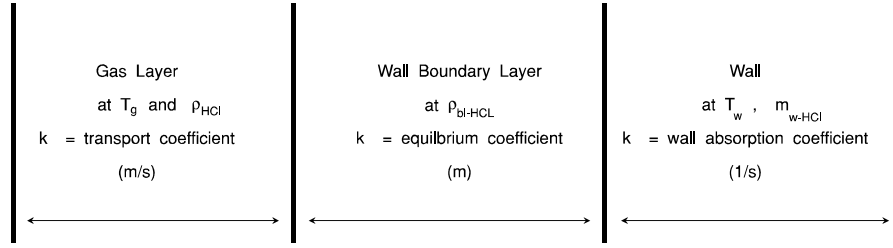


Figure 3-16. Schematic of hydrogen chloride deposition region.

The rate of addition of mass of hydrogen chloride to the gas layer is given by

$$\frac{d}{dt}m_{HCl} = \text{source} - k_c \times (\rho_{HCl} - \rho_{blHCl}) \times A_w \quad (126)$$

where source is the production rate from the burning object plus flow from other compartments.

For the wall concentration, the rate of addition is

$$\frac{d}{dt}d_{HCl,w} = k_c \times (\rho_{HCl} - \rho_{blHCl}) - k_s \times m_{HCl,w} \quad (127)$$

where the concentration in the boundary layer, ρ_{blHCl} , is related to the wall surface concentration by the equilibrium constant k_e ,

$$\rho_{blHCl} = d_{HCl,w} / k_e \quad (128)$$

We never actually solve for the concentration in the boundary layer, but it is available, as is a boundary layer temperature if it were of interest. The transfer coefficients are

$$k_c = \frac{\dot{q}}{\Delta T \rho_g c_p} \quad (129)$$

$$k_e = \frac{b_1 e^{1500/T_w}}{1 + b_2 e^{1500/T_w} \rho_{hcl}} \left(1 + \frac{b_5 (\rho_{H_2O})^{b_6}}{(\rho_{H_2O,sat} - \rho_{H_2O,g})^{b_7}} \right) \quad (130)$$

$$k_s = b_3 e^{-\left(\frac{b_4}{R T_w}\right)} \quad (131)$$

The only values currently available [69] for these quantities are shown in Table 4. The “b” coefficients are parameters which are found by fitting experimental data to eqs (126) through (131). These coefficients reproduce the adsorption and absorption of HCl reasonably well. Note though that error bars for these coefficients have not been reported in the literature.

Table 3.4 Transfer coefficients for HCl deposition from reference [69]

Surface	b_1	b_2	b_3	b_4	b_5	b_6	b_7
	(m)	(m ³ /kg)	(s ⁻¹)	(J/g-mol)	(note a)	(note b)	(note c)
Painted Gypsum	0.0063	191.8	0.0587	7476.	193	1.021	0.431
PMMA	9.6×10 ⁻⁵	0.0137	0.0205	7476.	29	1.0	0.431
Ceiling Tile	4.0×10 ⁻³	0.0548	0.123	7476.	30 ^b	1.0	0.431
Cement Block	1.8×10 ⁻²	5.48	0.497	7476.	30 ^b	1.0	0.431
Marinite®	1.9×10 ⁻²	0.137	0.030	7476.	30 ^b	1.0	0.431

a units of b_5 are (m³/kg)^{b₇-b₆}

b very approximate value, insufficient data for high confidence value

c non-dimensional

The experimental basis for poly(methyl methacrylate) and gypsum cover a sufficiently wide range of conditions that they should be usable in a variety of practical situations. The parameters for the other surfaces do not have much experimental backing, and so their use should be limited to comparison purposes.

3.8 Flame Spread

The Quintiere-Cleary flame spread model [70] incorporated into CFAST is based on five simple differential equations. One each for concurrent (eq (132)) and opposed flow flame spread (eq (133)). One each (eqs (135) and (134)) for the two burn-out fronts, and the last one for burn-out at the ignition point (eq (136)).

$$\frac{dy_p}{dt} = \frac{y_f - y_p}{\frac{\pi k \rho c [T_{ig} - T_s]^2}{4 q_f''}} \quad (132)$$

$$\frac{dx_p}{dt} = \frac{\phi}{k \rho c (T_{ig} - T_s)^2}, \text{ for } T_s \geq T_{s, \min} \quad (133)$$

$$\frac{dy_b}{dt} = \frac{q''(y_p - y_b)}{q_{TOT}''} \quad (134)$$

$$\frac{dx_b}{dt} = \frac{q''(x_p - x_b)}{q_{TOT}''} \quad (135)$$

and

$$\frac{dq''}{dt} = \frac{(q_f'' - \sigma T_{ig}^4 + \sigma T_{layer}^4)}{\Delta L} \Delta H \quad (136)$$

where y is the wind-aided coordinate direction, x is the opposed flow coordinate direction, $k\rho c$ is the thermal inertia (thermal conductivity x density x specific heat), T_{ig} is the ignition temperature, T_s is the surface temperature, $T_{s,min}$ is the minimum surface temperature for pyrolysis, q'' is heat flux, and ϕ is a flame heating parameter defined in eq. (168). The subscripts p , b , f , and TOT refer to pyrolysis front, burnout front, flame, and total respectively.

The equations describe the growth of two rectangles. At ignition a single rectangle, R_p , is defined and its growth is determined by eq (132) for spread up the wall and eq (133) for lateral spread as well as spread down the wall. When $q'' < 0$, a second rectangle, R_b , the same size as R_p was originally starts growing. It is governed by eqs (135) and (134). After R_b starts to be tracked the pyrolysis area is $R_p - R_b$.

When a flame spread object is defined, CFAST adds five additional differential equations to the equation set. A target is also placed at the prescribed location on the prescribed wall surface and the maximum time step is set to 1 s. This allows the temperature of the target to be tracked and the ignition temperature and time to be calculated. Once the object ignites, its mass loss and heat release rate are calculated and then treated like any other fire by CFAST.

3.9 Single Zone Approximation

A single zone approximation is appropriate for smoke flow far from a fire source where the two-zone layer stratification is less pronounced than in compartments near the fire. In this situation, a single zone approximation may be derived by using the normal two-zone source terms and the substitutions:

$$\begin{aligned} \dot{m}_U^{new} &= \dot{m}_L + \dot{m}_U, \\ \dot{m}_L^{new} &= 0, \\ Q_U^{new} &= Q_L + Q_U, \\ Q_L^{new} &= 0. \end{aligned} \quad (137)$$

This is used in situations where the stratification does not occur. Examples are elevators shafts, complex stairwells, and compartments far from the fire. In addition to a slight decrease in computing time, it allows one to benchmark simpler models such as CONTAM [71] and other network models.

3.10 Review of the Theoretical Development of the Model

The current version of ASTM E 1355-04 includes provisions to guide in the assessment of the theoretical basis of the model that includes a review of the model “by one or more recognized experts fully conversant with the chemistry and physics of fire phenomenon, but not involved with the production of the model. Publication of the theoretical basis of the model in a peer-reviewed journal article may be sufficient to fulfill this review” [1].

CFAST has been subjected to independent review in two ways, internal and external. First, all documents issued by the National Institute of Standards and Technology receive three levels of internal review by members of the staff not involved in the preparation of the report or underlying research. The theoretical basis of CFAST is presented in this document, and is subject to internal review by staff members who are not active participants in the development of the model, but who are members of the Fire Research Division and are considered experts in the fields of fire and combustion. The same was true of previous versions of the technical reference guide over the last decade [2],[72],[73]. Externally, the theoretical basis for the model has been published in peer reviewed journals [74],[75],[76] and conference proceedings [77]. In addition, CFAST is used worldwide by fire protection engineering firms who review the technical details of the model related to their particular application. Some of these firms also publish in the open literature reports documenting internal efforts to validate the model for a particular use. Many of these studies are discussed in more detail in the present document.

In addition to the formal review, procedures were in place during the development of CFAST to assure the quality of the model. These procedures included several components:

- Review of proposed changes to the code by at least two others involved in the development process to insure that a proposed change was consistent with the rest of the CFAST code and was implemented correctly. These reviews, while informal in nature, provided a comprehensive review of the changes to the model during its development. Significant changes were documented in internal memorandums covering such areas as the numerics and structure of the model [78], improvements in the chemistry [79] convection [80], HCl deposition [81] algorithms, and output formats for the model [82]. Comparisons of the impact of the changes on the output results were often described in internal memorandums (see, for example, reference [79]).
- Internal review of the model prior to public release. In addition to the normal NIST document review process, the CFAST software was circulated internally to Fire Research Division Staff to allow interested staff members to test the model [83],[84],[85]. These memorandums detail changes to the model since the last public release of the model and provide documentation of the history of the model development.
- For each major release of CFAST, NIST has maintained a history of the source code which goes back to March 1989. While it is not practical to reconstruct the programs for each release for use with modern software tools and computer operating systems, the source code history allows the developers to examine what changes were made at each release point. This provides detailed documentation of the history of model development and is often useful to understand the impact of changes to submodels over the development of the model.
- Once a release of CFAST was approved by NIST, it was announced with a letter to model users which provided a summary of model changes and available documentation. In essence, these were a condensation of the internal memorandums, without details or printout of specific code changes. These

memorandums provide documentation of the history of the model development [86], [87], [88], [89], [90].

Finally, CFAST has been reviewed and included in industry-standard handbooks such as the SFPE Handbook [91] and referenced in specific standards, including NFPA 805 [92] and NFPA 551 [93].

3.10.1 Assessment of the Completeness of Documentation

There are two primary documents on CFAST, this Technical Reference Guide and a Model User's Guide [94]. This document is the Technical Reference Guide and provides documentation of the governing equations, assumptions, and approximations of the various submodels. It also includes a summary description of the model structure, and numerics. The Model User's Guide includes a description of the model input data requirements and model results.

The extensive formal review process for all NIST publications in part insures the quality of the CFAST Guides. In addition, the model developers routinely receive feedback from users on the completeness of the documentation and add clarifications when needed. It is estimated that there are several thousand users of CFAST. Before new versions of the model are released, there is a "beta test" period in which the users test the new version using the updated documentation. This process is similar, although less formal, to that which most computer software programs undergo. Training courses for use of the model in fire hazard analysis have been developed from the model documentation and presented at training courses worldwide [95].

3.10.2 Assessment of Justification of Approaches and Assumptions

The technical approach and assumptions of the model have been presented in the peer reviewed scientific literature and at technical conferences. Also, all documents released by NIST are required to go through an internal editorial review and approval process. This process is designed to ensure compliance with the technical requirements, policy, and editorial quality required by NIST. The technical review includes a critical evaluation of the technical content and methodology, statistical treatment of data, uncertainty analysis, use of appropriate reference data and units, and bibliographic references. CFAST manuals are always first reviewed by a member of the Fire Research Division, then by the immediate supervisor of the author of the document, then by the chief of the Fire Research Division, and finally by a reader from outside the division. Both the immediate supervisor and the division chief are technical experts in the field. Once the document has been reviewed, it is then brought before the Editorial Review Board (ERB), a body of representatives from all the NIST laboratories. At least one reader is designated by the Board for each document that it accepts for review. This last reader is selected based on technical competence and impartiality. The reader is usually from outside the division producing the document and is responsible for checking that the document conforms with NIST policy on units, uncertainty and scope. This reader does not need to be a technical expert in fire or combustion.

Besides formal internal and peer review, CFAST is subjected to continuous scrutiny because it is available to the general public and is used internationally by those involved in fire safety design and postfire reconstruction. The source code for CFAST is also released publicly, and has been used at various universities worldwide, both in the classroom as a teaching tool as well as for research. As a result, flaws in the theoretical development and the computer program itself have been identified and fixed. The user base continues to serve as a means to evaluate the model, which is as important to its development as the formal internal and external peer review processes.

3.10.3 Assessment of Constants and Default Values

A comprehensive assessment of the numerical parameters (such as default time step or solution convergence criteria) and physical parameters (such as empirical constants for convective heat transfer or plume entrainment) used in CFAST is not available in one document. Instead, specific parameters have been tested in various verification and validation studies performed at NIST and elsewhere. Numerical parameters are described in this Technical Reference Guide and are subject to the internal review process at NIST, but many physical parameters are extracted from the literature and do not undergo a formal review. In addition, default values for the various model inputs have been specifically reviewed by a professional fire protection engineering university professor to insure appropriate default values and suggested limits for the various input values. The model user is expected to assess the appropriateness of default values provided by CFAST and make changes to the default values if need be.

DRAFT
FOR
FORMAT
REVIEW
ONLY

Chapter 4 Mathematical and Numerical Robustness

4.1 Introduction

The mathematical and numerical robustness of a deterministic computer model depends upon three issues: the code must be transparent so that it can be understood and modified by visual inspection; it must be possible to check and verify with automated tools; and there must be a method for checking the correctness of the solution, at least for asymptotic (steady state) solutions (numerical stability and agreement with known solutions).

In order to understand the meaning of accuracy and robustness, it is necessary to understand the means by which the numerical routines are structured. In this chapter, details of the implementation of the model are presented, including the tests used to assess the numerical aspects of the model. These include

- the structure of the model, including the major routines implementing the various physical phenomena included in the model,
- the organization of data initialization and data input used by the model,
- the structure of data used to formulate the differential equations solved by the model,
- a summary of the main control routines in the model that are used to control all input and output, initialize the model and solve the appropriate differential equation set for the problem to be solved,
- the means by which the computer code is checked for consistency and correctness,
- analysis of the numerical implementation for stability and error propagation, and
- comparison of the results of the system model with simple analytical or numerical solutions.

4.2 Structure of the Numerical Routines

A methodology which is critical to verification of the model is the schema used to incorporate physical phenomena. This is the subroutine structure discussed below. The method for incorporating new phenomena and insuring the correctness of the code was adopted as part of the consolidation of CCFM and FAST. This consolidation occurred in 1990 and has resulted in a more transparent, transportable and verifiable numerical model. This transparency is crucial to a verifiable and robust numerical implementation of the predictive model as discussed in the sections on code checking and numerical analysis.

4.2.1 Subroutine Structure

The model can be split into distinct parts. There are routines for reading data, calculating results and reporting the results to a file or printer. The major routines for performing these functions are identified in Figure **Figure 20**. These physical interface routines link the CFAST model to the actual routines which calculate quantities such as mass or energy flow at one particular point in time for a given environment.

The routines SOLVE, RESID and DASSL are the key to understanding how the physical equations are solved. SOLVE is the control program that oversees the general solution of the problem. It invokes the differential

equation solver DASSL [96] which in turn calls RESID to solve the transport equations. Given a solution at time t , what is the solution at time t plus a small increment of time, Δt , (where the time increment is determined dynamically by the program to insure convergence of the solution at $t + \Delta t$)? The differential equations are of the form

$$\begin{aligned}\frac{dy}{dt} &= f(y,t) \\ y(t_0) &= y_0\end{aligned}\tag{138}$$

where y is a vector representing pressure, layer height, mass, etc. and f is a vector function that represents changes in these values with respect to time. The term y_0 is an initial condition at the initial time t_0 . The subroutine RESID computes the right hand side of eq (138) and returns a set of residuals of that calculation to be compared to the values expected by DASSL. DASSL then checks for convergence. Once DASSL reaches an error limit (defined as convergence of the equations) for the solution at $t+\Delta t$, SOLVE then advances the solution of species concentration, wall temperature profiles, and mechanical ventilation for the same time interval.

Note that there are several distinct time scales that are involved in the solution of this type of problem. The fastest will be chemical kinetics. We avoid that scale by assuming that the chemistry is infinitely fast. The next larger time scale is that associated with the flow field. These are the equations which are cast into the form of ordinary differential equations. Then there is the time scale for mechanical ventilation, and finally, heat conduction through objects. Chemical kinetic times are typically on the order of milliseconds. The transport time scale are on the order of 0.1 s. The mechanical ventilation and conduction time scales are typically several seconds, or even longer. The time step is dynamically adjusted to a value appropriate for the solution of the currently defined equation set. In addition to allowing a more correct solution to the pressure equation, very large time steps are possible if the problem being solved approaches steady-state.

4.3 Code Checking

There are two means to automate checking the correctness of the language used by a numerical model. The first is the use of standard methods for checking the structure and interface. Programs such as Flint and Lint are standard tools to do such checking. They are applied to the whole model. There are three aspects of the model checked by this procedure: correctness of the interface, undefined or incorrectly defined (or used) variables and constants, and completeness of loops and threads. It does not check for the correctness of the numerical use of constants or variables only that they are used correctly in a syntactical sense. Lint is part of most C language distributions of Unix. Flint is the equivalent for the FORTRAN language. Though it is not usually included with FORTRAN distributions Flint is generally available⁵. Both have been used with CFAST.

The second is to use a variety of computer platforms to compile and run the code. Since FORTRAN and C are implemented differently for various computers, this represents both a numerical check as well as a syntactic check. CFAST has been compiled for the Sun (Solaris), SGI (Irix), the windows-based PCs (Lahey, Digital, and Intel FORTRAN), and the Concurrent Computer platforms. Within the precision afforded by the various hardware implementations, the answers are identical⁶

⁵ Cleanscape Software, 445 Sherman Ave, Ste. Q, Palo Alto, CA 94306

⁶ Typically one part in 10^6 , which is the error limit used for DASSL.

As discussed in section 4.1, many others have used the source for special applications, which provides another

check that the paradigm discussed in section 4.1 provides high reliability and robustness.

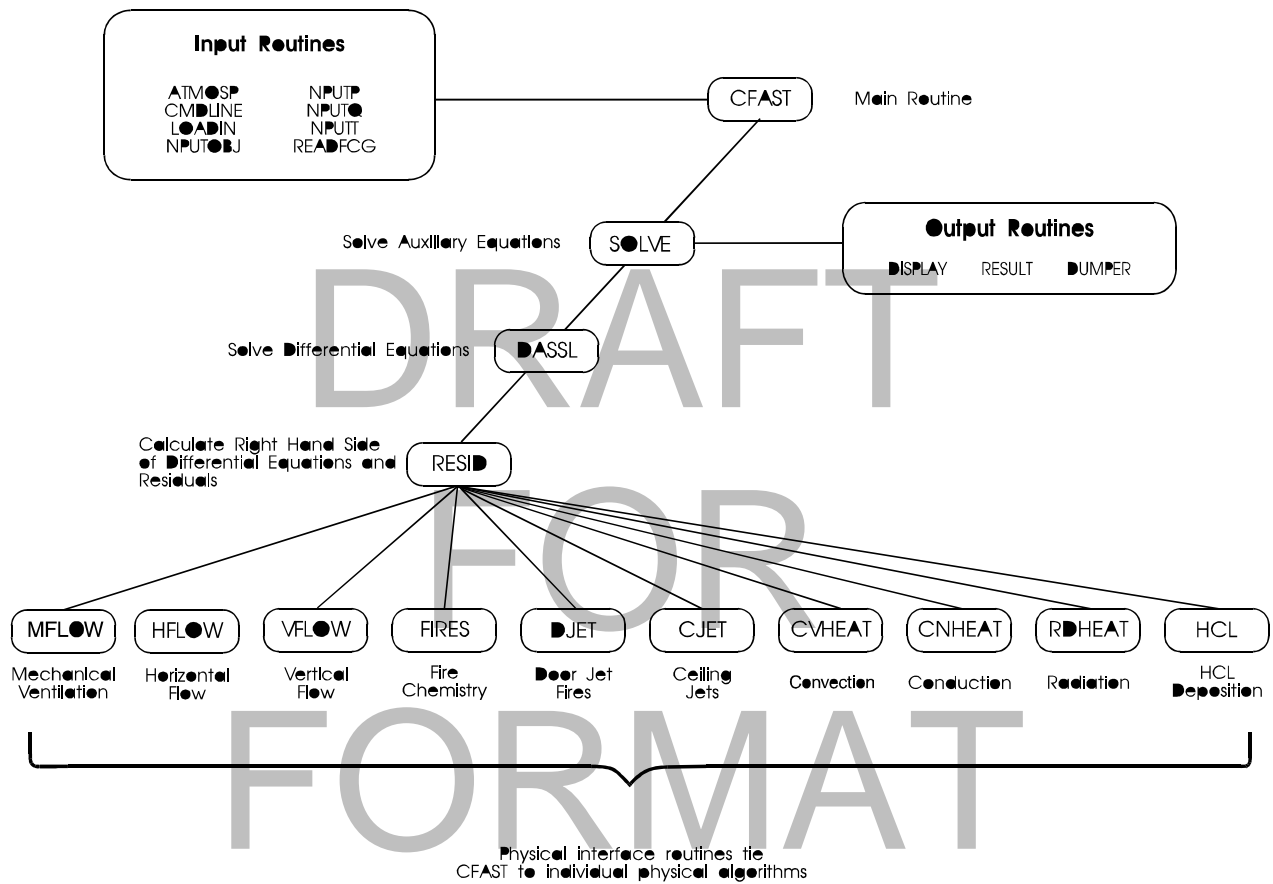


Figure 4-1. Subroutine structure for the CFAST Model.

DRAFT FOR

4.4 Numerical Tests

There are two components to testing the numerical solutions of CFAST. First, the DASSL solver is well tested for a wide variety of differential equations, and is widely used and accepted [96]. Also, the radiation and conduction routines are tested with known solutions. These are not analytical tests, but physical limits, such as an object immersed in a fluid of constant temperature, to which the temperature must equilibrate. The solver(s) must show that the differential equations asymptotically converge to these answers.

The second is to insure that the coupling between algorithms and the solver is correct. Most errors are avoided because of the structure discussed in section 4.1. The error due to the numerical solution is far less than that associated with the model assumptions. Two examples of this are the coupling of mechanical ventilation with buoyant flow, and the Nusselt number assumption for boundary layer convection. For the former, the coupling of a network of incompressible flow with an ODE for compressible flow has to deal with disparate calculations of pressure. For the latter, a very small time step occurs when a floor is heated and the thermal wave reaches the far (unexposed) side. This is a limitation of the physical implementation of the heat flow algorithm (convection). The solver arrives at the correct solution, but the time step becomes very small in order to achieve this.

Numerical error can be divided into three categories: roundoff, truncation and discretization error. Roundoff error occurs because computers represent real numbers using a finite number of digits. Truncation error occurs when an infinite process is replaced by a finite one. This can happen, for example, when an infinite series is truncated after a finite number of terms or when an iteration is terminated after a convergence criterion has been satisfied. Discretization error occurs when a continuous process such as a derivative is approximated by a discrete analog such as a divided difference. CFAST is designed to use 64-bit precision for real number calculations to minimize these effects.

Implicit in solving the equations discussed in Chapter 3, is that the solver will arrive at a solution. Inherent in the DASSL solver are convergence criteria for the mass and energy balance within CFAST to insure mass and energy conservation within 1 part in 10^6 . There are, however, limitations introduced by the algorithmic realization of physical models, that can produce errors and instabilities. Using the example above, if a mechanical ventilation system injects or removes mass and enthalpy from a small duct, then there can be a

stability issue with the layer interface bobbing up and down over the duct. These are annoyances to the user community and shortcomings of the implementation of algorithm rather than failure of the system model. Problems of this sort are noted in the “frequently asked questions” on the CFAST web site (<http://cfast.nist.gov>).

4.5 Comparison with Analytic Solutions

There do not exist general analytic solutions for fire problems, even for the simplest cases. That is, there are no closed form solutions to this type of problem. However, it is possible to do two kinds of checking. The first type is discussed in the section on the theoretical basis of the model, for which individual algorithms are validated against experimental work. The second is simple experiments, especially for conduction and radiation, for which the results are asymptotic. For example, for a simple, single compartment test case with no fire, all temperatures should equilibrate asymptotically to a single value. Such comparisons are common and not usually published.

DRAFT
FOR
FORMAT
REVIEW
ONLY

Chapter 5 Model Sensitivity

Sensitivity studies are conducted by parametric variation of inputs to models to examine the effect on output parameters. Sensitivities may be studied simply by examining a range of example input parameters that fall within expected ranges for fire scenarios of interest, or by systematically varying the input by specific amounts. The systematic variation of parameters can be accomplished deterministically (by incrementing inputs with a specified formula) or randomly using methods like Latin Hypercube Sampling.

5.1 Parametric Analysis

5.1.1 International Benchmarking and Validation Exercise # 1

Introduction

The following benchmark exercise was conducted and is presented here to examine the sensitivities of the CFAST code to variations in input parameters that fall within expected ranges for a typical NPP fire scenario.

A representative emergency switchgear room for a Pressurized Water Reactor (PWR) was selected for the study. The room is 15.2 m (50 ft) deep x 9.1 m (30 ft) wide and 4.6 m (15 ft) high. The room contains the power and instrumentation cables for the pumps and valves associated with redundant safety systems. The power and instrument cable trays run the entire depth of the room, and are separated horizontally by a distance, d . The cable trays are 0.6 m (~24 in.) wide and 0.08 m (~3 in.) deep. A simplified schematic of the room, illustrating critical cable tray locations, is shown in Figure 5.1*. The room has a door, 2.4 m x 2.4 m (8 ft x 8 ft), and a mechanical ventilation system with a flow rate of 5 volume changes per hour in and out of the room.

There are two parts to the exercise. The objective of Part I is to determine the maximum horizontal distance between a specified transient (trash bag) fire and tray A that results in the ignition of tray A. Part II examines whether the target cable tray B will be damaged for several heat release rates of the cable tray stack (A, C2, and C1), and horizontal distance, d . The effects of the fire door being open or closed, and the mechanical ventilation on or off, are examined in both parts of the benchmark exercise.

In order to provide a comprehensive discussion, the results of Part I of the analysis are presented here. The results of the analyses of Part II of the Benchmark Exercise with CFAST, along with several other fire models, may be found in NRC, 2002. The major sub-models used in CFAST for the scenarios specified in the benchmark exercise are (1) combustion chemistry (tracking O₂, and species); (2) plumes and layers; (3) vent flow, including forced ventilation; and (4) heat transfer, especially radiation and convection to the target. The following presents the major highlights of the results obtained for the analysis of the benchmark exercise. The trends of various parameters are examined to verify the adequacy of the basic sub-models for the specific scenarios, and to examine sensitivities.

The measured heat release rate of a large trash bag was used as input for the simulation as shown in Figure 2. In order to conduct a simplified and conservative analysis, the target is assumed to be a single power cable with a diameter of 50 mm at the bottom left corner of the cable tray A. Consistent with the target models in CFAST, the target cable is represented as a rectangular slab oriented horizontally with a thickness of 50 mm. The cable is assumed to ignite when the centerline of the cable reaches 643 K. Table 1 summarizes the cases

for Part I of the benchmark exercise. The peak heat release for the trash bag fire (Figure 2) for Part I is ~ 350 kW, and peaks at ~ 150 s.

* Figures for this section will be inserted later

Table 5-1: Summary of Cases for Part I

	Distance Between Trash Bag & Cable	Door	Ventilation System
Base Case	2.2 m	Closed	Off
Case 1	.3+		
Case 2	.9		
Case 3	1.5		
Case 4		Open	
Case 5			On

* For simulations with the door closed, a crack (2.4 m x 0.005 m) at the bottom of the doorway was assumed. +A value in a cell indicates the parameter was varied from the base case.

Base Case

Figure 3 shows the predicted oxygen depletion for the Base Case. The oxygen concentration in the lower layer stays approximately constant, as would be expected. The oxygen concentration in the upper layer decreases by ~ 1 % to 19.2 %. Therefore, the fire will not be limited by oxygen in this fire scenario.

Figure 2 also shows the plume flow development during this scenario. The main plume flow increases rapidly at the initiation of the fire, and does not follow the fire heat release rate, as expected. CFAST over predicts mass entrainment at the initial stages of the fire because of the plume height used in the calculation of the entrained air. Initially, the plume height is assumed to be from the fire to the ceiling. This leads to an over prediction of the initial mass flow to the upper layer, and the rate of descent of the gas layer interface.

Figure 4 shows the hot gas layer (HGL) temperature and the interface height development. The upper layer temperature peaks at ~ 230 s, about 80 s after the fire peaks, due to the lag time for the heating of the gas by the fire. In this scenario, the upper layer temperature increases only about 50 K. After peaking, the upper layer temperature decreases with time due to the heat loss to the boundaries. The interface height decreases rapidly initially due to high plume flow (see Figure 2). The rate of descent of the interface height decreases after ~ 230 s when the HGL temperature has peaked. The hot gas layer is prevented from reaching the floor due to air inflow at the crack below the door caused by a negative pressure in the compartment (see Figure 5).

Figure 5 shows the pressure development, and the resulting flows in and out of the compartment. The pressure peaks at ~ 150 s when the fire heat release rate peaks, as would be expected. The pressure decreases after the fire peaks due to outflow from the compartment at the crack under the door, and swings to a negative value. The small oscillations in the pressure after ~ 250 s is due to the small fluctuations in the heat release rate. The peak in the outflow is consistent with the pressure profile, and the outflow goes to zero when

the pressure in the compartment is less than the outside. The initiation of inflow is consistent with the pressure profile, and is much less than the outflow. The small oscillation of the inflow is caused by the fluctuations in the pressure.

Figure 6 shows the components of the heat flux to the target. The radiative flux on the target from the fire follows the fire heat release rate curve, as expected. The radiative flux on the target (lower side) from the hot gas increases at the point (~100 s) when the interface height reaches the target. The radiative flux from the hot gas on the target peaks at ~ 280 s, 50 s after the upper layer temperature peaks, and decreases in a similar manner to the upper layer temperature. The lag between the peak in the radiative flux from the hot gas and the upper layer temperature is because of the time needed for hot gas layer growth under the target. The convective flux is negative initially because the target temperature is greater than the lower layer temperature. The convective flux becomes positive and starts to increase at ~ 100 s when the hot gas layer interface reaches the target, as expected. The convective flux peaks at ~ 230 s when the upper layer temperature peaks, as expected.

Cases 1 to 3

Figure 7 shows the target surface temperatures versus time for the Base Case and Cases 1 -3. For the Base Case, the target temperature peaks at ~ 290 s, ~ 140 s after the fire and target flux reaches its peak due to the thermal inertia of the target. The target surface temperature only increases ~ 20 K for this case. Figure 8 is a plot of the maximum surface temperatures of the target versus the distance between the fire and target. The plot could be approximated by a straight line and does not show a rapid increase in temperature with decreasing distance between the fire and the target. This can be explained by examining Case 1. The radiative flux from the hot gas layer is the same as the Base Case since the only difference between the cases is the fire location. The radiation from the fire is the largest in Case 1 because the fire is closest to the target; however, the peak convective flux is half of that in the Base Case (100 vs. 200 W/m²). The decreased peak convective flux is caused by a smaller difference in temperature between the hot gas layer and the target surface (the target surface temperature is higher due to higher radiative flux).

Cases 4 and 5

The following presents some key features of the results of Case 4 and 5. Figure 9 shows the development of the interface height for Case 4 versus the Base Case. The interface height approaches a constant value at ~ 140 s, after the HGL reaches the top of the door at ~ 100 s. Figure 10 shows the development of the upper layer outflow and lower layer inflow after the HGL interface reaches the door at ~ 100 s, indicating the establishment of a neutral plane below the top of the door (at ~ 2.2 m). Figure 11 shows the HGL temperature development for Case 4 and 5. The HGL temperature for Case 4 is less than the Base Case after ~ 270 s because of the outflow of hot gas from the upper layer (which reaches its peak value at ~ 200 s) through the door, and higher plume flow. The HGL temperature for Case 5 is less than that in the Base Case after ~ 100 s when the HGL reaches the mechanical vents, and ambient air is injected into and hot gas ejected from the hot gas layer.

Figure 12 shows the development of flows in the mechanical ventilation system for Case 5. The transitions in flows from the mechanical vents in and out of the gas layers occurs at about ~ 100 s when the HGL reaches the mechanical vents. The mass flow rate into the upper layer is larger than the mass flow rate out of the upper layer because mechanical ventilation flows in CFAST are specified as volumetric flow rates. The temperature of the flow out of the compartment is higher than the ambient conditions of the flow into the compartment. Figure 3 shows that the oxygen concentration in the HGL layer is greater in Case 5 than the Base Case after ~ 160 s when the HGL reaches the mechanical vents, and air at ambient conditions is injected

in to the upper layer. Figure 7 shows the target surface temperature for Case 4 and 5 along with the other cases. The target surface temperature for Case 4 and 5 is less than in the Base Case because of cooler hot gas layer temperatures. The cable temperature does not approach the point of ignition (643 K) in any of the cases analyzed.

The above analyses of the results for Part 1 demonstrates that CFAST provides a comprehensive treatment of most physical phenomena of interest in the scenarios analyzed. The results indicate that the trends predicted by the sub-models in CFAST are accurate. The sensitivities are expected based on examination of the physical variation of phenomena in the cases.

5.2 Probabilistic Sensitivity Analysis

5.2.1 VTT Sensitivity Analysis with Probabilistic Fire Simulator

Sensitivity analysis for CFAST was performed using a risk analysis tool called Probabilistic Fire Simulator (PFS). The tool is used to estimate the failure probability of redundant cables in a cable tunnel fire and the failure and smoke filling probabilities of an electronics room during an electrical cabinet fire. PFS uses a combination of Monte Carlo simulations using a commercially available simulation software, @RISK, and a two-zone model from CFAST to model smoke spreading and gas temperature during the fire. The main output from the combined tool is the automatic generation of distributions of the selected result variables and their sensitivities to the input variables. Some examples of the outputs include times of component failure, fire detection, and flashover. Sensitivity of the output variables to the input variables is calculated in terms of the rank order correlations. Sensitivity calculations are performed using plausible input data distributions to find out the most important parameter.

The sensitivity of the output y to the different input variables x is studied by calculating the Spearman's rank-order correlation coefficients (RCC). A value's "rank" is determined by its position within the min-max range of possible values for the variable.

RCC is then calculated as

$$RCC = \frac{1-6\sum d^2}{n(n^2-1)}$$

Where d is the difference between ranks of corresponding x and y , and n is the number of data pairs. The RCC is independent of the distribution of the initial variable.

Two example cases have been studied: a fire in a nuclear power plant cable tunnel and a fire in an electronics room. The studies showed that CFAST two-zone model can be used to predict the thermal environment of a cable tunnel fire, at least in its early stages. The effects of the tunnel geometry and fire source properties are studied by sampling the input variables randomly from the distributions. The input distributions are based on data collected from the power plant. The results of the tunnel scenario show that the heat detector gives an alarm before the loss of the redundant cables, with a very high probability. This however doesn't take into consideration the reliability of the heat detector. According to the sensitivity measures the most important parameters for the safety of redundant cables are i) the growth rate of the fire, ii) the screen providing a physical separation of the burning and target cable trays, iii) the critical temperature of the cable, iv) the radius (mass) of the cable. However the failure time is also sensitive to the length of the virtual room of the fire origin, which is a purely numerical parameter.

5.2.2 Sensitivity Analysis

A sensitivity analysis considers the extent to which uncertainty in model inputs influences model output. For a sensitivity analysis, this uncertainty includes not only that inherent in the input of data for specific scenarios by the model user, but also uncertainty in empirical data or numerical parameters in the model such as the time step size used by the model to obtain a solution. Among the purposes for conducting a sensitivity analysis are to determine

- the important variables in the models,
- the computationally valid range of values for each input variable, and
- the sensitivity of output variables to variations in input data.

Conducting a sensitivity analysis of a complex model is not a simple task and it will differ depending on the application. CFAST typically requires the user to provide numerous input parameters that describe the building geometry, compartment connections, construction materials, and description of one or more fires.

Iman and Helton [97] studied the sensitivity of complex computer models developed to simulate the risk of severe nuclear accidents which may include fire and other risks. Consistent with the work of Iman and Helton [97], ASTM E1355 [1] provides overall guidance on typical areas of evaluation of the sensitivity of deterministic fire models. These areas may involve one or more of the following techniques: finite difference or direct analysis methods that provide an explicit solution of the sensitivity equations associated with the governing equations of the model, factorial design or Latin hypercube sampling studies that investigate the effect of varying the input parameters and consequential interactions between parameters that may be deemed important, and global or response surface methods that investigate the overall behavior of model outputs for a desired range of inputs.

This chapter provides a review of the sensitivity studies that have been conducted using CFAST with an emphasis on uncertainty in the input. Other sensitivity investigations of CFAST are also available [98],[99],[100].

5.2.2.1 Factorial Design Studies

Khoudja [101] has studied the sensitivity of an early version of the FAST [2] (predecessor to CFAST) model with a fractional factorial design involving two levels of 16 different input parameters. The statistical design, taken from the texts by Box and Hunter [102], and Daniel [103] reduced the necessary model runs from more than 65,000 to 256 by studying the interactions of input parameters simultaneously. The choice of values for each input parameter represented a range for each parameter. The analysis of the FAST model showed sensitivity to heat loss to the compartment walls and to the number of compartments in the simulation. Without the inclusion of surface thermophysical properties, this model treats surfaces as adiabatic for conductive heat transfer. Thus, consistent sensitivity should be expected. Sensitivity to changes in thermal properties of the surfaces were not explored.

Walker [104] discussed the uncertainties in components of zone models and showed how uncertainty within user-supplied data affects the results of calculations using CFAST as an example. The study systematically varied inputs related to the fire (heat release rate, heat of combustion, mass loss rate, radiative fraction, and species yields) and compartment geometry (vent size and ceiling height) ranging from $\pm 1\%$ to $\pm 20\%$ of base values for a one-compartment scenario. Heat release rate and ceiling height are seen to be the dominant input

variables in the simulations. Upper layer temperature changed $\pm 10\%$ for a $\pm 10\%$ change in heat release rate. Typical variation of ± 10 s in time to untenable conditions for a 20% variation in the inputs was noted for the scenarios studied.

Peacock *et al.* [98] studied the sensitivity of CFAST for a range of input parameters. They used simple factorial designs for model inputs deemed important to investigate local behavior of important model outputs along with response surface methods to evaluate overall model behavior. Results of the parametric investigations are discussed below and the application of response surface methods is summarized in section ?. Both are discussed in more detail in reference [98].

5.2.2.1.1 Model Inputs and Outputs

Most studies of modeling related to fire hazard and fire reconstruction present a consistent set of variables of interest to the model user [105],[106],[107]: upper and lower gas layer temperatures, gas species concentrations, and layer interface position. Other variables of interest include

- mass pyrolysis and heat release rate,
- room pressure, and
- vent flow.

Although there are certainly other comparisons of interest, these will provide evidence of the sensitivity of the model to most model inputs. Tables 5 and 6 show typical inputs and outputs for the CFAST model

Consider the following fire scenario: The building geometry (figure 22) includes four rooms on two floors with horizontal, vertical, and mechanical vents connecting the rooms and venting to the outdoors. The fire source in one of the rooms on the lower floor is a medium growth rate t^2 fire [108] chosen to simulate a mattress fire [109] (figure 5-1).

Table 5-2: Typical Inputs for a Two-Zone Fire Model.

Parameter	Inputs (Items in bold are inputs that may vary due to error in measurements)
Ambient Conditions	Inside temperature and pressure Outside temperature and pressure Wind speed Relative humidity (0%-100%)
Building Geometry	Compartment width, depth, height , and surface material properties (conductivity, heat capacity, density, thickness) Horizontal Flow Vents: Height of soffit above floor, height of sill above floor, width of vent, angle of wind to vent, time history of vent openings and closings Vertical Flow Vents: Area of vent , shape of vent Mechanical Ventilation, Orientation of vent, Center height of vent, area of vent, length of ducts, diameter of ducts, duct roughness, duct flow coefficients, fan flow characteristics
Fire Specification	Fire room, X, Y, Z position in room, fire area Fire Chemistry: Molar Weight, Lower oxygen limit, heat of combustion, initial fuel temperature, gaseous ignition temperature, radiative fraction Fire History: Mass loss rate, heat release rate , species yields for HCN, HCl, H/C, O₂/C, C/CO₂, CO/CO₂

Table 5-3: Typical Outputs for a Two-Zone Fire Model.

Parameter		Output (typically time histories)
Compartment Environment	for each compartment	Compartment pressure and layer interface height
	for each layer and compartment	temperature, layer mass density, layer volume, heat release rate, gas concentrations (N_2 , O_2 , CO_2 , CO , H_2O , HCl , HCN , soot optical density), radiative heat into layer, convective heat into layer, heat release rate in layer
	for each vent and layer	mass flow, entrainment, vent jet fire
	for each fire	heat release rate of fire, mass flow from plume to upper layer, plume entrainment, pyrolysis rate of fire
	for each compartment surface	surface temperatures
Tenability		Temperature Fractional Exposure Dose (FED)

DRAFT
FOR
FORMAT
REVIEW
ONLY

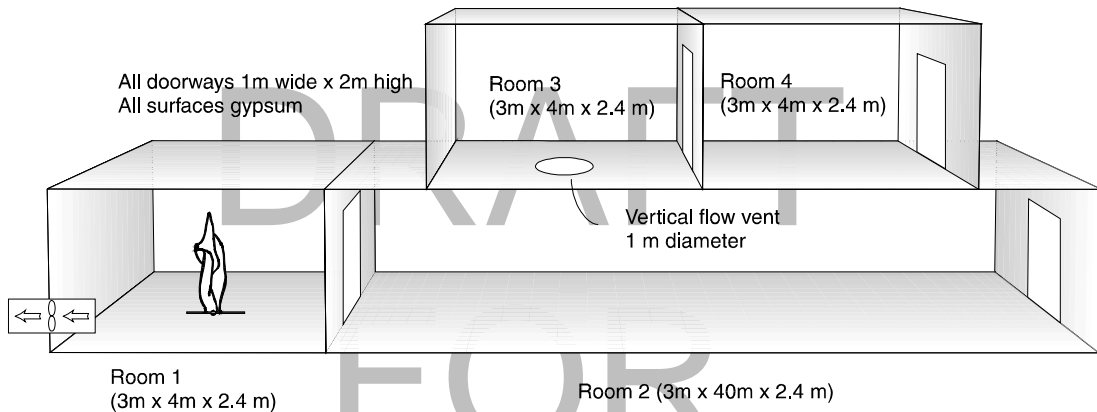


Figure 5-1. Building geometry for base case scenario.

FORMAT

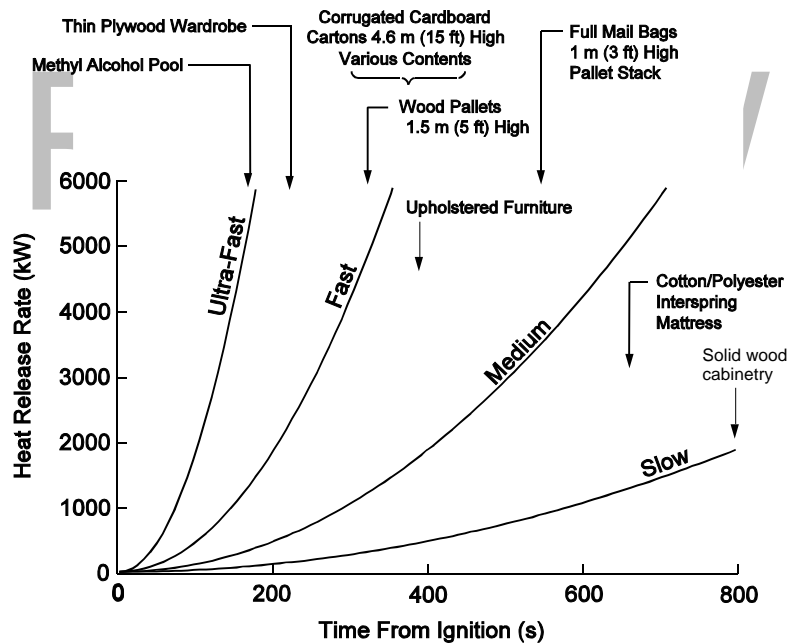


Figure 5-2 Characterization of heat release rate of growing fires as t^2 fires.

5.2.2.1.2

Sensitivity to Small Changes in Model Inputs

To investigate the sensitivity of the model, a number of simulations were conducted varying the input parameters about the base scenario discussed in the previous section. Both small ($\pm 10\%$) and larger (up to an order of magnitude) variations for selected inputs were studied. Varying most of the inputs by small amounts had little effect on the model outputs. **Figure 5-3** presents an example of the time dependent sensitivity of several outputs to a 10% change in room volume for the fire compartment in the scenario described above. For example, the pair of dotted-line curves labeled “Upper Layer Volume” were created by comparing the base case scenario with a scenario whose compartment volume was increased and decreased by 10%. The resulting curves presented on the graph are the relative difference between the variant cases and the base case defined by $(Variant\ value - Base\ value) / Base\ value$ for each time point. The graph shows that temperature and pressure are insensitive to changes in the volume of the fire room since a 10% change in room volume led to smaller relative changes in layer temperature and room pressure for all times. Upper layer volume can be considered neutrally sensitive (a 10% change in room volume led to about a 10% change in layer volume). Further, this implies that there is negligible effect on the average layer interface height. This is consistent with both experimental observations in open compartment room fires [110] and analytical solutions for single compartment steady-state fires [111]. For transient conditions early in the fire or when the fire burns out (illustrated in the figure at 300 s when the gas burner fire heat release rate goes to zero) higher uncertainties are noted. While these are transient effects, the early phases of the fire, in particular, may be important in calculating tenability for occupants during egress. While an uncertainty in the compartment

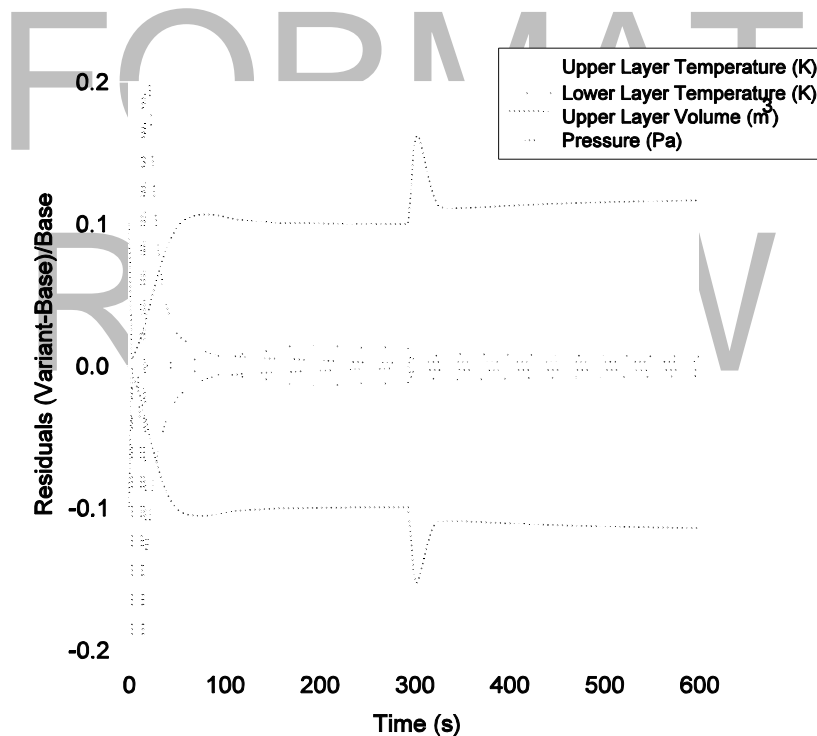


Figure 5-3. An example of time dependent sensitivity of fire model outputs to a 10% change in room volume for a single room fire scenario

volumes results in an equivalent uncertainty in calculated outputs, accurate specification of compartment dimensions within 5 % is often easily obtained.

In addition, **figure 5-3** shows a somewhat constant relative difference for the changes as a function of time. As suggested by Iman and Helton [97], an average relative difference could thus be used to characterize the model sensitivity for comparing individual inputs and outputs.

5.2.2.1.3 Sensitivity to Larger Changes in Model Inputs

To investigate the effects of much larger changes in the inputs, a series of simulations was conducted where the inputs were varied from 10 % to 400 % of base values. Simulations changing the heat release rate inputs from the base peak heat release rate of 750 kW are shown in **figure 5-4**.

Each set appears as families of curves with similar functional forms. This indicates that the heat release rate has a monotonic effect on the layer temperatures, with not as clear an effect on upper layer volume due to compartment filling and flow between compartments. Like the sensitivity to compartment volume in the previous section, changing the heat release rate by a factor of two results in a factor of two change in the upper layer temperature. Thus, in absolute terms, heat release rate and compartment volume are equally sensitive. However, compartment volume is easily determined accurately while heat release rate is typically estimated with far less accuracy and may be uncertain to within an order of magnitude or larger.

In the majority of fire cases, the most crucial question that can be asked by the person responsible for fire protection is: “How big is the fire?” Put in quantitative terms, this translates to: “What is the heat release rate of this fire?” Recently the National Institute of Standards and Technology (NIST) examined the pivotal nature of heat release rate measurements in detail [?]. Not only is heat release rate seen as the key indicator of real-scale fire performance of a material or construction, heat release rate is, in fact, the single most important variable in characterizing the “flammability” of products and their consequent fire hazard. Much of the remainder of this paper focuses on heat release rate as an example for examining sensitivity analysis.

DRAFT
FOR
REVIEW
ONLY

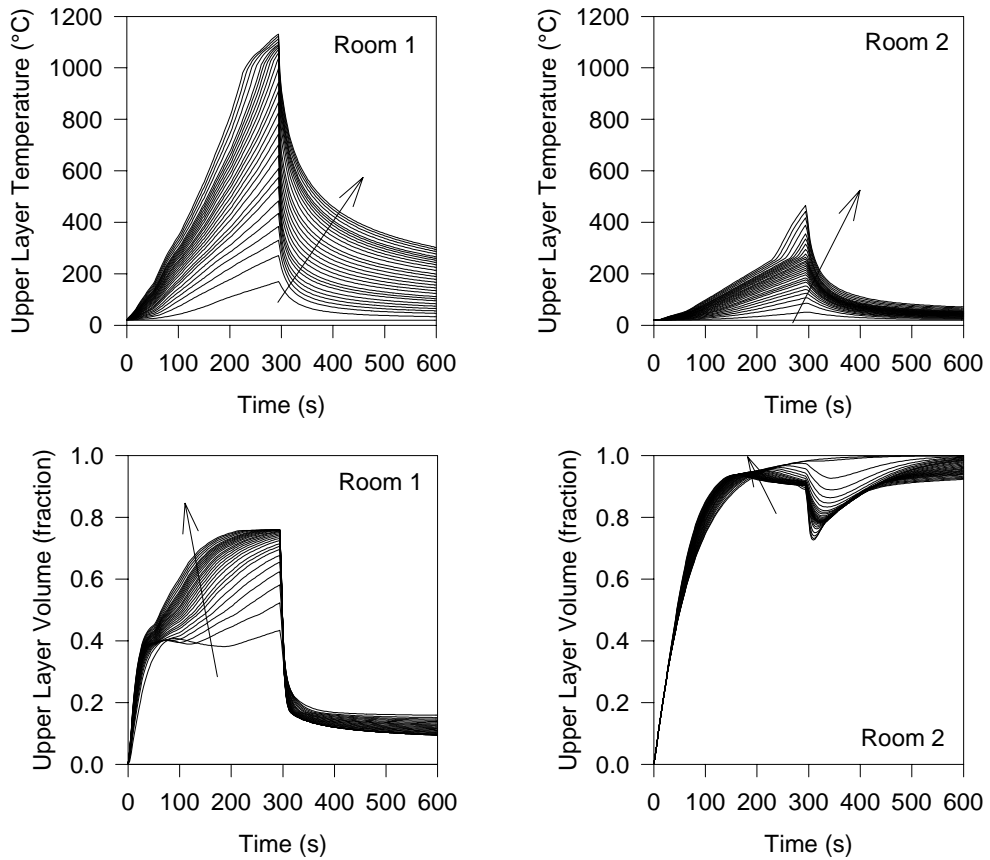


Figure 5-4. Layer temperatures and volumes in several rooms resulting from variation in heat release rate for a four-room growing fire scenario.

REVIEW
ONLY

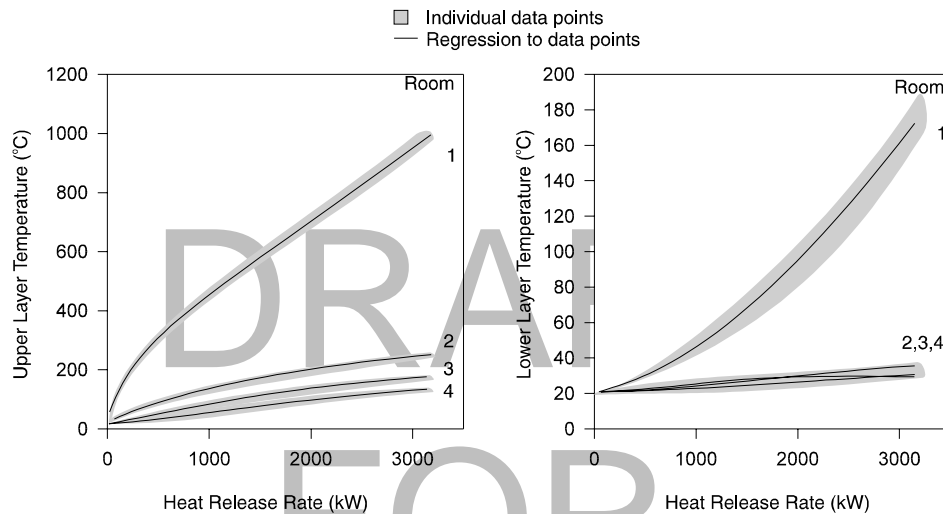


Figure 5-5. Comparison of the time dependent heat release rate and layer temperatures in several rooms for a four-room growing fire scenario.

5.2.2.2 Response Surface Studies

A next step beyond the simple plots presented in **figure 5-4** is a cross-plot of outputs of interest against heat release rate. **Figure 5-5** presents plots of the upper (presented in **figure 5-4**) and lower layer temperatures plotted against the heat release rate for all the simulations. The shaded areas on **figure 5-5** shows the locus of all the individual data points representing all the layer temperature time points for all the simulations shown in

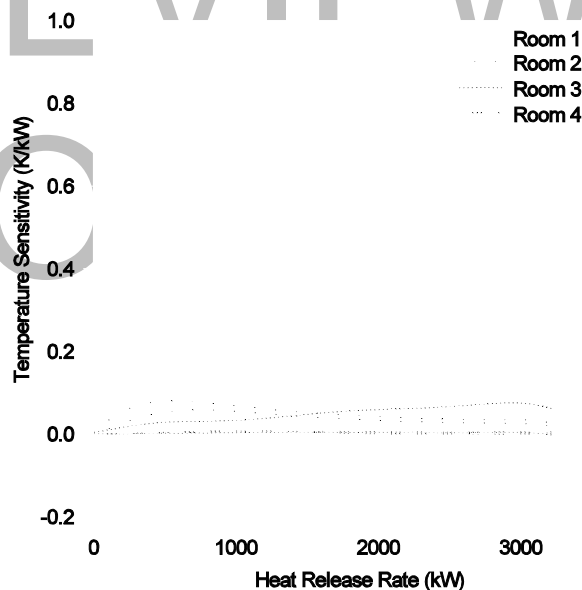


Figure 5-6. Sensitivity of temperature to heat release rate for a four-room growing fire scenario.

figure 5-4. For each room, a regression fit to the data for each room overlays the locus. The temperature curves for both upper and lower layer temperature in all four rooms (**figure 5-5**) show a strong functional dependence on heat release rate. Even for the wide variation in inputs, the heat release rate provides a simple predictor of the temperature in the rooms. In addition, this relationship allows calculation of the sensitivity of the temperature outputs to the heat release rate inputs as a simple slope of the resulting correlation between heat release rate and temperature.

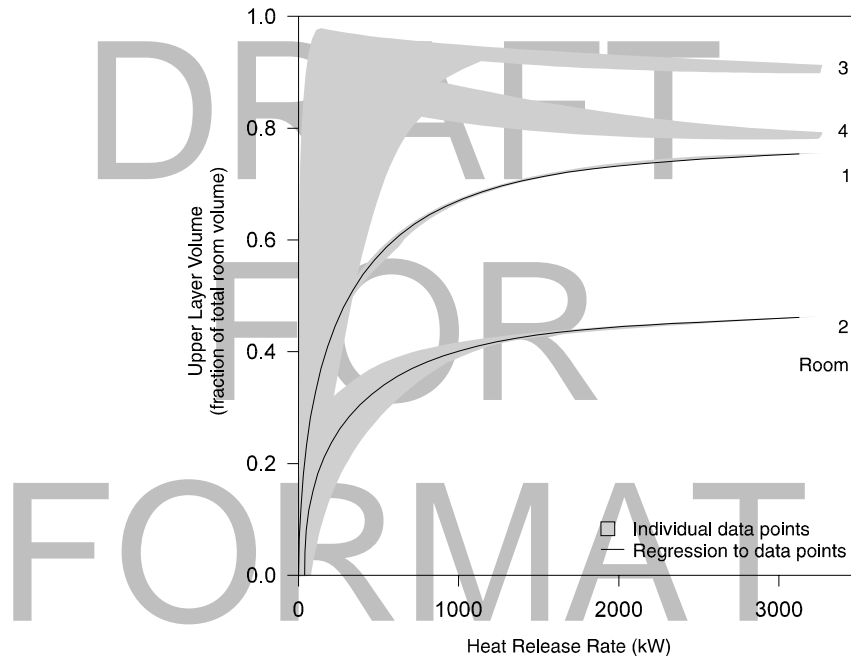


Figure 5-7. Comparison of heat release rate and upper layer volume in several rooms for a four-room growing fire scenario.

Figure 5-6, simply a plot of the slope of the regression curves in **figure 5-5**, shows this sensitivity, $\partial(T)/\partial(\text{heat release rate})$, for the four-room scenarios studied and represents all time points in all the simulations in which the peak heat release rate was varied from 0.1 to 4.0 times the base value. Except for relatively low heat release rate, the upper layer temperature sensitivity is less than 1 K/kW and usually below 0.2 K/kW. Not surprisingly, the layer that the fire feeds directly is most sensitive to changes. The lower layer in the fire room and all layers in other rooms have sensitivities less than 0.2 K/kW. This implies, for example, that if the heat release rate for a 1 MW fire is known to within 100 kW, the resulting uncertainty in the calculation of upper layer temperature in the fire room is about ± 30 K.

For upper layer volumes (**figure 5-7**) of both rooms 1 and 2, it is again a simple correlation between heat release rate and volume fraction (upper layer volume expressed as a fraction of the total room volume). The shaded gray area on the graph shows the locus of all individual time point values of temperature and volume in the four compartments of the simulation. The correlations for the upper layer volumes of room 1 and room 2 could also be differentiated as was done for the temperature correlations to obtain sensitivities for the upper layer volume. For rooms 3 and 4, the relationship is not as clear. The flow into the layers of these rooms is more complicated than for rooms 1 and 2, resulting from flow from the first floor through a vent in the floor of

room 3 and from a vent to the outside in room 4. However, even these rooms approach a constant value for higher heat release rate values, implying near zero sensitivity for high heat release rate.

Figure 5-8 presents the effect of both peak heat release rate and vent opening (in the fire room) on the peak upper layer temperature. In this figure, actual model calculations, normalized to the base scenario values are indicated by circles overlaid on a surface grid generated by a spline interpolation between the data points. At high heat release rate and small vent openings, the fire becomes oxygen limited and the temperature trails off accordingly, but for the most part, the behavior of the model is monotonic in nature. Although more laborious, the approaches used to calculate sensitivities for single variable dependencies illustrated earlier are thus equally applicable to multivariate analyses.

From the surface, it is clear that heat release rate has more of an effect on the peak temperature than does the vent width. Until the fire becomes oxygen limited, the trends evident in the surface are consistent with expectations – temperature goes up with rising heat release rate and down with rising vent width. The effects are not, of course, linear with either heat release rate or vent opening. Plume theory and typically used algorithms for estimating upper layer temperature in a single room with a fire [112] suggest that the dependence is on the order of $Q_f^{2/3}$ for heat release rate and $A\sqrt{h}$ for the vent opening where A is the area of the vent and h is the height of the vent. Although these correlations are based on a simple analysis of a single room fire, the dependence suggested is similar to that illustrated in **figure 5-8**.

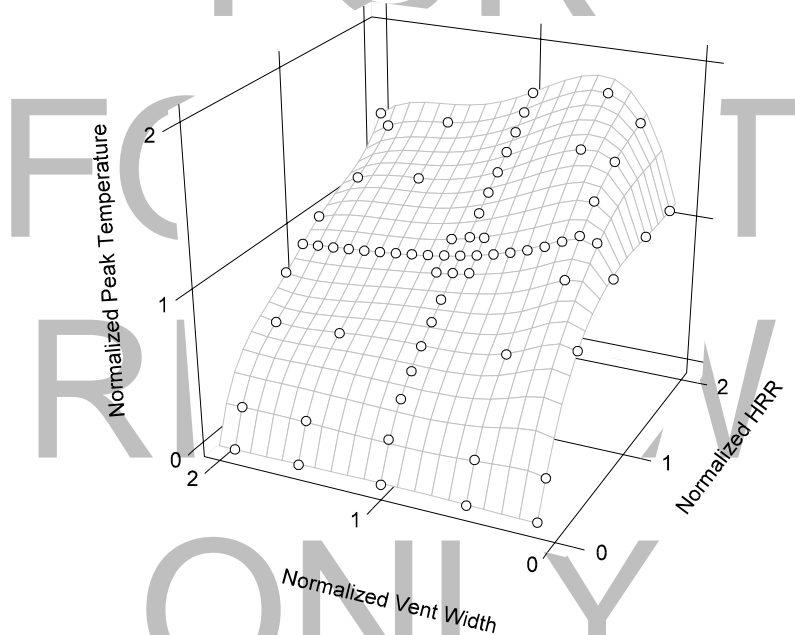


Figure 5-8. Effect of both heat release rate and vent opening size on upper layer temperature for a four-room growing fire scenario.

5.2.2.3 Latin Hypercube Sampling Studies

Notarianni [100] developed an iterative methodology for the treatment of uncertainty in fire-safety engineering calculations to identify important model parameters for detailed study of uncertainty. She defines a nine-step process to identify crucial model inputs and parameters, select sampling methods appropriate for the important parameters, and evaluate the sensitivity of the model to chosen outcomes. Both factorial designs and Latin hypercube sampling are included in a case study involving the CFAST model. In a performance-based design of a sixteen-story residential structure, the impact of model uncertainty on a chosen design and inclusion of residential sprinklers in the design would effect the resulting safety of the design. For a seven-compartment scenario representing one living unit in the structure, distributions of input variables based on Latin hypercube sampling of selected ranges of the inputs were developed and used as input for a series of 500 CFAST simulations for the scenario. The results of the calculations are presented in a series of cumulative distribution functions which show the probability that a chosen criterion of the design is exceeded within a given time. Depending on the evaluation criterion chosen, times to unacceptable designs varied by as little as 10 s to as much as 470 s. To determine important input variables, Notarianni used a multivariate correlation of the input and output variables to determine statistical significance at a 95 % confidence level. Input variables deemed important in the analysis included fire-related inputs (growth rate, heat of combustion, position of the base of the fire, and generation rates of products of combustion) and door opening sizes. Other inputs were determined to be less important.

5.2.2.4 Summary

Many of the outputs of the CFAST model are quite insensitive to uncertainty in the input parameters for a broad range of scenarios. Not surprisingly, heat release rate was consistently seen as the most important variable in a range of simulations. Heat release rate and related variables such as heat of combustion or generation rates of products of combustion provide the driving force for fire-driven flows. For CFAST, all of these are user inputs. Thus, careful selection of these fire related variables are necessary for accurate predictions. Other variables related to compartment geometry such as compartment height or vent sizes, while deemed important for the model outputs, are typically more easily defined for specific design scenarios than fire related inputs. For some scenarios, such as typical building performance design, these vents may need to include the effects of leakage to insure accurate predictions. For other scenarios, such as shipboard use or nuclear power facilities, leakage (or lack thereof) may be easily defined and may not be an issue in the calculations.

DRAFT
FOR
FORMAT
REVIEW
ONLY

Chapter 6 Model Validation

This chapter initially summarizes the studies used for the validation of the CFAST fire model. This is followed by a discussion of the applicability of the results of the validation studies to the NPP scenarios identified in Chapter 2, accuracies of the prediction of parameters of interest for these scenarios, and the final validation results.

6.1 Summary of Validation Studies

Four blind validation studies conducted recently by the NRC as part of the International Collaborative Fire Model Project (ICFMP) are summarized here, as well as validation studies conducted in the past by various organizations.

Blind Studies

6.1.1 International Benchmarking and Validation Exercise # 2

Specification of Exercise

The objective of the second benchmark exercise [Miles, 2004] of the International Collaborative Fire Model project (ICFMP) was to examine scenarios that are more challenging for zone models, in particular to fire spread in a multi-level larger volume representative of turbine halls in nuclear power plants. The full specification of the benchmark exercise and results are documented in Miles, 2004.

Part I was based on a series of full scale experiments inside the VTT Test Hall (Fig. 6-1) in Finland, for which the sloping roof provided a challenge to zone models in particular. The dimensions of the test hall was 19 m high by 27 m long by 14 m wide (i.e. floor area 378 m² and total volume 5409 m³). Each case involved a single heptane pool fire, in the range 2 to 4 MW, for which there were experimental measurements of gas temperature at three thermocouple trees and above the fire source. For two cases the hall was nominally sealed, and 'infiltration ventilation' was incorporated by including small openings. For the third case mechanical exhaust ventilation (11 m³/s) was employed, and two doorway openings (3.2 m² each) were provided. There were no cable or other targets in the hall. Part I was conducted as an open exercise with the measured temperature data available to participants prior to the simulations. Eleven organizations participated in Part I, collectively making simulations with three zone models, two lumped parameter models and four CFD models. CFAST was one of the models used in the exercise (Miles, 2004).

Although for Part II there was no experimental measurements, formulating a hypothetical problem extended the scope of the exercise to examine the effect of a bigger lube oil pool fire, growing to approximately 70 MW, and a building with dimensions representative of a turbine hall 100 m by 50 m (i.e., floor area 5000 m²). The building was divided into a lower and an upper deck (each 10 m high), connected by two 5 m by 10 m open hatches (Fig. 2). Case 1 involved a nominally sealed building, for which small 'infiltration' openings were specified. The other cases included smoke exhaust ventilation using, in one case, purely natural ventilation and in the other a combination of natural and mechanical ventilation (i.e. natural wall vents combined with natural or mechanical roof vents respectively) as listed in Table 6.1.1. There were several cable and beam targets in this part of the exercise. For Part II, there were nine participating organizations, making simulations with three zone, one lumped parameter and four CFD models. CFAST was exercised for this scenario. The model predictions were compared against each other as there was no experimental data for this hypothetical problem. The complete validation of CFAST and FDS for this scenario can be found in Dey, 2004a.

Table 6.1.1 Summary of Cases

Table 6-1 Summary of Cases

Case 1	Case 2
Nearly-sealed. Two 1 m x 1 m openings.	Natural ventilation. 36 roof vents. 24 make-up wall vents.
Case 3	
Mechanical (extract) and natural ventilation. 194.4 m ³ s ⁻¹ mechanical exhaust ventilation (divided evenly between 36 roof vents) 24 make-up wall vents.	

Summary of Results - TBD

6.1.2 International Benchmarking and Validation Exercise # 3

Specification of Exercise

The Nuclear Regulatory Commission (NRC) and the National Institute of Standards and Technology (NIST) sponsored full-scale NPP compartment fire experiments for the International Collaborative Fire Model Project (ICFMP) to assess and validate fire computer codes for a range of nuclear power plant applications. The goal of this validation study was to provide data from a large-scale fire test series of a simulated nuclear power plant cable room. The experimental configuration was designed to mimic a cable room including representative mechanical ventilation (5 acph), a door (4 m²), and targets such as an electrical junction box, as well as vertically and horizontally aligned cables and cable trays.

The experiments consisted of heptane and toluene spray fires varying from 350 kW to 2 MW in heat release rate burning in a single compartment 7 m wide, 22 m long, and 4 m tall with a floor area and volume of 152 m² and 578 m³ respectively (see Figure 6-2). The experimental results were composed of 15 tests with more than 370 channels of data.

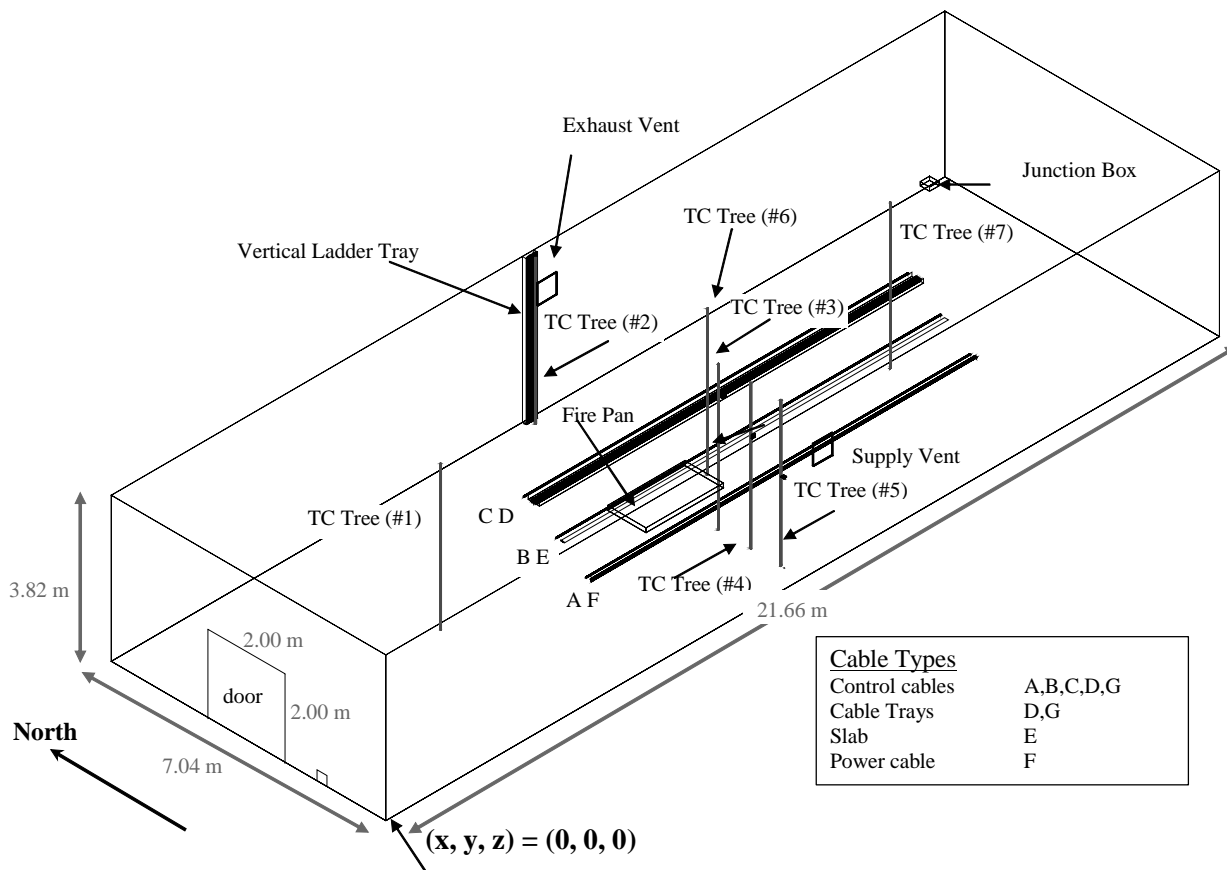


Figure 6-2 Compartment Isometric with thermocouple trees

REVIEW

ONLY

The test configuration and fire scenarios were selected to examine the following effects:

- Heat release rate
- Natural ventilation with an open door
- Mechanical ventilation system operation
- A combination of mechanical and natural ventilation
- Distance between fire and target
- Heating of cables and a PVC slab directly in the plume region

Experimental measurements and model predictions of the following parameters were compared:

- Heat release rates

- Compartment pressure
- Radiative and total heat flux at various targets in the compartment
- Surface and core cable temperatures and a PVC slab temperature
- Hot gas layer (HGL) temperature, depth, soot density, and concentrations of oxygen, carbon monoxide and carbon dioxide
- Gas temperatures at loss from walls, ceiling, and floor
- Total heat loss from the door and mechanical exhaust vent

Summary of Results - TBD

6.1.3 International Benchmarking and Validation Exercise # 4

Specification of Exercise

For the investigation of large compartment fires inside nuclear power plants, large kerosene pool fire experiments were performed at the iBMB (Institut für Baustoffe, Massivbau und Brandschutz) of Braunschweig University of Technology, Germany and used in ICFMP Benchmarking and Validation Exercise # 4. Depending on the plant specific scenario, such fires may lead to high temperatures, relative long-standing fire loads and low oxygen conditions. To be able to predict the potential consequences of such fires these kerosene pool fire experiments are important for the validation of available fire models and codes for this application.

Within the kerosene pool fire test series the fire compartment OSKAR of iBMB with a floor size of 3.6 m x 3.6 m and a height of 5.7 m (floor area 13 m² and 74 m³ total volume) has been used. This facility has openings for the natural ventilation (door - 2.1 m² and window - 0.7 m²) of the fire room. During the experiments, gas and surface temperatures, gas composition, velocities and heat flux densities were measured. Figure 6-2 shows the test facility. Plate targets composed of steel, concrete, aerated concrete, as well as a typical barrel that would contain radioactive waste were include in the experiments. The peak HRRs were between 3.5 MW to 18.8 MW in the compartment.

For measuring the temperatures inside the fire compartment 3 mm thick thermocouples were used. These were not protected against flame radiation. The position of the thermocouples were fixed within a grid in the compartment as shown in Figure 6-3. Surface temperatures were measured with thermo-wire, as well as “coated thermocouples.” Temperatures of typical targets in NPPs (concrete, aerated concrete, and steel) and the convective and radiative heat flux to the targets were measured by water cooled heat transfer blocks. Temperatures along three vertical lines inside the barrel were also measured. The velocity inside the plume, and at the door were measured by bi-directional probes. Gas concentrations and pressures were also recorded. Predictions of all these parameters were made with fire models exercised in the benchmarking and validation exercise.

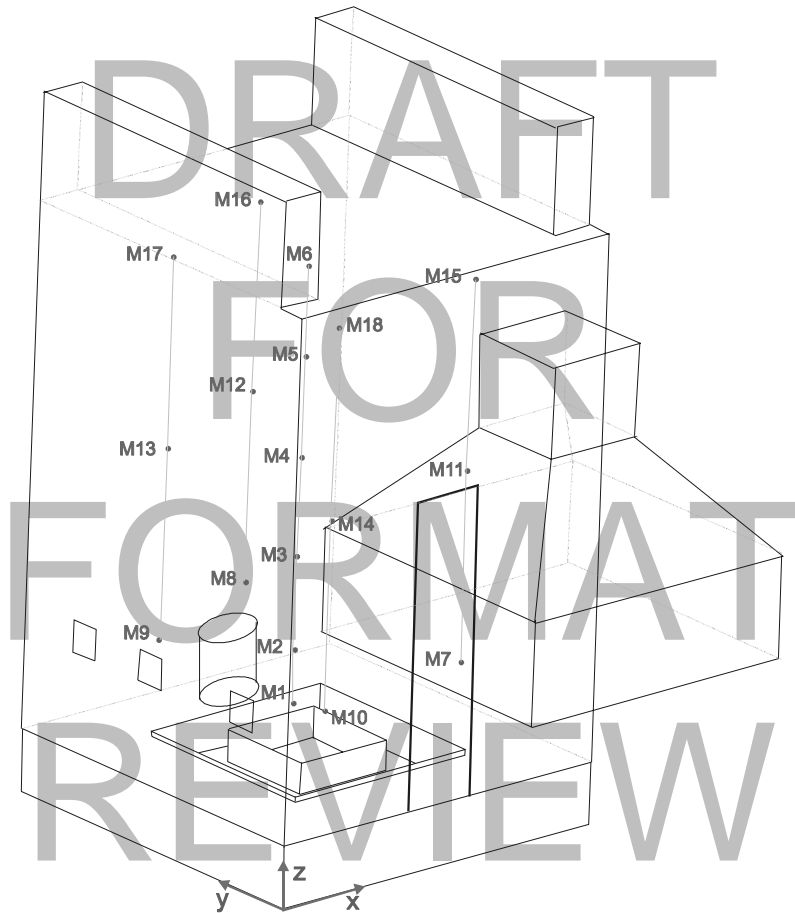


Figure 6-3 3-D View of Fire Compartment

Summary of Results - TBD

6.1.4 International Benchmarking and Validation Exercise # 5

Specification of Exercise

In a first large scale fire test series performed at the "Institut für Baustoffe, Massivbau und Brandschutz" (iBMB) of Braunschweig University of Technology in Germany cable flame spread experiments with different types of cable types and insulation materials were performed from 1999 until 2002. It could be shown that pre-heating of

the cables strongly increases the fire propagation risk such that high fire spreading velocities can be reached even in case of cable insulation materials with improved characteristics.

By means of the actual cable fire series the effects of a naturally ventilated fire of vertically routed cables (as worst case) with different cable insulation materials were investigated, in particular, the functional failure of equipment in case of such a cable fire. One of the major goals of these analyses is the applicability of various fire models of different types, such as zone models, lumped parameter codes and three-dimensional computational fluid dynamics codes (CFD models), for such cable flame spread scenarios with and without pre-heating of the fire compartment.

In the fire compartment of iBMB four large scale fire experiments with realistically routed vertical cable trays will be carried out. The cable fire experiments were carried out in a special fire compartment (iBMB test facility) with a floor 3.6 m x 3.6 m (13 m²) and room height of 5.6 m. The total volume of the room is 73 m³. A schematic of the room is shown in Figure 6-4. Pre-heating of the cables was accomplished with an ethanol pool fire of 1 m² resulting in the a peak HRR of 350 kW. The vertical cable tray is directly ignited by means of a propane gas burner. Natural ventilation takes place through an opening of 0.7 m width and 3.6 m height (2.1 m²). Smoke gases released are collected in a hood with a exhaust duct located over the opening leading to a smoke gas cleaning system.

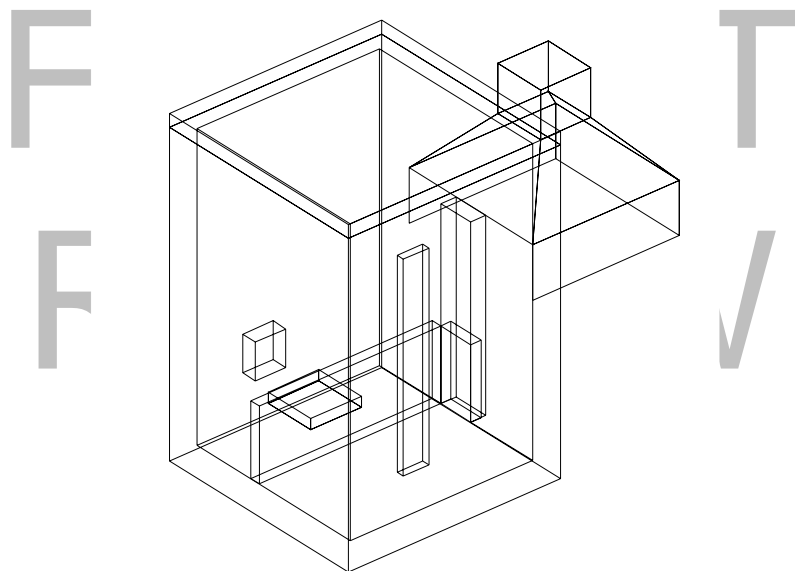


Figure 6-4 Three dimensional view of fire compartment

For each of the cable insulation materials, PVC and FRNC, two experiments will be carried out. One of these experiments with an identical amount and type of cable was performed without pre-heating, the other with pre-heating of the fire compartment. The main target in the compartment were cables in vertical cable trays.

The following parameters were measured and predicted :

- Temperatures above the fire (plume) at 7 heights,
- Temperatures in the fire compartment at 4 locations at each of 7 heights,
- Temperatures in front of the cable tray at 7 heights,
- Temperatures at the wall surfaces,
- Weight loss of the pool,
- Weight loss of the cable tray,
- Gas velocities and temperatures in the openings and in the plume,
- Difference Pressure distribution at 3 heights in the fire compartment,
- Gas analysis (O_2 , CO_2 und CO) at 2 heights in the fire compartment,
- Heat flux densities at the level of the cable bundles at 5 heights,
- Cable surface and inner temperatures at 9 heights,
- Gas velocity and temperature in the exhaust channel,
- Gas analysis (O_2 , CO_2 und CO) in the exhaust channel,
- Smoke gas density in the exhaust channel,
- Functional failure tests for the cables,
- Flame front height.

Summary of Results - TBD

Open Studies

6.1.5 HDR T51 and T52 Tests

Specification of Exercise

The HDR T51 and T52 test series were two of four test series performed in the HDR (Heiss-Dampf Reaktor) test facility located in the containment building of a decommissioned German nuclear reactor. The T51 and T52 test series were compared to results from three computational methods to examine their predictive capabilities: hand calculations, CFAST, and FDS. The two specific subtests that were used in these comparisons are the T51.23 gas fire experiment and the T52.14 oil pool fire experiment. The full description of these experiments and the comparison of the experimental results to the above mentioned computational

methods is located in Floyd, 2002. A brief description of the two subtests used in the comparisons is provided below.

The HDR facility is cylindrical in shape and divided into eight levels with each level subdivided into smaller compartments. A special set of fire test rooms was prepared at the 1.400 level of the containment building to conduct the T51 experiments and at the 1.900 level to conduct the T52 experiments.

The T51.23 test was a gas fire experiment involving a 1 MW propane gas fire located low in the containment building.

The dimensions of the compartment used in the T51 test series are shown in the table below.

Table 6-2: T51 Fire Compartment Dimensions

Compartment	Height(m)	Area (m ²)	Volume (m ³)	Doorway (m wide x m tall)	Hatch (m x m)
Fire Room	2.750	10	27	1.01x1.975	n/a
Doorway	1.9575	2	3	1.01x1.975	n/a
Hallway	2.485	11	22	1.80x2.485	n/a
Curtained	5.350	12	63	7.40x0.50	

The fire source used in the T51 test series was propane gas fed at a constant rate through one or more of six burners located along the wall of the fire room opposite the fire room doorway.

The table below shows some of the T51 experimental data compared to the simulation results from CFAST, FDS, and Hand Calculations.

Table 6-3: T51 Experimental Data

Quantity	Data	Hand Calc.	CFAST	FDS
Upper Temperature	730	834	870	8008
Layer Height	1.0	0.7	0.7	0.9

The T52.14 experiment was an oil fire test that ranged in power from 2 to 4 MW with the fire lasting approximately 30 minutes. The tests were conducted high in the containment building in a special fire compartment constructed on the 1.900 level just below the operating deck. The fuel for the fires in this experiment consisted of an initial volume of oil in a pool with surface area ranging from 1 m² to 3 m² in size. A

nozzle augmented the initial amount of fuel by feeding a continuous supply of oil once the initial pool was nearly consumed. The nozzle mass flow rate varied with each test. In this test series special attention was paid to the buoyant fire plume entering the upper dome.

The geometric details of the T52 Fire compartment are given in the table below.

Table 6-4: T52 fire Compartment Dimensions

Compartment	Height (m)	Area (m ²)	Volume (m ³)	Flow Area (m ²)
Fire Room	2.8	4.58x1.75=7.88	24	n/a
Doorway	1.975	0.95x0.78=0.74	2	3.0x0.95=2.85
Maintenance Hatch Area	2.485	3.6x3.05=10.98	52	1.85x2.6=4.81

The diagram below illustrates the basic layout of the fire rooms used in the T52 experiments.

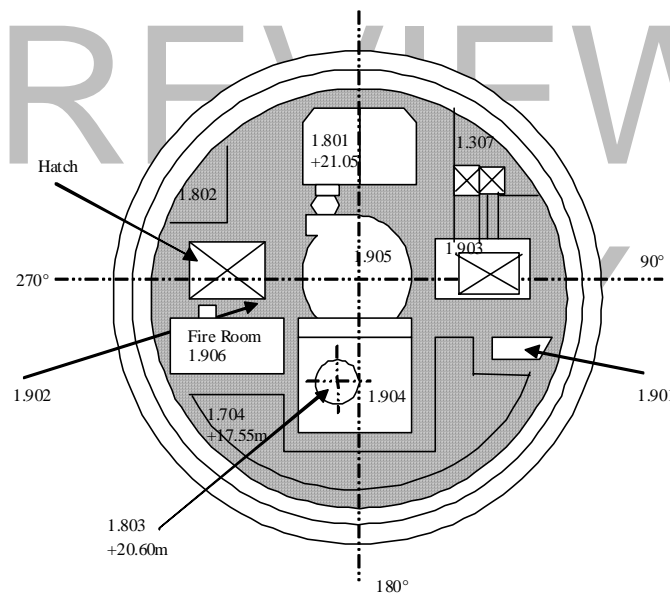


Figure 6-4 Layout of HDR T52 Test Facility

The fire source for the T52 test series was Shellsol T which is a hydrocarbon solvent manufactured by Shell Chemicals of Norway. It is a clear liquid that generates less soot than common fuel oils such as kerosene.

Summary of Results - TBD

6.1.6 NIST Multi-Compartment Tests

Specification of Exercise

The National Institute of Standards and Technology (NIST) conducted a series of comparisons between zone based modeling tool, CFAST, and a range of real-scale fire experiments. The purpose of conducting these comparisons was to determine, within limits, the accuracy of the predictions for those quantities of interest to a model user and to highlight the strengths and weaknesses of the underlying algorithms in the models to guide future improvements. A set of five different real scale fire tests were selected for comparison with CFAST (consolidated fire and smoke transport model). These tests were chosen to represent a range of challenges for the CFAST model. Three of the five tests involved a multi-compartment configuration. These tests included a three room test, a four room configuration, and a series of full-scale experiments conducted in a seven-story hotel with multiple rooms on each floor. The final configuration was chosen because it would be beyond the scope of fire models available at the time of testing. The three and four room configuration tests are briefly summarized here.

The three room data set is actually an average of a series of 11 replicate tests. In this test series simple steady-state gas burner fires are used as the fire source. The fire size was about 100 kW with a total volume of 100m³. The room configuration was similar to the illustration below.

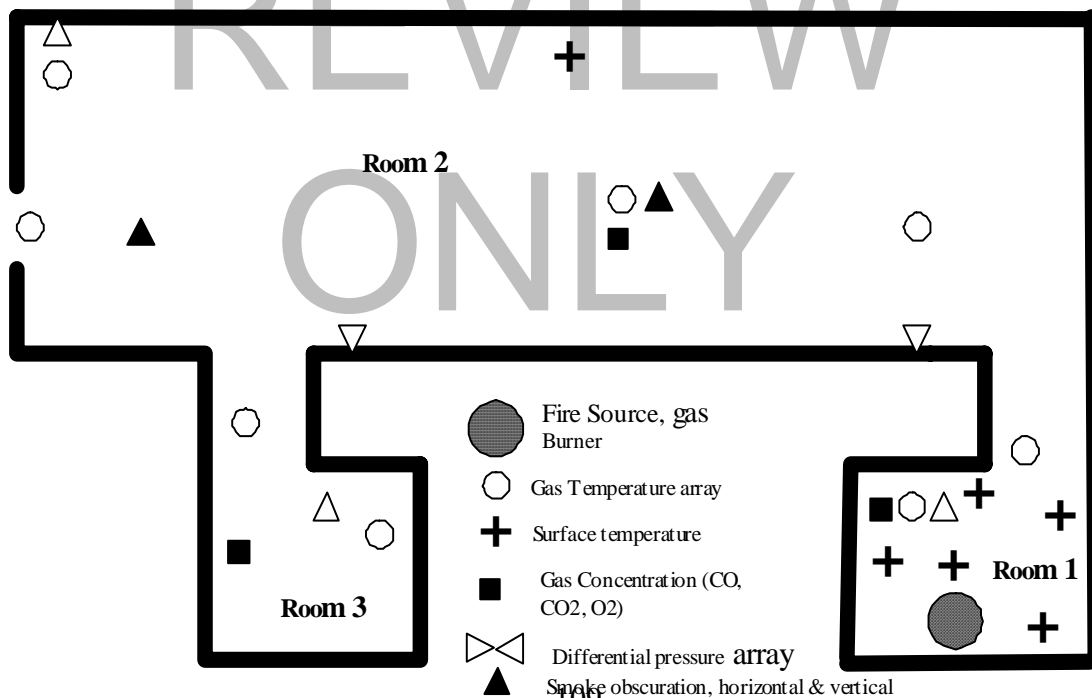


Figure 6-5 Three-room gas burner tests with a corridor.

The four room data set is part of a series of tests conducted with more complex gas burner fires than the previous test set. This test set provided larger time varying gas burner fires in a room-corridor configuration. The fire size was up to 1 MW with a total volume of 200 m³. The diagram below illustrates the layout of the four room test compartments.

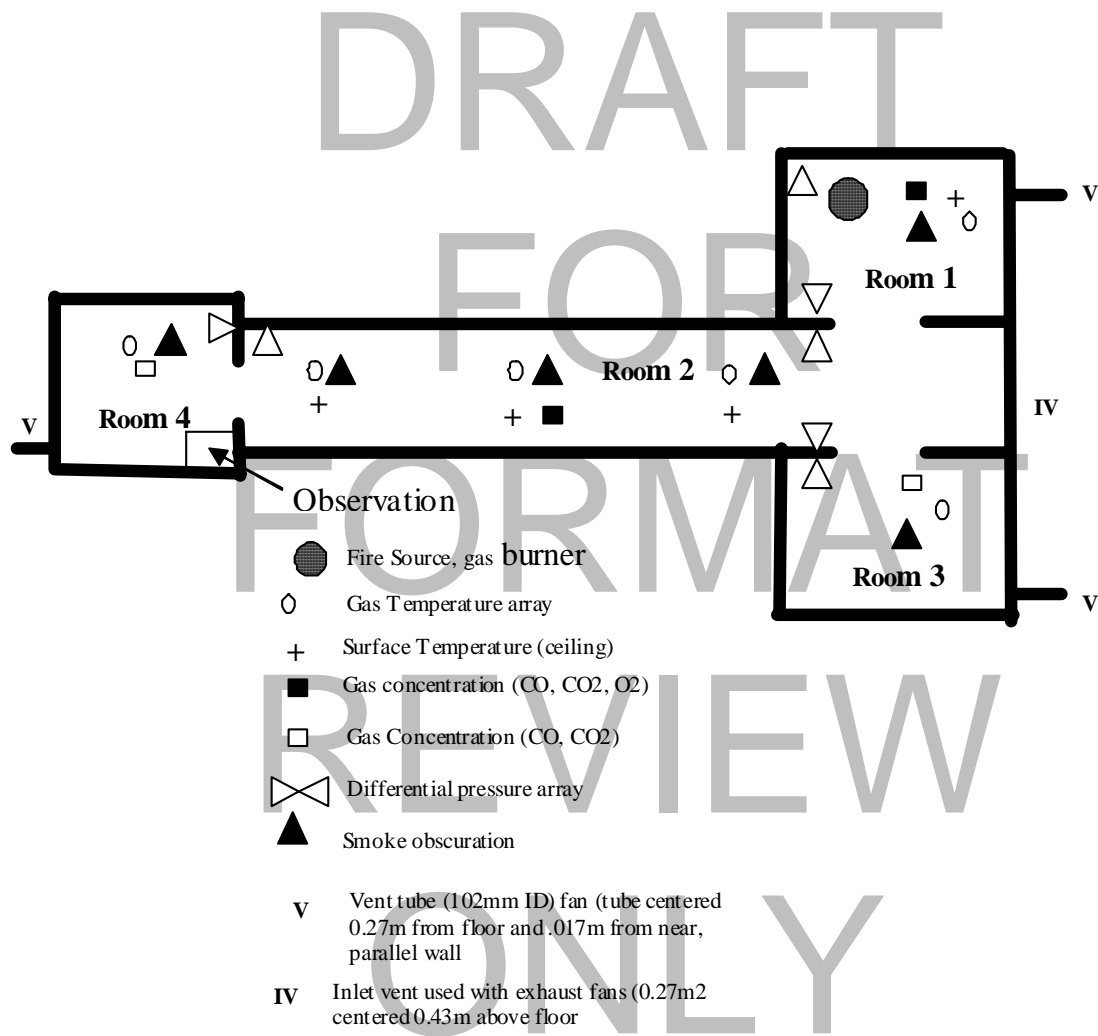


Figure 6-6 Four Room Gas Burner with a corridor

Summary of Results - TBD

6.2 Applicability of Validation Studies to NPP Scenarios

Chapter 2 presented the range of NPP fire scenarios for which the application of fire models is expected. The following specific attributes of the scenarios were defined to allow the evaluation of fire models for those applications:

- Fire Source
- Peak HRR
- Geometry
- Ventilation
- Targets
- Fire Protection

The attributes of the selected scenarios and presented in Chapter 2 are summarized in Table 6.1. For the purpose of correlating the Benchmark Exercises and other tests described in Section 6.1, the same attributes of the scenarios in these validation exercises described above are summarized in Table 6.2. A key parameter, the HRR per Unit Volume (kW/m³), is listed in the Tables for the NPP scenarios and the scenarios studied in the validation exercises. The HRR Per Unit Volume indicates the size of the fire in relationship to the compartment volume and is an important parameter in determining the bounds of the assumptions in the different types of models. CFAST incorporates a point source model for the fire with a correlation for plume flows developed from tests for fires with specific entrainment patterns. The point source model and plume correlations will not be valid when these conditions and ranges are exceeded in a fire scenario to be studied.

Based upon examination of the attributes of the postulated NPP fire scenarios (Table 6.5) and the attributes of the scenarios in the validation studies (Table 6.6), the correlation matrix of the two sets are shown in Table 6.3. Specific parameters in the benchmark exercises/other tests that are of interest for validating models for the NPP fire scenarios are identified in Table 6.7. The validation exercises include a range of conditions that are representative of the ranges specified in the NPP fire scenarios. In some cases, parameters from other tests are included if they are not available in the primary test series or they provide a broader range of conditions for validation.

Based upon examination of the attributes, the results of Benchmark Exercise # 3 may be used for the validation of cable target parameters (hot gas layer, ceiling jet, and cable surface temperatures , and total heat flux to the cable surface) in the switchgear, cable spreading, battery, and diesel generator rooms; control cabinet target parameters (hot gas layer temperature and total heat flux to wall surfaces) in the computer room, and human habitability conditions (gas temperature, CO, and visibility) in the control room. The attributes of Benchmark Exercise # 3 and these room scenarios are similar, including the HRR per Unit Volume. The performance criteria for cable damage may be simply specified in terms of hot gas layer, plume, or ceiling jet temperatures assuming the target instantaneously reaches the temperature of the hot gas it is exposed to. Alternately, the

performance criterion may be specified in terms of the total heat flux to the cable or the cable temperature. The alternate parameters are provided to allow the choice of establishing performance criteria.

Since there were no measurements made of plume temperatures in Benchmark Exercise # 3, Benchmark Exercise # 4 and 5, which represent a range of plume conditions, are used to determine the uncertainties of predicting plume temperatures as shown in Table 6.3. The HRR Per Unit Volume in the Pump room exceeds the conditions in Benchmark Exercise # 3, therefore, Benchmark Exercise # 4 which has tests with HRR per Unit Volume in this range is used for evaluating models for this scenario. Cable target parameters will be evaluated with the gas, plume, ceiling jet, and plate temperatures and flux. Plate temperature and fluxes are used to represent cable characteristics since Benchmark Exercise # 4 did not include any cable targets. Wall target parameters are evaluated with wall temperature and flux.

The turbine hall is a very large hall (28,000 to 215,000 m³) and presents unique challenges for model evaluation. Benchmark Exercise # 2, Part I is used for the evaluation of models for this scenario. The height of the hall in these tests, ~ 15 m, is similar to that of a turbine hall, although it is acknowledged that the floor area of a turbine hall is much greater. However, the test hall is one of the largest enclosures for which fire test data is available for comparison with model predictions. Gas and plume temperatures are available for evaluating cable and beam targets.

Recent or blind validation exercises are not available for the multi-compartment scenario. An old validation exercise conducted in 1988 for small rooms typical in office buildings is used to determine the uncertainties of predictions of gas temperatures, the only measured parameter relevant to cable damage. There were no measurements of heat flux or any target temperatures. The results of this validation exercise is included here for completeness, however, its use should recognize that multi-compartment configurations in NPPs would be significantly different from those in the old 1988 exercise for typical office buildings.

The multi-level scenario presents a unique challenge since these configurations are only present in industrial structures such as a nuclear power plant. Presently, there is no experimental data available that would allow the evaluation of key issues, such as vertical flow through horizontal hatches, in these scenarios. With the aim of including all available analysis for evaluating fire models for this scenario, the results of Benchmark Exercise # 2, Part II, is presented here. This exercise was a code-to-code comparison of model results for a hypothetical scenario that was developed to represent a multi-level turbine hall. The uncertainties in model predictions are only estimates based on the code-to-code comparison of results. Code-to-code comparisons of hot gas layer, ceiling jet, plume, and cable temperatures, and heat flux to the cables are available from this exercise.

The only experimental data for the containment scenario is available from tests conducted in the mid-1980s at the containment facility for the experimental HDR reactor in Germany. Open validation studies using this experimental data was sponsored by NIST and conducted with CFAST and FDS by the University of Maryland. This study is used for validating models for predictions of cable target response with gas temperature.

None of the Benchmark Exercises and Other Tests are applicable to the outdoors scenario since they are all validation studies for compartment studies. The SFPE Engineering Guide for Assessing Flame Radiation to External Targets from Pool Fires [] is used for estimating the uncertainties of FDTs calculations of radiative heat flux to cable targets. FDS

Table 6.5 Attributes of NPP Fire Scenarios

Scenario	Fire Source	Peak HRR	Geometry area, ht	Ventilation	Target - [Damage Criteria]
1. Switchgear Room	Cabinet Cable tray ignition	65-200 kW ____ kW 0.02 - 0.7 kW/m ³	81-490 m ² 3.7-6.0 m 300-2940m ³	Door 2-4 m ² MV 2 acph	Cables [Surf. Temp.]
2. Cable Spreading Rm	- Trash can - Cable tray (elevated) - multiple fires	135-300 kW ____ kW 0.02-0.16 kW/m ³	334-1048m ² 5.7-6.4 m 1904-6707m ³	2 doors - 4 m ² each MV 1-5 acph	Cables [Surf. Temp.] Electrical cabinets
3. Control Room	- Control cabinet - MCB - Transient	200-950 kW 0.08-1.13 kW/m ³	145-854 m ² 2.8-5.8 m 841-2391 m ³	MV 5-10 acph	-cable or SSD inside cabinet -human . temp. . toxicity . visibility
4. Pump Room	- oil spill	3.6-7.2 MW 8.6-84 kW/m ³	15-86 m ² 4.9-5.7 m 86-421m ³	Door 4 m ² MV ____	Cables [Surf. Temp.] Walls
5. Turbine Hall	- oil spill - hydrogen	7.2-18.1MW 0.6 kW/m ³ max	3809-14,052m ² 7.5-15.3 m 28,568-214,996 m ³	NV, MV, & NV/MV NV-windows MV 6.6 acph	- Cables - Beams [Surf. Temp.]
6. Multi-Compartment	- oil spill - cable tray	3.6-7.2 MW	- 3 rooms like Pump Room - Corridor 1.4 m wide	Doors MV ____	Cables [Surf. Temp.]
7. Multi-Level Building	Oil spills	7.2-18 MW	3809-14,052m ² 10 m each lvl 38,090-140,052 m ³	NV, MV, & NV/MV NV-windows MV 6.6 acph	Cables [Surf. Temp.]

8. Containment PWR	- oil spills	7.2-18 MW	1555 m ² 63 m 97,965 m ³ multi- level & compartment		Cables [Surf. Temp.]
9. Outdoors	- oil spill	7.2-18 MW	N/A	Ambient	Cables [Surf. Temp.]
10. Battery Room	- hydrogen - cable tray wood pallets	75-150 kW 0.04-3.1 kW/m ³	20-334 m ² 2.4-5.7 m 48-1904 m ³	Door MV 5 acph	Cables [Surf. Temp.]
11. Diesel Generator Rm	- oil spill	3.6-10.9 MW 0.9-8 kW/m ³	155-372 m ² 8.8-11 m 1364-4092 m ³	Door MV 5 acph	Cables [Surf. Temp.]
12. Computer Room	- furniture - workstation	135-300 kW 0.07-1.15 kW/m ³	54-334 m ² 4.8-5.7 m 260-1904 m ³	Door MV 5 acph	Control cabinet

FORMAT

REVIEW

Table 6.6 Attributes of Benchmark Exercises and Other Tests

Benchmark Exercise/ Other Tests	Fire Source	Peak HRR HRR/Vol max	Geometry area, ht, vol	Ventilation	Target - [Damage Criteria]
BE # 1 (Code to code)	Trash bag Cable tray - elevated	350 kW, 1 MW 1.6 kW/m ³ (for 1 MW)	138 m ² 4.6 m 635 m ³	Door - 5.8 m ² MV 5 acph	Cables - horiz [Temp inside cable]
BE # 2 Part I (Open exercise)	Heptane pool	2-4 MW 0.7 kW/m ³	373 m ² 14.5 m 5409 m ³	Doors - 3.2 m ² ea MV 11m ³ /s (7.3 acph)	None

BE # 2 Part II (Code to code)	Lube oil pool	63.5 MW 1.3 kW/m ³ (per level)	5000 m ² 10 m - 2 levels 50,000 m ³ x 2	24 doors - 4 m ² each 36 roof vents - -4.5 m ² each MV 194.4 m ³ /s (7 acph)	Cables (horiz) [Temp inside cable] Beams [Surface temp]
BE # 3	Heptane spray/pool	350 kW 1, 2 MW 0.6, 1.7, 3.5 kW/m ³	152 m ² 3.8 m 578 m ³	Door - 4 m ² MV 5 acph	Cables (horiz&vert) Junction box Walls [Temp inside & surface for all]
BE # 4	Kerosene pool	3.5, 18.8MW 47 kW/m ³ , 254kW/m ³	13 m ² 5.7 m 74 m ³	Door - 2.1 m ² Window - 0.7 m ²	- Steel & concrete plates - Barrel - Walls [Temp inside & surface for all]
BE # 5	Methanol pool cables - vertical	350 kW 4.8 kW/m ³	13 m ² 5.6 m 73 m ³	Door - 2.1 m ²	Cables (vert) Walls [Temp inside & surface for both]
NIST Multi-Room 3 Room Test 4 Room Test	- steady state gas burner -complex gas burner	100KW 1 KW/m ³ 1MW 5 KW/m ³	100 m ³ 200 m ³	3 Vent Tubes 102mm ID Inlet vent .27 m ²	none
HDR Containment	T51 gas fire T52 oil pool 1m ² to 3m ²	2-4MW .11KW/m ³ - .22KW/m ³ 1.011MW .057KW/m ³	cylinder diameter 20 m height 50 m dome - radius 10 m area-314 m ² total facility height- 60 m vol- 17801.4 m ³	(Both) doorway 1.01m x1.975m vent 2m ²	none

Table 6.7 NPP Scenario to Benchmark Exercise/Other Tests Correlation Matrix

Scenario	BE#1	BE # 2	BE # 3	BE # 4	BE # 5	Multi-R	HDR
1.Switchgear Room			- Gas temp - Cable temp - CJ temp - Flux	Plume temp	Plume temp		
2. Cable Spreading Rm (same as Switchgear Room)							
3. Control Room			- Gas temp - CO - Visibility				
4. Pump Room				- Plume temp - CJ temp - Gas temp - Flux - Plates temp - Wall temp			
5. Turbine Hall ⁷		Part I - Gas temp Plume temp					
6. Multi-Compartment ⁸						- Gas temp?	
7. Multi-Level Building ⁹		Part II: - Gas temp - Cable temp - CJ temp - Plume temp - Flux					

⁷Scaling of experimental data to a larger enclosure may not be valid.

⁸No mechanical ventilation and flux measurements, open validation study available only.

⁹No experimental data available.

8. Containment PWR ¹⁰								- Gas temp - Cable temp - CJ temp - Plume temp - Flux
9. Outdoors								
10. Battery Room			- Gas temp - Cable temp - CJ temp - Flux	Plume temp	Plume temp			
11. Diesel Generator Rm			- Gas temp - Cable temp - CJ temp - Flux	Plume temp	Plume temp			
12. Computer Room			- Gas temp - Flux					

DRAFT FOR
FORMAT
REVIEW
ONLY

¹⁰Open validation study available only.

6.3 Comparison of Predictive Capability with Actual Events

There are two ways of comparing predictive capability with actual events. The first is simply graphing the time series curves of model results with measured values of sensible variables such as temperature. Another approach is to consider the time to critical conditions such as flashover. Making direct comparisons between theory and experiment gives a good sense of whether predictions are reasonable. This chapter provides a review of CFAST validation efforts by NIST and others to better understand the quality of the predictions by the model.

6.3.1 Comparisons with Full-Scale Tests Conducted Specifically for the Chosen Evaluation

Several studies have been conducted specifically to validate the use of CFAST in building performance design. Dembsey [113] used CFAST to predict the ceiling jet temperatures, surface heat fluxes and heat transfer coefficients for twenty compartment fire experiments in a compartment that is similar in size, geometry, and construction to the standard fire test compartment specified in the Uniform Building Code[114]¹¹. Results from 330 kW, 630 kW, and 980 kW fires were used. In general, CFAST made predictions which were higher than the experimental results. In these cases, the temperature prediction is typically 20 to 30% higher than measured values. Much of this can be attributed to not knowing the species production (soot) and relative absorption of radiation by the gas layers which highlights the importance of scenario specification. This is the most common cause of “over prediction” of temperature by CFAST. A secondary source of discrepancy is correcting for radiation from thermocouple beads. The authors do this, but the corrections cited are not as large as has been reported in similar fire experiments [115].

He *et al.* [116] describe a series of full-scale fire experiments that were designed to investigate the validity of two zone models including CFAST. The experiments, involving steady state burning rates and a number of ventilation conditions, were conducted in a four-story building. Temperature, pressure, flow velocity, smoke density and species concentrations were measured in various parts of the building. The stack effect and its influence on temperature distribution in a stair shaft were observed. Comparisons were then made between the experimental results and the model predictions. Early in the fire there is very good agreement (a few percent difference) between the predictions and measurements, beyond 10 minutes, there are significant variations. Both the experiment and the model are internally consistent; that is, higher flow leads to a higher interface height (figure 13 in this paper). Once again, the difference is about 25%. The authors discuss the effect of fuel composition and correction for radiation from thermocouple beads but cannot draw firm conclusions based on their measurements of fuel products.

A series of experimental results for flaming fires, obtained using realistic fires in a prototype apartment building were performed by Luo *et al.* [117]. Fuel configurations in the fire test included a horizontal plain polyurethane slab, mock-up chair (polyurethane slabs plus a cotton linen cover), and a commercial chair. CFAST typically over-predicted upper layer temperatures by 10% to 50 % depending on the test conditions and measurement location in that test. The predicted and experimental time dependent upper layer temperatures were similar in shape. The time to obtain peak upper layer temperatures was typically predicted to within 15 % of the

¹¹ The 1997 Uniform Building Code has been superceded by the International Building Code, 2003 Edition, International Code Council, Country Club Hills, Illinois.

experimental measurements. The authors concluded that CFAST was conservative in terms of life safety calculations, and that in these experiments, the layer was not uniform.

In order to optimize fire service training facilities, the best use of resources is imperative. The work reported by Poole *et al.* [118] represents one aspect of a cooperative project between the city of Kitchener Fire Department (Canada) and the University of Waterloo aimed at developing design criteria for the construction of a fire fighter training facility. One particular criterion is that realistic training with respect to temperature, heat release and stratification be provided in such a facility. The purpose of this paper was to compare existing analytical heat release and upper and lower gas temperature rise correlations and models with data from actual structures which were instrumented and burned in collaboration with the Kitchener Fire Department. The CFAST model was used successfully to predict these conditions and will be used in future design of such facilities.

A report by Bailey *et al.* [119] compares predictions by CFAST to data from real scale fire tests conducted onboard ex-USS SHADWELL, the Navy's R&D damage control platform. The phenomenon of particular interest in this validation series was the conduction of heat in the vertical direction through compartment ceilings and floors. As part of this work, Bailey *et al.* [120] compared CFAST temperature predictions on the unexposed walls of large metal boxes, driven by steady state fires. This tested the model's prediction of radiation and conduction in both the vertical and horizontal directions. Indirectly it quantifies the quality of the conduction/convection/radiation models. The model and experiment compared well within measurement error bounds of each. The comparison was particularly good for measurements in the fire compartment as well as for the compartment and deck directly above it, with predictions typically agreeing with experiments within measurement uncertainty. The model under-predicted the temperatures of the compartments and decks not directly adjacent to the fire compartment early in the tests. Most of the error arose due to uncertainty in modeling the details of the experiment. The size of the vent openings between decks and to the outside must be included, but these were not always known. Cracks formed in the deck between the fire compartment and the compartment above due to the intense fire in the room of origin, but a time dependent record was not kept. The total size of the openings to the outside of warped doors in both compartments was not recorded. As can be seen in figures 7 and 8 of reference [119], the steady state predictions are identical (within error bounds of the experiment and prediction). The largest error is after ignition (uncertainty in the initial fire) and during development of the cracks between the compartments. While this does not affect the agreement in the room of origin, it does lead to an error of about 30% in the adjacent compartment.

6.3.2 Comparisons with Previously Published Test Data

A number of researchers have studied the level of agreement between computer fire models and real-scale fires. These comparisons fall into two broad categories: fire reconstruction and comparison with laboratory experiments. Both categories provide a level of verification for the models used. Fire reconstruction, although often more qualitative, provides a higher degree of confidence for the user when the models successfully simulate real-life conditions. Comparisons with laboratory experiments, however, can yield detailed comparisons that can point out weaknesses in the individual phenomena included in the models.

NIST has studied the predictive capability of CFAST in detail for several scenarios where experimental data were available. In this section, we will consider these variables for comparison:

- upper and lower layer gas temperature,
- layer interface position,

- gas species concentration.
- fire pyrolysis and heat release rate,
- room pressure, and
- vent flow.

Although there are certainly other comparisons of interest, these will provide an indication of the match of the model to the experimental data. The intent is to do a general comparison of each of the sensible output variables with full scale experiments. Additional comparisons for additional specific applications are discussed later.

6.3.2.1 Experimental Data Selected for Comparison

Peacock *et al.* [121] compared the performance of the CFAST model with experimental measurements for the variables presented above. Using a range of laboratory tests, they presented comparisons of peak values, average values, and overall curve shape for a number of variables of interest to model users. A total of five different real-scale fire tests were selected for the comparisons to represent a range of challenges for the CFAST model. Details of the experimental measurements and procedure for model calculations are available in the original paper [121]. Five sets of tests were considered for comparison:

- 1) A single-room test using upholstered furniture as the burning item was selected for its well-characterized and realistic fire source in a simple single-room geometry [122]. Heat release rate, mass loss rate, and species yields measurements were made available for the test. This should allow straightforward application of the model. Peak fire size was about 2.9 MW with a total room volume of 21 m³.
- 2) Like the first test, this test was a single-room fire test using furniture as the fire source [123]. It expanded upon that data set by adding the phenomenon of wall burning. Peak fire size was about 7 MW. Room size was similar to the first test.
- 3) This data set is actually an average of a series of 11 replicate tests in a three-room configuration with simple steady-state gas burner fires [26]. It provides a basic set of measured quantities for small to medium size fires. Since all fires were gas burner fires, simulation should be straightforward. It is of particular interest since it was undertaken as a part of a program to develop a methodology for the evaluation and accuracy assessment of fire models. Fire size was about 100 kW with a total volume of 100 m³.
- 4) This data set is part a series of tests conducted in a multiple room configuration with more complex gas burner fires than the three-room configuration [120] , [124]. This study was included because it expands upon that data set by providing larger and time-varying gas burner fires in a room-corridor configuration. Fire size was about up to 1 MW with a total volume of 200 m³.
- 5) By far the most complex test, this data set is part of a series of full-scale experiments conducted to evaluate zoned smoke control systems, with and without stairwell pressurization [10]. It was conducted in a seven story hotel with multiple rooms on each floor and a stairwell connecting all floors. This data set was chosen because it would be considered beyond the scope of most current fire models.

Measured temperatures and pressure differences between the rooms and floors of the building are extensive and consistent. Peak fire size was 3 MW with a total building volume of 140,000 m³.

All of the simulations were performed with version 4 of the CFAST model. For each of the data sets, the model data were developed from the building and fire descriptions provided in the original reports. Obtaining building geometry, construction materials, and room interconnections was straightforward. Usually, description of the fire source was more difficult. Where freeburn data were available, such data were used to describe the heat release rate, pyrolysis rate, and species yields. In other cases, estimates from tests of similar materials or text-book values were used to determine missing quantities.

6.3.2.2 Layer Temperature and Interface Position

Arguably the most frequent question asked about a fire is, "How hot did it become?" Temperature in the upper layer of a compartment is an obvious indicator to answer this question. Peak temperature, time to peak temperature, or time to reach a chosen temperature tenability limit are typical values of interest. Quality of the prediction (or measurement) of layer interface position is more difficult to quantify. Although observed valid in a range of experiments, the two-layer assumption is in many ways just a convenience for modeling. From a standpoint of hazard, time of descent to a chosen level may be a reasonable criterion (assuming some in the room will then either be forced to crawl beneath the interface to breathe the "clean" atmosphere near the floor or be forced to breath the upper layer gases). Minimum values may also be used to indicate general agreement. For the single-room tests with furniture or wall-burning, these are appropriate indicators to judge the comparisons between model and experiment. For the more-closely steady-state three- and four-room tests with corridor or the multiple-story building tests, a steady-state average better characterizes the nature of the experiment.

Figures 6-4 – 6-6 and Tables 7 – 9 show the upper layer temperature, lower layer temperature, and interface position for the tests studied. Like all zone-based fire models, CFAST calculates conditions within each room as an upper and a lower volume (layer), each with uniform conditions throughout the volume at any instant of time. Thus, for the model, the temperature environment within a room can be described by an upper and lower layer temperature and by the position of the interface between these two layers. By contrast, experimental measurements often take the form of a vertical array of measurement points describing a profile of temperature. Techniques for collapsing these profiles to data that can be compared to zone fire models are available [110] and are used here to facilitate the comparison.

For the single-room tests, predicted temperatures and layer interface position show obvious similarities to the measured values. Peak values occurred at similar times with comparable rise and fall for most comparisons. Interface height for the single-room with wall-burning is a notable exception. Unlike the model prediction, the experimental measurement did not show the rise and fall in concert with the temperature measurement. Peak values were typically higher for upper layer temperature and lower for lower layer temperature and layer interface position. For all the tests, including the single-room tests, times to peak values and times to 100 °C predicted by the model were within 25 s of experimentally measured values on average.

DRAFT
FOR
FORMAT
REVIEW
ONLY

Table 6.8 Comparison of experimental measurements and model predictions of upper layer temperature (°C) for several tests

Numbers in parentheses are model predictions	Peak ^a Value (°C)	Time to Peak (s)	Time to 100°C (s)	Steady-State Value (°C)	Similar Shape?
Single-room furniture tests ^b (Tests 1 and 6)	790 (780) 920 (780)	500 (510) 450 (510)	290 (250) 290 (250)	-- ^b	✓
	590 (660) 900 (660)	510 (520) 510 (520)	330 (260) 330 (260)	--	✓
Single-room tests with wall burning (Tests 1 and 2)	750 (620)	710 (230)	100 (140)	--	✓
	810 (1190)	520 (470)	100 (80)	--	✓
Three-room tests with corridor ^d (SET 4, 11 replicates)	--	--	100 (120) 830 (n.r.) n.r.	230 (215) 75 (90) 45 (50)	
Four-room tests with corridor ^d (Tests 19 and 21)	--	--	195 (195) n.r. n.r. n.r.	240 (370) 70 (90) 55 (35) 40 (35)	✓
	--	--	200 (195) n.r. (240) n.r. n.r.	260 (370) 80 (100) 65 (50) 50 (50)	
Multiple-story building (Test 7)	--	--	390 (180) 210 (390) n.r.	270 (340) 110 (110) 15 (15)	✓

a Experimental data for these comparisons come from references [26],[122],[123],[124],[10] discussed in section •.

b Two measurement positions within the room were available from the experimental data.

c Not appropriate for the experiment.

d Multiple entries indicate multiple measurements were available for comparison with model predictions.

ONLY

Table 6.9 Comparison of experimental measurements and model predictions of lower layer temperature (°C) for several tests

Numbers in parentheses are model predictions	Peak Value (°C)	Time to Peak (s)	Time to 100°C (s)	Steady-State Value (°C)	Similar Shape?
Single-room furniture tests ^a	570 (430) 590 (430)	500 (510) 420 (510)	370 (400) 390 (400)	-- ^b	✓
	230 (230) 590 (230)	510 (520) 500 (520)	410 (460) 390 (460)	--	✓
Single-room tests with wall burning	710 (240)	710 (230)	240 (220)	--	✓
	700 (950)	520 (470)	290 (290)	--	✓
Three-room tests with corridor ^c	--	--	n.r. n.r. n.r.	70 (50) 30 (30) 23 (30)	
Four-room tests with corridor ^c	--	--	n.r. n.r. n.r.	75 (50) 21 (22) 21 (17)	✓
	--	--	n.r. n.r. n.r.	70 (52) 20 (22) 20 (17)	
Multiple-story building	--	--	520 (n.r.) n.r. n.r.	85 (95) 40 (45) 14 (16)	✓

See notes for Table 7.

Table 6.10 Comparison of experimental measurements and model predictions of layer interface position (m) for several tests

Numbers in parentheses are model predictions	Peak Value (m)	Time to Peak (s)	Time to 1 m (s)	Steady-State Value (m)	Similar Shape?
Single-room furniture tests ^a	0.8 (0.3) 0.8 (0.3)	420 (480) 450 (480)	400 (390) 380 (390)	-- ^b	✓
	0.8 (0.5) 0.9 (0.5)	480 (510) 460 (510)	420 (430) 430 (430)	--	✓
Single-room tests with wall burning	0.2 (0.7)	710 (220)	120 (210)	--	✓
	0.1 (0.6)	500 (410)	80 (280)	--	✓
Three-room tests with corridor ^c	--	--	360 (n.r.) 1210 (n.r.) 90 (n.r.)	1.0 (1.7) 1.2 (1.6) 0.9 (1.3)	✓
Four-room tests with corridor ^c	--	--	n.a.	0.7 (1.7) 1.0 (1.8) 1.0 (1.7) 0.7 (1.7)	
	--	--	n.a.	0.8 (1.5) 0.9 (1.4) 0.8 (1.2) 0.6 (1.2)	
Multiple-story building	--	--	n.a.	0.3 (0.6) 0.8 (0.8) 1.8 (0.9)	

See notes for Table 7.

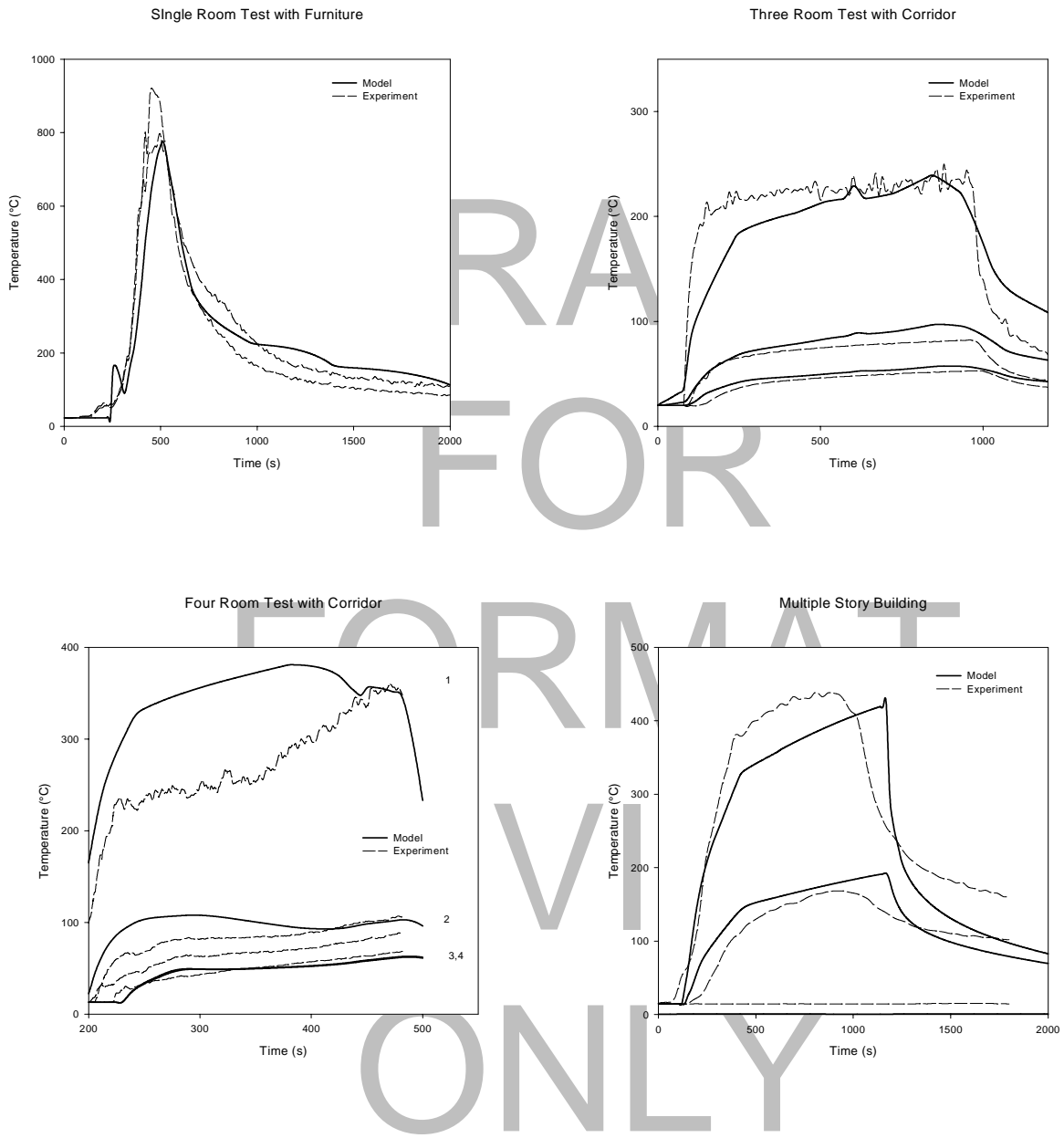


Figure 6-7. Comparison of measured and predicted upper layer temperatures for several tests.

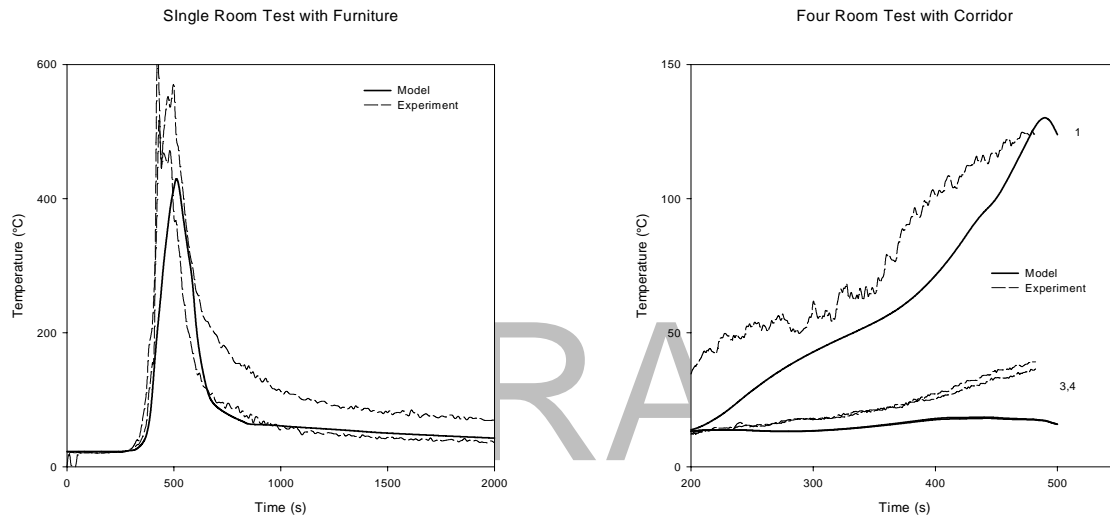


Figure 6-8. Comparison of measured and predicted lower layer temperatures for several tests.

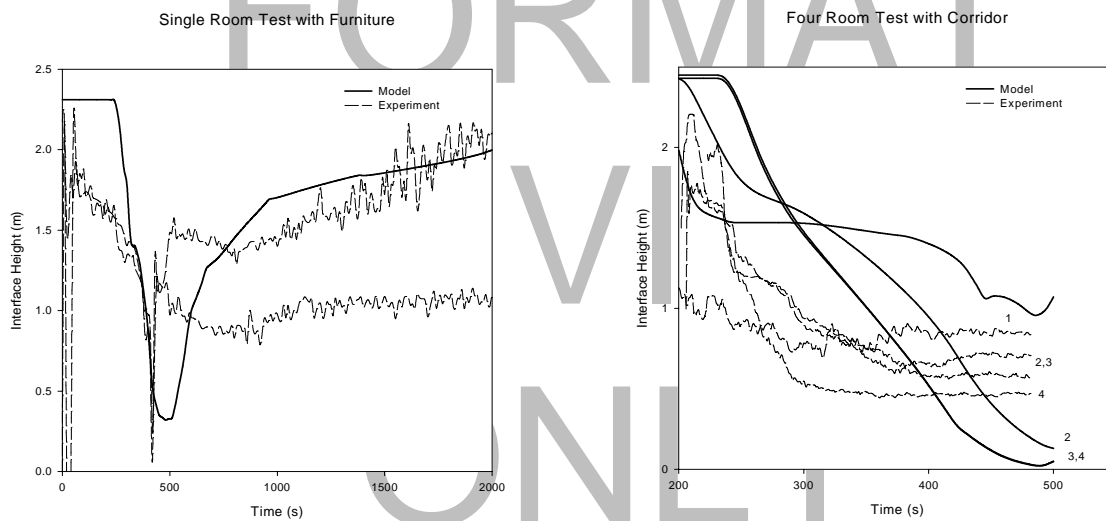


Figure 6-9. Comparison of measured and predicted layer interface position for several tests.

Systematic deviations exist for the remaining three data sets. Differences between model predictions and experimental measurements changed monotonically over time (rising for the three-room test and falling for the four-rooms tests. Modeling of heat conduction (losing too much or too little heat to the surfaces) or lack of modeling of leakage (rooms in CFAST are presumed perfectly sealed unless vents are included to simulate

leakage) may account for the trends. The comparison of interface position for the four-room test with corridor seems an anomaly. Although a nearly closed space, the roughly level interface position from the experiment seems more typical of a test more open to the ambient. The model calculations appear to better represent the mixing which would occur in a closed volume. Again, leakage may be a factor. With some leakage in the space, lower temperatures for both the lower and upper layers and higher (and more uniform) interface position would be calculated.

In general, upper layer temperature and interface position predicted by the model were somewhat higher than the experimental measurements [125], with the differences ranging from $-140\text{ }^{\circ}\text{C}$ to $380\text{ }^{\circ}\text{C}$ for the temperature and -0.5 to 0.8 m for the interface position. Conversely, the lower layer temperature was somewhat lower for the model than for the experiments ($-470\text{ }^{\circ}\text{C}$ to $250\text{ }^{\circ}\text{C}$). Presuming conservation of energy (an underlying assumption in *all* fire models), these three observations were consistent. A higher interface position gives rise to a smaller upper volume (and larger lower volume) within a room. With the same enthalpy in a smaller upper volume, higher temperatures result. This lends credence to the assumption of enthalpy conservation. Layer interface position is primarily affected by entrainment by the fire or at vents. Plume entrainment in CFAST is based on the work of McCaffrey [20] on circular plumes in relatively small spaces. For large fires in small spaces where the fire impinges on the ceiling (such as the single room tests with wall burning) or very small fires in large spaces (such as atria), these correlations may not be as valid.

6.5.2.3 Gas Species

The fire chemistry scheme in CFAST is essentially a species balance from user-prescribed species yields and the oxygen available for combustion. Once generated, it is a matter of bookkeeping to track the mass of species throughout the various control volumes in a simulated building. It does, however, provide another check of the flow algorithms within the model. Since the major species (CO and CO_2) are generated only by the fire, the relative accuracy of the predicted values throughout multiple rooms of a structure should be comparable. Figure 6-10 and table 6.12 show measured and predicted concentrations of O_2 , CO_2 , and CO in two of the tests studied.

REVIEW
ONLY

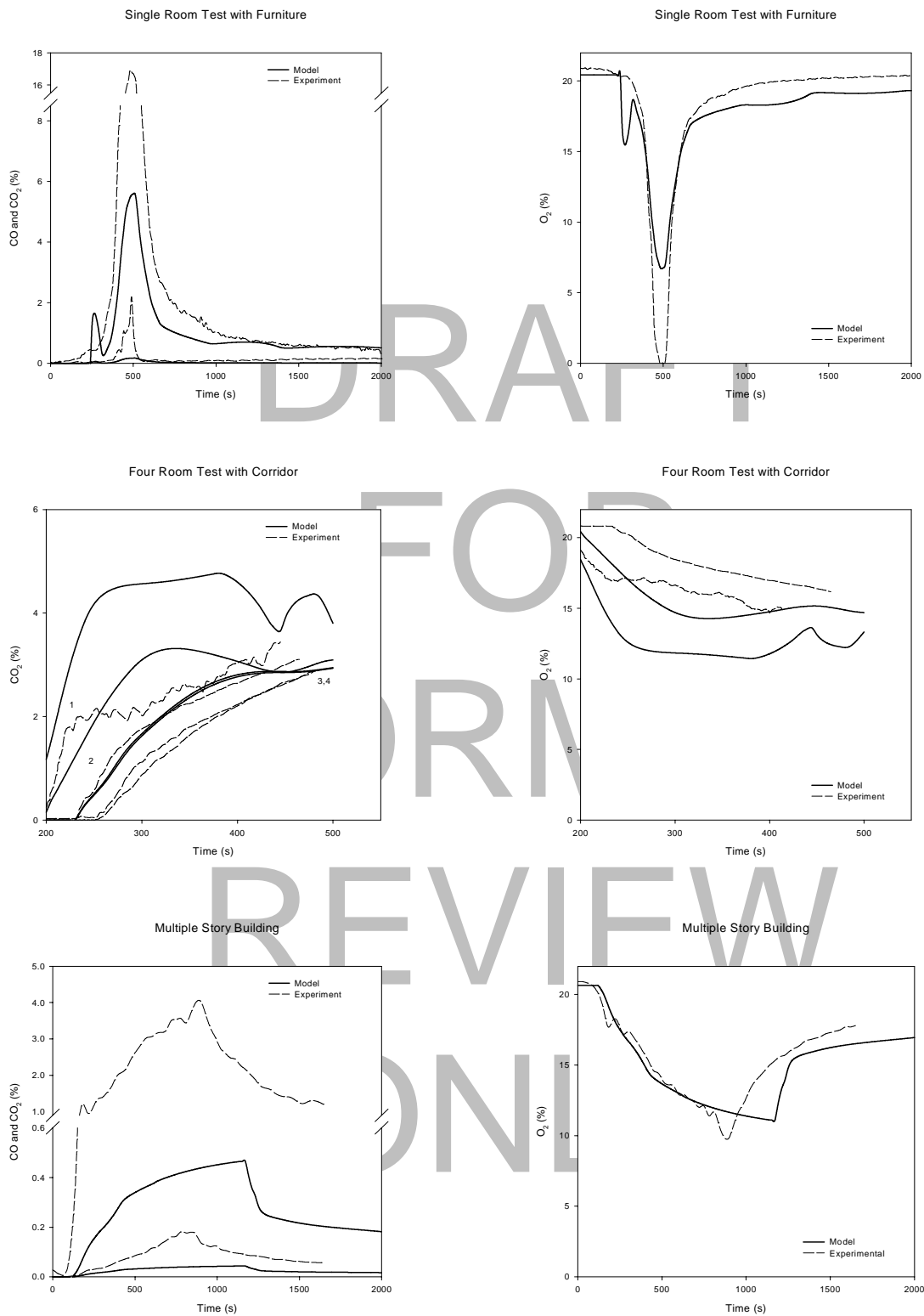


Figure 6-10. Comparison of measured and predicted gas species concentrations for several tests.

Table 6.11 Comparison of experimental measurements and model predictions of oxygen concentration for several tests

Oxygen Concentration

Numbers in parentheses are model predictions	Peak Value ^a (%)	Time to Peak (s)	Steady-State Value (%)	Similar Shape?
Single-room furniture fire tests	0.01 (6.7)	510 (490)	-- ^a	✓
	6.9 (10.6)	490 (510)	--	✓
Four-room tests with corridor ^c	--	--	17.9 (12.8) 18.0 (15.4)	✓
	--	--	16.1 (11.8) 18.1 (16.5)	✓
Multiple-story building test ^c	--	--	15.5 (11.1) 20.9 (20.3)	

Carbon Dioxide Concentration

Single-room furniture fire tests	17.0 (5.6)	480 (510)	-- ^b	✓
	10.6 (4.1)	490 (510)	--	✓
Four-room tests with corridor ^c	--	--	2.3 (4.1)	✓
	--	--	2.4 (4.8)	✓
Multiple-story building test ^c	--	--	2.0 (0.5)	

Carbon Monoxide Concentration

Single-room furniture fire tests	2.2 (0.2)	490 (510)	-- ^a	✓
	0.6 (0.1)	440 (510)	--	✓
Multiple-story building test ^c	--	--	0.8 (0.04)	

a Experimental data for these comparisons come from references [26],[122], [123],[124],[10] discussed in section •.

b not appropriate for the test.

c multiple entries indicate comparable rooms in the test structure.

For the single-room tests with furniture, the predicted concentrations are lower than those measured experimentally (averaging 5 percent low). This is probably due to the treatment of oxygen limited burning. In CFAST, the burning rate simply decreases as the oxygen level decreases. A user prescribed lower limit determines the point below which burning will not take place. This parameter could be finessed to provide better agreement with the experiment. For the present comparisons, it was always left at the default value of 14 %.

For the four room test with corridor, the asymptotic values of the gas concentrations agree quite well. At first glance, the model predictions reach this equilibrium more quickly. An appreciation of the differences between the modeled parameters and the experimental measurements put this in perspective. From figure 6-4, it takes

about 100 s for the upper layer to descend to the level of the gas sampling port in the test. In addition, it is assumed that this point measurement is the bulk concentration of the entire upper layer. In reality, some vertical distribution not unlike the temperature profile (figure 6-4) exists for the gas concentration as well. Since this measurement point is near the lower edge of the upper layer for a significant time, it should underestimate the bulk concentration until the layer is large in volume and well mixed.

For the multiple-story building test, predicted values for CO_2 , CO , and O_2 are far lower than measured experimentally. Both the lower burning rate limit as well as leakage in the 100 year-old structure probably contributed to the differences between the experiments and model. In addition, values for species yields were simply literature values since no test data were available.

6.5.2.4 Heat Release and Fuel Pyrolysis Rate

Heat release rate and its intimately related pyrolysis rate are key indicators of fire hazard [?]. Peak values and time to reach peak values are typical scalar estimates used to represent the time-variant heat release rate and fire pyrolysis rate. For the single-room tests with furniture or wall-burning, these are appropriate indicators to judge the comparisons between model and experiment. For the three- and four-room tests with corridor or the multiple-story building tests, a steady state average is more appropriate.

Table 11 and figure 6-8 compare measured and predicted heat release rates for the tests. In the CFAST model, the fire is prescribed as a series of straight line segments describing the pyrolysis rate, heat release rate, and species yields. Thus, the model predictions could be expected to agree quite well with experimental measurements. For tests where experimental data were available, the agreement is excellent – usually within 5 percent of the peak experimental values. Since this effectively just shows how well a series of line segments reproduces experimental measurement, this level of agreement is expected.

Times to peak values are always close. For two tests (the single-room with furniture and wall burning and the multiple-story building), the heat release rate in the room is limited by the available oxygen. Additional burning outside the room (seen in the single-room with furniture) accounts for the remainder of the heat released.

For the three-room test with corridor, multiple replicate tests put the agreement between the model and experiments in perspective. For all tests in the original study [26], the coefficients of variation (the standard deviation expressed as a percentage of the mean) ranged from 4 % to 52 %. In another study, precision to within 15 percent for fires of 2.5 MW was noted [122]. Thus, the simplification of specifying the fire growth as a series of straight lines is easily justified with the expected accuracy of experimental measurements.

Table 6.12 Comparison of measured and prescribed heat release rate for several tests

Numbers in parentheses are model predictions	Peak Value ^a (kW)	Time to Peak (s)	Steady-State Value (kW)	Similar Shape?
Single-room furniture fire tests	2450 (2200)	480 (480)	— ^b	✓
	2600 (2350)	500 (510)	--	✓
Single-room tests with wall-burning	2050 (2000)	230 (200)	--	✓
	4000 (3150)	420 (370)	--	✓
Three-room test with corridor	--	--	86 (87)	✓
Four-room tests with corridor	--	--	n.r. ^c	✓
	--	--	n.r.	✓
Multiple-story building test	--	--	n.r.	✓

a Experimental data for these comparisons come from references [26],[122], [123],[124],[10] discussed in section •.

b not appropriate for the test.

c not available from experimental data.

For the multiple-story building test, no pyrolysis rate or heat release rate data were available. Estimates of the

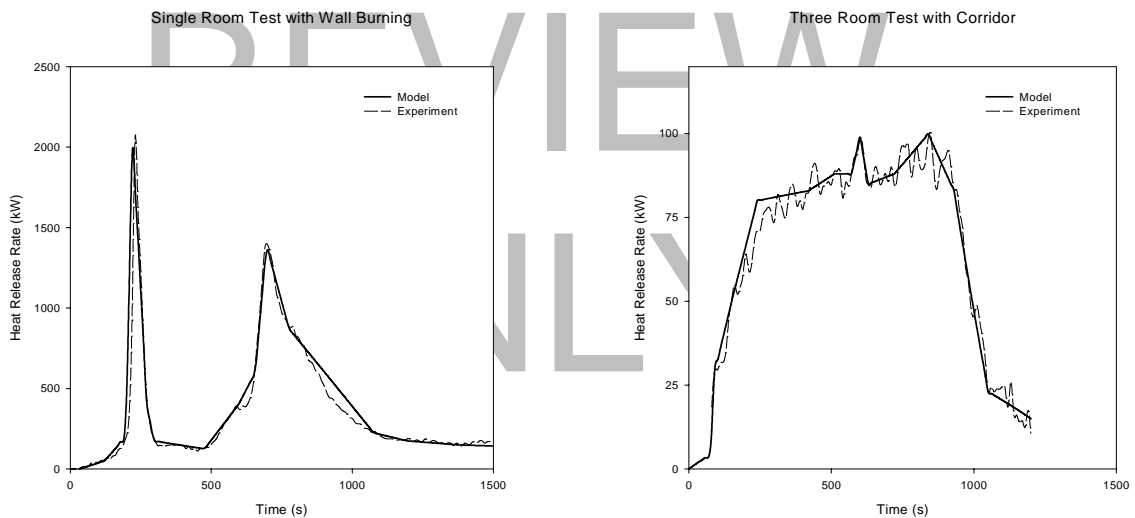


Figure 6-11. Comparison of measured and prescribed heat release rates for two selected tests.

“steady-state” burning rate, time to reach “steady-state,” and duration of “steady-state” burning were made from available correlations for wood cribs [126], [127]. Although the comparisons for this test should be considered approximate, it was included since, if successful, the scope of the model is extended considerably to a large multiple-story building with mechanical ventilation.

6.5.2.5 Pressure

The differential pressure across an opening drives the flow through the opening. For each room, the CFAST model calculates a differential pressure at floor level, referenced to ambient. Noting that the ambient pressure is approximately 100 kPa, typical pressure drops across openings induced by fires are but a small fraction of the ambient pressure – typically from less than 1 Pa to perhaps a few hundred Pascals in well-sealed enclosures. The ability to model these extremely small differential pressures provides another check on the flow algorithms in the model. These are, however, expected to be difficult to model and measure accurately. Thus, agreement within a few pascals is often considered acceptable. In four of the five experimental test series, measurements (corrected to floor level) were available which could be compared to these predicted values (measurements were not available for the single room tests with furniture).

Figure 6-7 and table 12 show the comparisons. For most cases, the agreement is reasonable, with the difference between measured and predicted values typically less than 2 Pa and for some experiments, less than 0.5 Pa. Trends displayed in the experimental data are replicated by the model predictions. Some interesting exceptions are apparent however. In major part, these are due to quantities unknown in the experiments (leakage). Not all of the onus for agreement should be placed on the model, however. Only one of the test series included any estimate of leakage through cracks in the buildings. Logically, unless directed otherwise, the model assumes *no* leakage from any room. This leakage can have a dramatic effect on the results predicted by the model. Figure 6-10 illustrates the effect of leakage for a single room with a single doorway and an upholstered chair used as the fire source. Leakage areas from 0 to 100 percent of the vent area were simulated with a second vent of appropriate size and placed at floor level (much of the leakage in rooms take place at floor level). Both temperatures and pressures change by more than a factor of two (other variables can be expected to change with similar variation). Temperature changes by about 20 percent with only a 10 percent leakage area. The effect on pressure is not quite as straightforward, but for larger leakages changes in concert with the temperature. For the four-room tests with corridor, leakage from the “well sealed rooms” was estimated via measurement at not more than 25 percent of the total vent area.

ONLY

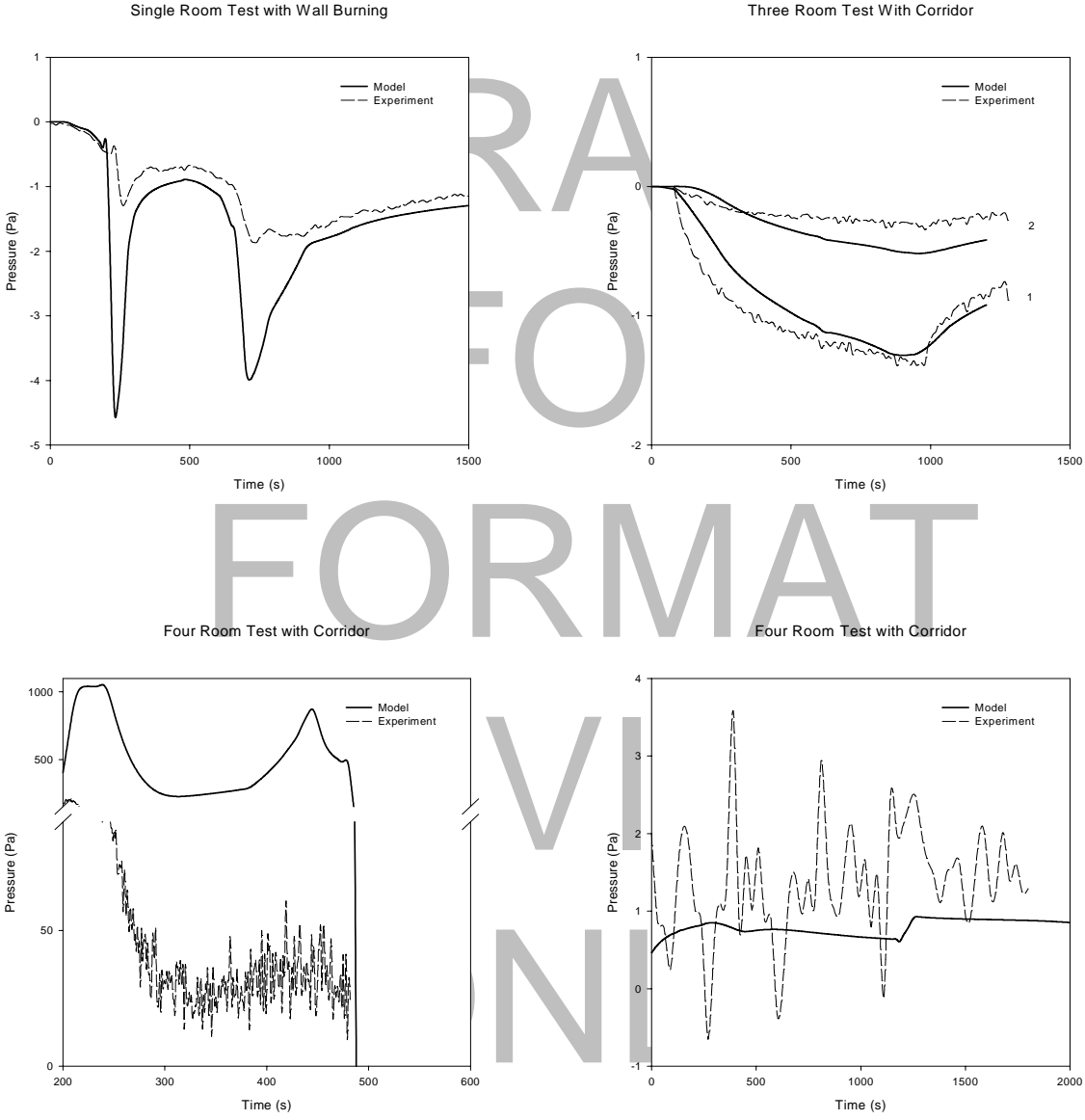


Figure 6-12. Comparison of measured and predicted pressures for several tests.

Table 6.13 Comparison of experimental measurements and model predictions of room pressure for several tests

Numbers in parentheses are model predictions	Peak Value	Time to Peak	Steady-State Value	Similar Shape?
Single-room tests with wall-burning	-1.9 (-4.5)	730 (230)	--	✓
	-1.9 (-6.4)	520 (490)	--	✓
Three-room test with corridor	--	--	-1.1 (-0.6) -0.2 (-0.5)	✓
Four-room tests with corridor	--	--	-1.0 (-2.1)	✓
	--	--	36 (22)	
Multiple-story building test	--	--	2.4 (1.3)	✓

Experimental data for these comparisons come from references [26],[122], [123],[124],[10] discussed in section •.
^a not appropriate for the test.

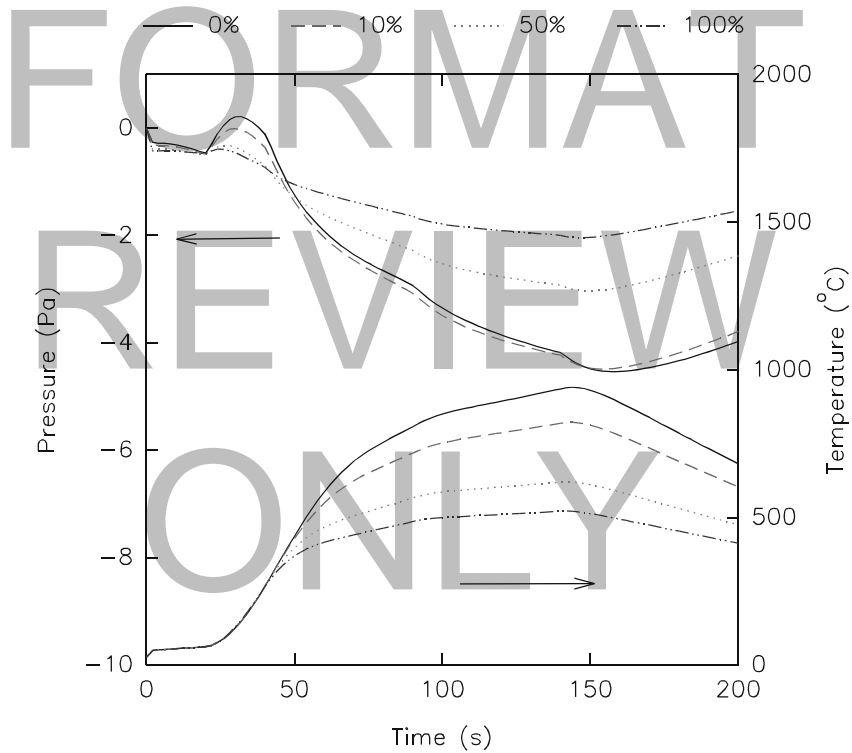


Figure 6-13: Effect of leakage in an arbitrary single-room fire.

6.5.2.6 Flow Through Openings

In the control volume approach, the differential form of the momentum equation for the zones is not solved directly. Rather, the momentum transfer at the zone boundaries is included by using Bernoulli's approximation for the velocity equation. This solution is augmented for restricted openings by using flow coefficients [28], [55] to allow for constriction in vents. The flow coefficients allow for an effective constriction of fluid flow which occurs for vents with sharp edges. In CFAST, these coefficients are for rectangular openings in walls whose surfaces are much larger than the opening.

Figure 6-11 and table 13 compare measured and predicted mass flows through doorways in two of the tests studied. For the three-room test with corridor, flow through two doorways of the same test are shown (one between the fire room and the corridor and one between the corridor and the outdoors). Not surprisingly, the flow is typically somewhat underpredicted by the model (averaging 0.1kg/s). The vent flow in CFAST includes mixing phenomena at the vents. As hot gases from one compartment leave that compartment and flow into an adjacent compartment, a door jet can exist which is analogous to a normal fire plume, but with an extended flat plume similar to a waterfall. This places its use outside the normal range of the plume model [20] and perhaps beyond its range of validity. However, no reliable correlation yet exists for the extended flat plume which occurs in vent flow. Examining the trends of prediction of upper layer temperature in tests with multiple rooms (Tables 7 and 8), the typical over-prediction in the room of fire origin is far greater than for other rooms in the structures. The under-prediction of the mass flows probably accounts for this as a cascading effect with distance from the room of fire origin.

Table 6.14 Comparison of experimental measurements and model predictions of mass flow through openings for several tests

Numbers in parentheses are model predictions	Peak Value	Time to Peak	Steady-State Value	Similar Shape?
Single-room furniture fire tests	1.2 (1.3)	380 (410)	-- ^a	✓
	1.9 (1.9)	560 (460)	--	✓
Three-room test with corridor	--	--	0.4 (0.3)	✓

Experimental data for these comparisons come from references [26],[122], [123],[124],[10] discussed in section •.

^a not appropriate for the test.

Sections • through • show comparisons of the experiments with the model predictions. The differences are quantified based on time to peak (e.g. temperature), closeness of the two curves in a time varying sense, and the steady state predictions. The latter are valuable since they iron out impreciseness of the explanation of the experiment. In addition to these comparisons, it is possible to quantify the relative difference between the time dependent curves and the relative shape of the curves. For these experiments such a detailed quantification was done by Peacock et. al.[128].

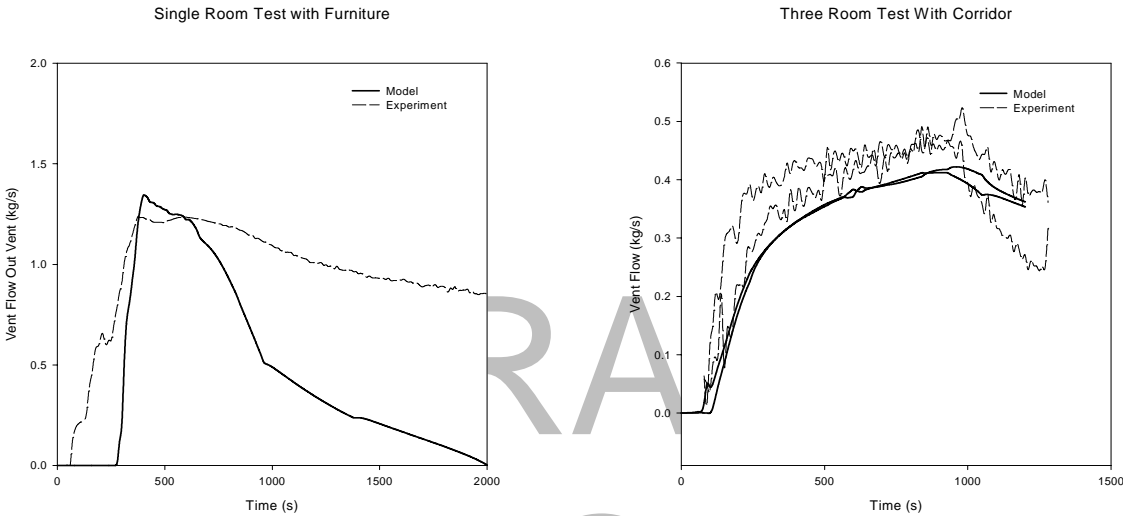


Figure 6-14: Comparison of measured and predicted mass flow through vents for several tests. (Numbers indicate comparable rooms in the test structure.)

6.5.2.7 Plume Model

Davis compared predictions by CFAST (and other models) for high ceiling spaces [129]. In this paper, the predictive capability of two algorithms designed to calculate plume centerline temperature and maximum ceiling jet temperature in the presence of a hot upper layer were compared to measurements from experiments and to predictions using CFAST's ceiling jet algorithm. The experiments included ceiling heights of 0.58 m to 22 m and heat release rates of 0.62 kW to 33 MW. When compared to the experimental results CFAST's ceiling jet algorithm tended to over-predict the upper layer temperature by 20%. With proper adjustment for radiation effects in the thermocouple measurements, some of this difference disappears. The effect of entrainment of the upper layer gases needs to be improved.

6.5.2.8 Other Comparisons with Previously Published Test Data

Jones and Peacock [130] presented a limited set of comparisons between the FAST model and a multi-room fire test. The experiment involved a constant fire of about 100 kW in a three-compartment configuration of about 100 m³. They observed that the model predicted an upper layer temperature that was too high by about 20% with satisfactory prediction of the layer interface position. These observations were made before the work of Pitts *et al.* [115] showed that the thermocouple measurements need to be corrected for radiation effects. Convective heating and plume entrainment were seen to limit the accuracy of the predictions. A comparison of predicted and measured pressures in the rooms showed within 20%. Since pressure is the driving force for flow between compartments, this agreement was seen as important.

Levine and Nelson [131] used a combination of full-scale fire testing and modeling to simulate a fire in a residence. The 1987 fire in a first-floor kitchen resulted in the deaths of three persons in an upstairs bedroom, one with a reported blood carboxyhemoglobin content of 91 percent. Considerable physical evidence remained. The fire was successfully simulated at full scale in a fully-instrumented seven-room two-story test structure. The data collected during the test have been used to test the predictive abilities of two multiroom computer fire models: FAST and HARVARD VI. A coherent ceiling layer flow occurred during the full-scale test and quickly carried high concentrations of carbon monoxide to remote compartments. Such flow is not directly accounted for in either computer code. However, both codes predicted the carbon monoxide buildup in the room most remote from the fire. Prediction of the pre-flashover temperature rise was also good. Prediction of temperatures after flashover that occurred in the room of fire origin was less good. Other predictions of conditions throughout the seven test rooms varied from good approximations to significant deviations from test data. Some of these deviations are believed to be due to phenomena not considered in any computer models.

Deal [132] reviewed four computer fire models (CCFM [8], FIRST [6], FPETOOL [133] and FAST) to ascertain the relative performance of the models in simulating fire experiments in a small room (about 12 m³ in volume) in which the vent and fuel effects were varied. Peak fire size in the experiments ranged up to 800 kW. All the models simulated the experimental conditions including temperature, species generation, and vent flows, quite satisfactorily. With a variety of conditions, including narrow and normal vent widths, plastic and wood fuels, and flashover and sub-flashover fire temperatures, competence of the models at these room geometries was demonstrated.

Duong [134] studied the predictions of several computer fire models (CCFM, FAST, FIRST, and BRI [6]), comparing the models with one another and with large fires (4 MW to 36 MW) in an aircraft hanger (60,000 m³). For the 4 MW fire size, he concluded that all the models are reasonably accurate. At 36 MW, however, none of the models did well. Limitations of the heat conduction and plume entrainment algorithms were thought to account for some of the inaccuracies.

6.5.3 Prediction of Flashover

A chaotic event that can be predicted by mathematical modeling is that of flashover. Flashover is the common term used for the transition a fire makes from a few objects pyrolyzing to full room involvement. It is of interest to the fire service because of the danger to fire fighters and to designers buildings because of life safety and the attendant impact on occupants. Several papers have looked at the capability of CFAST to predict the conditions under which flashover can occur.

Chow [135] concluded that CFAST correctly predicted the onset of flashover if the appropriate criteria were used. The criteria were gas temperature near the ceiling, heat flux at the floor level and flames coming out of the openings. This analysis was based on a series of compartment fires.

A paper by Luo *et al.* [136]. presents a comparison of the results from CFAST against a comprehensive set of data obtained from one flashover fire experiment. The experimental results were obtained from a full-scale prototype apartment building under flashover conditions. Three polyurethane mattresses were used as fuel. It was found that the predicted temperatures from the CFAST fire model agreed well with the experimental results in most areas, once radiation corrections are applied to the thermocouple data..

Collier [137] makes an attempt to quantify the fire hazards associated with a typical New Zealand dwelling, a series of experiments. These tests, done in a three-bedroom dwelling, included both non-flashover and flashover fires. The predictions were consistent with the experiments within the uncertainty of each.

Post-flashover fires in shipboard spaces have a pronounced effects on adjacent spaces due to highly conductive boundaries. The CFAST model predictions for the gas temperature and the cold wall temperature were compared with shipboard fires [138]. The comparisons between the model and experimental data show conservative predictions. The authors attribute this to an overestimation of the average hot wall temperature and an underestimation of external convective losses due to wind effects.

Finally, a more general comparison of CFAST with a number of simple correlations was used by Peacock and Babrauskas [139], [140] to simulate a range of geometries and fire conditions to predict the development of the fire up to the point of flashover. The simulations represent a range of compartment sizes from 8 m³ to 1327 m³, with ceiling height varying from 2.4 m to 12.2 m and vent openings from 10 % to 100 % of the length of the short wall (plus a “standard” door, 0.76 m in width). For most of the simulations, the surface lining material was gypsum wallboard, 12.7 mm in thickness, consistent with the values used in the correlations. A simple constant fire size was varied until the calculated upper layer temperature reached 600 °C at the end of the simulation. For some simulations, the surface linings ranged from aluminum to a highly insulating foam and the fire source diverged from the simple steady-state fire to more complex shapes.

The important test of all these prediction methods is in the comparison of the predictions with actual fire observations. Figure 6-12 presents estimates of the minimum energy required to achieve flashover for a range of room and vent sizes. This figure is an extension of the earlier work of Babrauskas [141] and includes additional experimental measurements from a variety of sources, most notably the work of Deal and Beyler [142]. In addition, figure 6-12 includes predictions from the CFAST model.

DRAFT
FOR
REVIEW
ONLY

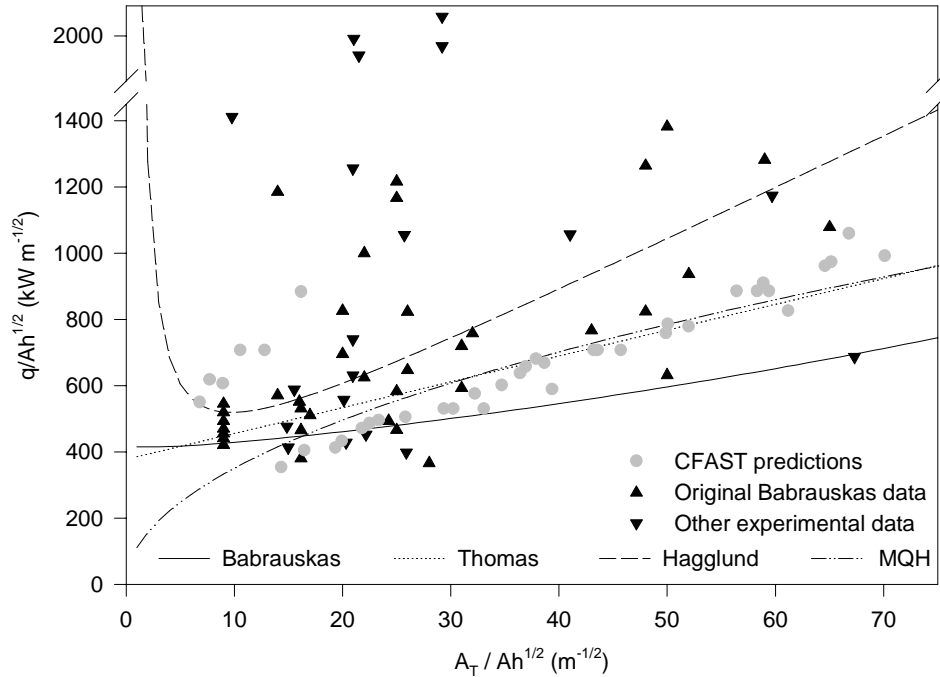


Figure 6-15: Comparison of correlations, CFAST predictions, and experimental data for the prediction of flashover in a compartment fire.

As with some of the experimental data defining flashover as an upper layer temperature reaching 600 °C, many experimental measures were reported as peak values rather than minimum values necessary to achieve flashover. Thus, ideally all the predictions should provide a lower bound for the experimental data. Indeed, this is consistent with the graph – the vast majority of the experimental observations lie above the correlations and model predictions. For a considerable range in the ratio $A_T/A\sqrt{h}$, the correlations of Babrauskas [122] Thomas [143], and the MQH correlation of McCaffrey *et al.* [144] provide similar estimates of the minimum energy required to produce flashover. The estimates of Hägglund [145] yields somewhat higher estimates for values of $A_T/A\sqrt{h}$ greater than 20 $m^{-1/2}$.

The results from the CFAST model for this single compartment scenario provide similar results to the experiments and the correlations for most of the range of $A_T/A\sqrt{h}$. For small values of $A_T/A\sqrt{h}$, the CFAST values rise somewhat above the values from the correlations. These small values of $A_T/A\sqrt{h}$ result from either very small compartments (small A_T) or very large openings (large $A\sqrt{h}$), both of which stretch the limits of the assumptions inherent in the model. For very small compartments, radiation from the fire to the compartment surfaces becomes more important, enhancing the conductive heat losses through the walls. However, the basic two-zone assumption may break down as the room becomes very small. For very large openings, the calculation of vent flow via an orifice flow coefficient approach is likely inaccurate. Indeed, for such openings, this limitation has been observed experimentally [122]. The estimates are close to the range of uncertainty shown by the correlations which also diverge at very small values of $A_T/A\sqrt{h}$.

Perhaps most significant in these comparisons is that all the simple correlations provide estimates similar to the CFAST model and all the models are consistent with a wide range of experimental data. For this simple scenario, little is gained with the use of the more complex models. For more complicated scenarios, the comparison may not be as simple.

6.5.4 Comparison with Documented Fire Experience

There are numerous cases of CFAST being used to adjudicate legal disputes. Since these are discussed in courts of law, there is a great deal of scrutiny of the modeling, assumptions, and results. Most of these simulations and comparisons are not available in the public literature. A few of the cases which are available are discussed below. In these scenarios, there are, of course, no detailed measurements. The metric for how good the model performed is its ability to reproduce the time-line as observed by witnesses and the death of occupants or the destruction of property as was used in evidence in legal proceedings.

As mentioned in section •, Levine and Nelson describe the use of CFAST for understanding the deaths of two adults in a residence in Sharon, Pennsylvania in 1987 [131]. The paper compared the evidence of the actual fire, a full scale mockup done at NIST and the results from CFAST (FAST 18 [75]) and Harvard VI [146]. The most notable shortcoming of the models was the lower than actual temperatures in the bedrooms, caused by loss of heat through the fire barriers. This led to the improvement in CFAST in the mid-90s to couple compartments together so that both horizontal and vertical heat transfer occur to adjacent compartments.

Bukowski used CFAST to analyze a fire in New York City [147] in 1994 which resulted in the death of three fire fighters. The CFAST model was able to (very accurately) reproduce the observable conditions and supported the theory as to how the fire began and the cause of death of the three fire fighters.

Chow describes the use and comparison of CFAST simulations with a recent (circa 1996) high-rise building fire in Hong Kong [148]. CFAST simulations were performed to help understand the probable fire environment under different conditions. Three simulations were performed to study the consequences of a fire starting in the lift shaft. Smoke flow in the simulations qualitatively matched those observed during the incident.

In the early morning hours of March 25, 1990 a tragic fire took the lives of 87 persons at a neighborhood club in the Bronx, New York [149]. The New York City Fire Department requested the assistance of the Center for Fire Research (CFR) in understanding the factors which contributed to this high death toll and to develop a strategy that might reduce the risk of a similar occurrence in the many similar clubs operating in the city.

These are examples of CFAST being validated by corroboration with eye witness accounts, and forensic evidence.

6.5.5 Comparison with Experiments Which Cover Special Situations

There are several sets of comparisons used in the development of the model or specific applications beyond those discussed more generally above.

6.5.5.1 Nuclear Facilities

Floyd validated CFAST by comparing the modeling results with measurements from fire tests at the Heiss-Dampf Reaktor (HDR) facility [150]. The structure was originally the containment building for a nuclear power reactor in Germany. The cylindrical structure was 20 m in diameter and 50 m in height topped by a hemispherical dome 10 m in radius. The building was divided into eight levels. The total volume of the building was approximately 11,000 m³. From 1984 to 1991, four fire test series were performed within the HDR facility. The T51 test series consisted of eleven propane gas tests and three wood crib tests. To avoid permanent damage to the test facility, a special set of test rooms were constructed, consisting of a fire room with a narrow door, a long corridor wrapping around the reactor vessel shield wall, and a curtained area centered beneath a maintenance hatch. The fire room walls were lined with fire brick. The doorway and corridor walls had the same construction as the test chamber. Six gas burners were mounted in the fire room. The fuel source was propane gas mixed with 10 % air fed at a constant rate to one of the six burners.

In general, the comparison between CFAST and the HDR results was good, with two exceptions. The first is the over estimate of the temperature of the upper layer, typically within about 15 % of the experimental measurements. This is common and generally results from the using too low a value for the production of soot, water (hydrogen) and carbon monoxide. The other exception consists of predictions in spaces where the zone model concept breaks down, for example in the stairways between levels. In this case, CFAST has to treat the space either in the filling mode (two layer approximation) or as a fully mixed zone (using the SHAFT option). Neither is quite correct, and in order to understand the condition in such spaces in detail (beyond the transfer of mass and energy), a more detailed CFD model must be used, for example FDS [44].

6.5.5.2 Small Scale Testing

As an implementation of the zone model concept, CFAST is applicable to a wide range of scenarios. One end of this spectrum are small compartments, one to two meters on a side. Several research efforts have looked at small scale validation. There are three papers by Chow [151],[152],[153] which examine this issue. The first is the use of an electric heater with adjustable thermal power output was to verify results predicted by CFAST. The second were closed chamber fires studied by burning four types of organic liquids, namely ethanol, N-heptane, thinner and kerosene. The burning behavior of the liquids was observed, and the hot gas temperature measured. These behaviors along with the transient variations of the temperature were then compared with those predicted by the CFAST model. Finally, in another series of experiments, three zone models, one of which was CFAST, were evaluated experimentally using a small fire chamber. Once again, liquid fires were chosen for having better control on the mass loss rate. The results on the development of smoke layer and the hot gas temperature predicted by the three models were compared with those measured experimentally. According to Chow, fairly good agreement was found if the input parameters were chosen properly.

6.5.5.3 Unusual Geometry and Specific Algorithms

A zone model is inherently volume calculation. There is an assumption in the derivation of the equations, that gas layers are strongly stratified. This allows for the usual interpretation that a volume can then be thought of as a rectangular parallel-piped, which allows the developers to express the volume in terms of a floor area and height of a compartment, saying simply that the height times the floor area is the volume. However, there are other geometries which can be adequately described by zone models. Tunnels, ships, and attics are the most common areas of application which fall outside of the usual scope.

6.5.5.3.1 *Railway and Vehicle Tunnels*

Altinakar *et al.* [154] used a modified version of CFAST for predicting fire development and smoke propagation in vehicle or railroad tunnels. The model was tested by simulating several full-scale tests carried out at memorial Tunnel Ventilation Test Program in West Virginia, and the Offeneg Tunnel in Switzerland. His article compares simulated values of temperature, opacity and similar sensible quantities with measured values and discusses the limits of the applicability of zone models for simulating fire and smoke propagation in vehicle and railroad tunnels. The two major modifications made to the model dealt with mixing between the upper and lower layers and friction losses along the tunnel.

Peacock *et al.* [155] compared times to untenable conditions determined from tests in a passenger rail car with those predicted by CFAST for the same car geometry and fire scenarios. For a range of fire sizes and growth rates, they found agreement that averaged approximately 13 %.

6.5.5.3.2 *Non-Uniform Compartments*

In January 1996, the US Navy began testing how the CFAST model would perform when tasked with predicting shipboard fires. These conditions include mass transport through vertical vents (representing hatches and scuttles), energy transport via conduction through decks, improvement to the radiation transport sub model, and geometry peculiar to combat ships. The purpose of this study was to identify CFAST limitations and develop methods for circumnavigating these problems [156]. The approach taken was to apply CFAST to the modeling of a full-scale shipboard fire test and then compare to model conditions. A retired ship representing the forward half of a USS LOS ANGELES class submarine was used during this test. Compartments in combat ships are not square in floor area, nor do they have parallel sides.

Application of CFAST to these scenarios required a direct integration of floor area over height to interpret the layer interface and provide correct predictions for flow through doors and windows (vertical vents). The most vexing part of this was development of the user specification (ROOMA and ROOMH) to provide a description for the model to use. For most applications of CFAST, the effort required to for the input outweighs any additional precision in the calculated results.

6.5.5.3.3 *Long Corridors*

Prior to development of the corridor flow model, the implementation of flow in compartments assumed that smoke traveled instantly from one side of a compartment to another. The work of Bailey *et al.* [157] provided the basis for the corridor flow model discussed in the section ?. It shows good agreement for the delay time calculated using CFAST and measured flow along high aspect ratio passageways.

6.5.5.3.4 *Mechanical Ventilation*

There have been two papers which have looked at the effectiveness of the mechanical ventilation system. The first considered a fire chamber of length 4.0 m, width 3.0 m and height 2.8 m with adjustable ventilation rates [158]. Burning tests were carried out with wood cribs and methanol to study the preflashover stage of a compartmental fire and the effect of ventilation. The mass loss rate of fuel, temperature distribution of the compartment and the air intake rate were measured. The heat release rates of the fuel were calculated and the

smoke temperature was used as a validation parameter. A scoring system was proposed to compare the results predicted by the three models. CFAST does particularly well, though there are some differences which can be attributed to the zone model approach.

A second series of experiments by Luo [159] indicate that the CFAST model generally over predicts the upper layer temperature in the burn room because the zonal assumption is likely to break down in the burn room. It was found that the room –averaged temperatures obtained from CFAST were in good overall agreement with the experimental results. The discrepancies can be attributed to the correction needed for thermocouple measurements. The CO concentration, however, was inconsistent. CFAST tended to overestimate CO concentration when the air handling system was in operation. This is probably due to inconsistencies in what is measured (point measurements) and predicted (global measurements).

6.5.5.3.5 *Sprinkler Activation*

A suppression algorithm [64] was incorporated into CFAST. This paper [160] evaluates the predictive capability for a sprinkler installed in an atrium roof. There were three main points being considered: the possibility of activating the sprinkler, thermal response, and water requirement. The zone model CFAST was used to analyze the possibility of activation of a sprinkler head. Results derived from CFAST proved to be accurate, that is providing good agreement with experimental measurements.

6.5.5.3.6 *t² Fires*

In this study, a series of full-scale experiments [161] were carried out using t²-fires. Fire room and corridor smoke filling processes were measured. The size of the corridors and arrangements of smoke curtains were varied in several patterns. Comparisons were then made between the experimental results and those predicted by CFAST. The author concludes that while the model does a good job of predicting experimental results, there are systematic differences which could be reduced with some revision to zone model formulation to include the impact of smoke curtains.

6.5.6 Summary

How to best quantify the comparisons between model predictions and experiments is not obvious. The necessary and perceived level of agreement for any variable is dependent upon both the typical use of the variable in a given simulation (for instance, the user may be interested in the time it takes to reach a certain temperature in the room), the nature of the experiment (peak temperatures would be of little interest in an experiment which quickly reached steady state), and the context of the comparison in relation to other comparisons being made (a true validation of a model would involve proper statistical treatment of many compared variables).

Insufficient experimental data and understanding of how to compare the numerous variables in a complex fire model prevents a true validation of the model. Thus, the comparisons of the differences between model predictions and experimental data discussed here are intentionally simple and vary from test to test and from variable to variable due to the changing nature of the tests and typical use of different variables.

In general, upper layer temperatures predicted by the CFAST model are higher than experimental measurements, with the differences typically in the 10 % to 25 % range. Conversely, the lower layer temperature is

somewhat lower for the model than for the experiments. Presuming conservation of energy (an underlying assumption in *all* fire models), these observations are consistent. Limitations inherent in the model also account partially for these trends. In the current version of CFAST, energy exchange in the lower layer is *only* by mixing or convection from surfaces. Adding radiative exchange to the lower layer would reduce the upper layer temperature and increase the lower layer temperature. Layer interface position is primarily affected by entrainment by the fire or at vents. Underestimation of the conduction would also account for the effect. Plume entrainment in CFAST is based on the work of McCaffrey [20] on circular plumes in relatively small spaces. For large fires in small spaces where the fire impinges on the ceiling (such as the single room tests with wall burning) or very small fires in large spaces (such as atria), these correlations may not be as valid.

DRAFT
FOR
FORMAT
REVIEW
ONLY

Chapter 7 Bibliography and References

Miles, S., "International Collaborative Project to Evaluate Fire Models for Nuclear Power Plant Applications: International Panel Report on Benchmark Exercise # 2 Pool Fires in Large Halls," U.S. Nuclear Regulatory Commission, NUREG-____, _____, 2004.

Dey, M., "Fire Modeling of Pool Fires in Multi-Level Turbine Halls in Nuclear Power Plants," U.S. Nuclear Regulatory Commission, NUREG-____, _____, 2004a.

Dey, M., "Large Fires in Compartments," U.S. Nuclear Regulatory Commission, NUREG-____, _____, 2004c.

Floyd, Jason E. "Comparison of CFAST and FDS for Fire Simulation with the HDR T51 and T52 Tests." National Institute of Standards and Technology, NISTIR 6866

Electric Power Research Institute "Fire Modeling Guide for Nuclear Power Plant Applications," EPRI TR-1002981, Palo Alto, CA, August 2002.

"Standard Guide for Evaluating the Predictive Capability of Fire Models," ASTM E 1355, American Society for Testing and Materials, Philadelphia, PA, 1992.

Memorandum from Sunil Weerakkady to Joseph G. Gitter dated September 5, 2003. Subject: Fire Scenarios for Fire Model Evaluation and Review Guidance, "Fire Scenarios for NFPA 805 Verification and Validation (V&V) Guide"

U.S. Nuclear Regulatory Commission, "Fire Dynamics Tools (FDT) Quantitative Fire Hazard Analysis Methods for the U.S. Nuclear Regulatory Commission Fire Protection Inspection Program," Draft NUREG 1805, June 2003.

Hostikka, Simo, Keski-Rahkonen, Olavi, Korhonen, Timo. "Probabilistic Fire Simulator Theory and User's Manual". VTT Technical Research Centre of Finland 2002.

Dey, M. "Analysis of Pool Fires in Large Multi-Level Halls with the CFAST and FDS Fire Codes," National Institute of Standards and Technology, Gaithersburg, MD, 2003.

[1] ASTM Standard Guide for Evaluating the Predictive Capability of Deterministic Fire Models, ASTM E1355-04, West Conshohocken, PA (2004).

- [2] Jones, W.W., Peacock, R.D., "Technical Reference Guide for FAST Version 18," National Institute of Standards and Technology, TN 1262 (1989).
- [3] Cooper L.Y. and Forney, G. P., "The consolidated compartment fire model (CCFM) computer application CCFM-VENTS – part I: Physical reference guide," National Institute of Standards and Technology, NISTIR 4342 (1990).
- [4] Peacock, R. D.; Jones, W. W.; Forney, G. P.; Portier, R. W.; Reneke, P. A.; Bukowski, R. W.; Klote, J. H., "Update Guide for HAZARD I Version 1.2," National Institute of Standards and Technology, NISTIR 5410 (1994).
- [5] Peacock, R.D., Reneke, P.A., Jones, W.W., Bukowski, R.B., and Forney, G.P., "A User's Guide for FAST: Engineering Tools for Estimating Fire Growth and Smoke Transport," National Institute of Standards and Technology, Special Publication 921, 2000 Edition (2000).
- [6] Gross, D., "Data Sources for Parameters Used for Predictive Modeling of Fire Growth and Smoke Spread," National Institute of Standards and Technology, NISTIR 85-3223 (1985).
- [7] Incorpera, F. P. and DeWitt, D. P., "Fundamentals of Heat Transfer," John Wiley & Sons, New York (1981).
- [8] Rehm, R., and Forney, G., "A Note on the Pressure Equations Used in Zone Fire Modeling," National Institute of Standards and Technology, NISTIR 4906 (1992).
- [9] Steckler, K.D, Quintiere, J.G., and Rinkinen, W.J., "Flow Induced by Fire in a Compartment," National Bureau of Standards, NBS IR 82-23520 (1982).
- [10] Klote, J. H., "Fire Experiments of Zoned Smoke Control at the Plaza Hotel in Washington DC," National Institute of Standards and Technology, NISTIR 90-4253 (1990).
- [11] Standard Test Method for Heat and Visible Smoke Release for Materials and Products Using and Oxygen Consumption Calorimeter, ASTM E1354-04a, *American Society for Testing and Materials*, Philadelphia, PA (2004).
- [12] Thornton, "The Relation of Oxygen to the Heat of Combustion of Organic Compounds," *Philosophical Magazine and Journal of Science* **33** (1917).
- [13] Huggett, C., "Estimation of the Rate of Heat Release by Means of Oxygen Consumption," *Journal of Fire and Flammability* **12**, 61 (1980).
- [14] Morehart, J. H., Zukowski, E. E. and Kubota, T., "Characteristics of Large Diffusion Flames Burning in a Vitiated Atmosphere," *Third International Symposium on Fire Safety Science*, Edinburgh (1991).
- [15] Bryant, R. A.; Ohlemiller, T. J.; Johnsson, E. L.; Hamins, A.; Grove, B. S.; Guthrie, W. F.; Maranghides, A.; Mulholland, G. W., "NIST 3 Megawatt Quantitative Heat Release Rate Facility," National Institute of Standards and Technology, Special Publication 1007

- (2003).
- [16] Babrauskas, V., Lawson, J. R., Walton, W. D., Twilley, W. H., "Upholstered Furniture Heat Release Rates Measured with a Furniture Calorimeter," National Bureau of Standards (U.S.), NISTIR 82-2604 (1982).
- [17] Babrauskas, V. and Krasny, J. F., "Fire Behavior of Upholstered Furniture," National Bureau of Standards (U.S.), Monograph 173 (1985).
- [18] Lee, B.T., "Effect of Ventilation on the Rates of Heat, Smoke, and Carbon Monoxide Production in a Typical Jail Cell Fire," National Bureau of Standards (U.S.), NISTIR 82-2469 (1982).
- [19] Alterman, Z., "Effect of Surface Tension on the Kelvin-Helmholtz Instability of Two Rotating Fluids," *Proceedings of the National Academy of Sciences (USA)* **47** (2), 224–227 (1961).
- [20] McCaffrey, B.J., "Momentum Implications for Buoyant Diffusion Flames," *Combustion and Flame* **52**, 149 (1983).
- [21] Cetegen, B. M., "Entrainment and Flame Geometry of Fire Plumes," National Bureau of Standards (U.S.) GCR 82-402 (1982).
- [22] Drysdale, D., "An Introduction to Fire Dynamics," John Wiley and Sons, New York, (1985).
- [23] Tewarson, A., "Combustion of Methanol in a Horizontal Pool Configuration," Factory Mutual Research Corp., Norwood, MA, Report No. RC78-TP-55 (1978).
- [24] McCaffrey, B.J., "Entrainment and Heat Flux of Buoyant Diffusion Flames," National Bureau of Standards (U. S.), NBS IR 82-2473 (1982).
- [25] Koseki, H., "Combustion Properties of Large Liquid Pool Fires," *Fire Technology* **25**, 241 (1989).
- [26] Peacock, R. D., Davis, S., Lee, B.T., "An Experimental Data Set for the Accuracy Assessment of Room Fire Models," National Bureau of Standards (U.S.), NBS IR 88-3752 (1988).
- [27] Zukoski, E. E., Kubota, T., Lim, C. S., "Experimental Study of Environment and Heat Transfer in a Room Fire. Mixing in Doorway Flows and Entrainment in Fire Plumes," National Bureau of Standards, GCR 85-493; 173 p. (1985).
- [28] Quintiere, J.G., Steckler, K., and Corley, D., "An Assessment of Fire Induced Flows in Compartments," *Fire Science and Technology* **4**, 1 (1984).
- [29] Quintiere, J.G., Steckler, K. and McCaffrey, B.J., "A Model to Predict the Conditions in a Room Subject to Crib Fires," First Specialist Meeting (International) of the Combustion Institute, Talence, France (1981).

- [30] Cooper, L.Y., "Calculation of the Flow Through a Horizontal Ceiling/Floor Vent," National Institute of Standards and Technology, NISTIR 89-4052 (1989).
- [31] Klote, J.K. and Milke, J.A., "Principles of Smoke Management," American Society of Heating, Refrigerating and Air Conditioning Engineers, Atlanta, GA (2002).
- [32] ASHRAE Handbook - HVAC Systems and Equipment, American Society of Heating, Refrigerating and Air Conditioning Engineers, Atlanta, GA (1992).
- [33] Klote, J.H., "A Computer Model of Smoke Movement by Air Conditioning Systems," National Bureau of Standards, NBS IR 87-3657 (1987).
- [34] 2001 ASHRAE Handbook - Fundamentals, American Society of Heating, Refrigeration and Air Conditioning Engineers, Inc., Atlanta, GA (2001).
- [35] Jorgensen, R., "Fan Engineering," Buffalo Forge Co., Buffalo, NY (1983).
- [36] Murdock, J.W., "Mechanics of Fluids, Marks' Standard Handbook for Mechanical Engineers," 8th ed., Baumeister *et al.* editors, McGraw, New York, NY (1978).
- [37] Schlichting, H., Boundary Layer Theory, 4th ed., Kestin, J. Translator, McGraw, New York, NY (1960).
- [38] Huebscher, R.G., "Friction Equivalents for Round, Square and Rectangular Ducts," ASHVE Transactions (renamed ASHRAE Transactions), Vol. 54, pp 101-144 (1948).
- [39] Heyt, J.W. and Diaz, J. M., "Pressure Drop in Flat-Oval Spiral Air Duct," *ASHRAE Transactions*, **81**, Part 2, p 221-230 (1975).
- [40] Colebrook, C.F., "Turbulent Flow in Pipes, With Particular Reference to the Transition Region Between the Smooth and Rough Pipe Laws," *Journal of Institution of Civil Engineers (London)*, **11**, 133 (1938-1939).
- [41] Moody, L.F., "Friction Factors for Pipe Flow," *Transactions of ASME*, **66** p 671-684 (1944).
- [42] Klote, J. H. and Fothergill, J. W., Jr., "Design of Smoke Control Systems for Buildings," National Bureau of Standards, *Handbook 141*, 272 (1983).
- [43] McGrattan, K. B., Baum, H. R., and Rehm, R. G., "Large Eddy Simulations of Smoke Movement," *Fire Safety Journal* **30** (2), pp 161-178 (1998).
- [44] McGrattan, K. B., Baum, H. R., Rehm, R.G., Hamins, A., Forney, G.P., Floyd, J.E., Hostikka, S., "Fire Dynamics Simulator (Version 2): Technical Reference Guide," National Institute of Standards and Technology, NISTIR 6783 (2001).
- [45] Forney, G. P., "Computing Radiative Heat Transfer Occurring in a Zone Fire Model," National Institute of Standards and Technology, NISTIR 4709 (1991).

- [46] Siegel, R. and Howell, J. R., "Thermal Radiation Heat Transfer," Hemisphere Publishing Corporation, New York, second ed. (1981).
- [47] Hottel, H. C., "Heat Transmission," McGraw-Hill Book Company, New York, third ed. (1954).
- [48] Hottel, H. and Cohen, E., "Radiant Heat Exchange in a Gas Filled Enclosure: Allowance for non-uniformity of Gas Temperature," *American Institute of Chemical Engineering Journal* **4**, 3 (1958).
- [49] Yamada, T. and Cooper, L.Y., "Algorithms for Calculating Radiative Heat Exchange Between the Surfaces of an Enclosure, the Smoke Layers and a Fire," Building and Fire Research Laboratory Research Colloquium, July 20 (1990).
- [50] Jones, W.W. and Forney, G. P., "Improvement in Predicting Smoke Movement in Compartmented Structures," *Fire Safety Journal* **21**, 269 (1993).
- [51] Tien C.L., K.Y. Lee, and A.J. Stretton, "Radiation Heat Transfer" in *The SFPE Handbook of Fire Protection Engineering*, 3rd Ed., National Fire Protection Association (1988).
- [52] G. Hubbard and C. Tien, Infrared Mean Absorption Coefficients of Luminous Flames and Smoke, *J. Heat Transfer* **100**, p. 235 (1978).
- [53] Edwards, D. K., "Radiation Properties of Gases," in Rohsenow, W. M., *Handbook of Heat Transfer Fundamentals*, 2nd ed. pp. 74-75 (1985).
- [54] Hottel, H. C., "Radiant Heat Transmission," Chapter 3 in *Heat Transmission*, McAdams, W. H., McGraw-Hill Book Company, New York (1942).
- [55] Atreya, A., "Convection Heat Transfer," in *The SFPE Handbook of Fire Protection Engineering*, 3rd Edition, National Fire Protection Association (2002).
- [56] Golub, G. H. and Ortega, J.M., "Scientific Computing and Differential Equations, An Introduction to Numerical Methods," Academic Press, New York (1989).
- [57] Moss, W. F. and Forney, G.P., "Implicitly coupling heat conduction into a zone fire model," National Institute of Standards and Technology, NISTIR 4886 (1992).
- [58] Cooper, L. Y., "Fire-Plume-Generated Ceiling Jet Characteristics and Convective Heat Transfer to Ceiling and Wall Surfaces in a Two-Layer Zone-Type Fire Environment," National Institute of Standards and Technology, NISTIR 4705 (1991).
- [59] Cooper, L. Y., "Heat Transfer in Compartment Fires Near Regions of Ceiling-Jet Impingement on a Wall," *Journal of Heat Transfer* **111**, 455 (1990).
- [60] Cooper, L. Y., "Ceiling Jet-Driven Wall Flows in Compartment Fires," *Combustion Science and Technology* **62**, 285 (1988).

- [61] Jaluria, Y. and Cooper, L.Y., "Negatively Buoyant Wall Flows Generated in Enclosure Fires," *Progress in Energy and Combustion Science*, **15**, 159 (1989).
- [62] Cooper, L.Y., "Fire-plume-generated ceiling jet characteristics and convective heat transfer to ceiling and wall surfaces in a two-layer zone-type fire environment: Uniform temperature and walls," National Institute of Standards and Technology, Technical Report 4705 (1991).
- [63] Heskestad, G. and Smith, H.F., "Investigation of a new sprinkler sensitivity approval test: The plunge test," *Technical Report Serial No. 22485 2937*, Factory Mutual Research Corporation, Norwood, MA, 1976. RC 76-T-50.
- [64] Madrzykowski, D. and Vettori, R.L., "A sprinkler fire suppression algorithm for the gsa engineering fire assessment system," National Institute of Standards and Technology, Technical Report 4833 (1992).
- [65] Evans, D.D., "Sprinkler fire suppression for hazard," National Institute of Standards and Technology, Technical Report 5254 (1993).
- [66] Madrzykowski, D., "Evaluation of Sprinkler Activation Prediction Methods," International Conference on Fire Science and Engineering, Interscience Communications Limited, ASIAFLAM (Kowloon, 1995).
- [67] Seader, J., and Einhorn, I., "Some Physical, Chemical, Toxicological and Physiological Aspects of Fire Smokes," *Sixteenth Symposium (International) on Combustion*, The Combustion Institute, Pittsburgh, PA 1976, pp. 1423-1445.
- [68] Galloway, F. M., Hirschler, M. M., "A Model for the Spontaneous Removal of Airborne Hydrogen Chloride by Common Surfaces," *Fire Safety Journal* **14**, 251 (1989).
- [69] Galloway, F. M., Hirschler, M. M., "Transport and Decay of Hydrogen Chloride: Use of a Model to Predict Hydrogen Chloride Concentrations in Fires Involving a Room-Corridor-Room Arrangement," *Fire Safety Journal* **16**, 33 (1990).
- [70] Cleary, T. G. And Quintiere, J. G., "Framework for Utilizing Fire Property Tests." National Institute of Standards and Technology, NISTIR 4619 (1991); also *Proceedings of the 3rd International Symposium*, International Association of Fire Safety Science, Edinburgh, Scotland, Elsevier Applied Science, New York, Cox, G.; Langford, B., Editors, 647-656 pp, (1991).
- [71] Dols, W. S. And Walton, G. N., "CONTAMW 2.0 User Manual. Multizone Airflow and Contaminant Transport Analysis Software," National Institute of Standards and Technology NISTIR 6921; 161 p. (2002).
- [72] Jones, W., Forney, G., Peacock R., and Reneke, P., "A Technical Reference for CFAST: An Engineering Tool for Estimating Fire and Smoke Transport," National Institute of Standards and Technology, TN 1431 (2003).
- [73] Peacock, R.D., Forney, G.P., Reneke, P. A., Portier, R.W., Jones, W.W., "CFAST, The Consolidated Model of Fire Growth and Smoke Transport," National Institute of Standards and Technology, TN 1299 (1993).

- [74] Jones, W. W., "Modeling Smoke Movement Through Compartmented Structures," *Journal of Fire Sciences* **11**(2), 172 (1993).
- [75] Jones, W.W., "Multicompartment Model for the Spread of Fire, Smoke and Toxic Gases," *Fire Safety Journal* **9**(1), 55 (1985).
- [76] Jones, W.W. and Quintiere, J.G. , "Prediction of Corridor Smoke Filling by Zone Models," *Combustion Science and Technology* **35**, 239 (1984).
- [77] Jones, W.W. and Forney, G.P., "Modeling Smoke Movement Through Compartmented Structures," Proceedings of the Fall Technical Meeting of Combustion, Institute/Eastern States Section, Ithaca (1991).
- [78] Peacock, R.D., Forney, G.P., and Reneke, P.A. (2-11-1992). Improved Numerics and Structure in CFAST. Unpublished Memorandum.
- [79] Peacock, R.D. (4-11-1994). Fix for Chemistry Algorithm in CFAST. Unpublished Memorandum.
- [80] Peacock, R.D. (1-5-1993). New Convection Algorithm in CFAST. Unpublished Memorandum.
- [81] Peacock, R.D. (1-5-1993). HCl Deposition. Unpublished Memorandum
- [82] Peacock, R. D. (9-16-1993). New Output and History File Formats for CFAST. Unpublished Memorandum.
- [83] Jones, W.W. (2-12-1996). Internal memo dated February 1996 Announcing Version 3.0 of CFAST. Unpublished Memorandum.
- [84] Jones, W.W. (11-8-1997). Internal memo dated November 1997 Announcing Version 3.1.1 of CFAST. Unpublished Memorandum.
- [85] Jones, W.W. (3-10-2000). Differences in the 4.0.1 Code from the Beta Release of September 1, 1999 to March 1, 2000. Unpublished Memorandum.
- [86] Fire Hazard Analysis Group. (12-1991). Description of the CFAST 1.4 Release, Letter to CFAST Users.
- [87] Fire Hazard Analysis Group. (10-5-1992). Description of the CFAST 1.6 Release, Letter to CFAST Users.
- [88] Fire Hazard Analysis Group. (10-14-1993). Description of the CFAST 2.0 Release, Letter to CFAST Users.
- [89] Fire Hazard Analysis Group. (1-22-1996). Description of the CFAST 2.0.1 (Hazard 1.2) Release, Letter to CFAST and Hazard I Users.
- [90] Fire Hazard Analysis Group. (8-20-1996). Description of the CFAST 3.0 Release

- [91] Walton, W.D., "Zone Fire Models for Enclosures," in SFPE Handbook of Fire Protection Engineering, Third Edition, DiNenno, P. J, Beyler, C. L., Custer, R. L. P., Walton, W. D., and Watts, J. M., eds., National Fire Protection Association, Quincy, MA (2002).
- [92] NFPA 805, Performance-Based Standard for Fire Protection for Light Water Reactor Electric Generating Plants, 2001 Edition, 2004/2005 National Fire Codes, National Fire Protection Association, Quincy, MA (2004).
- [93] NFPA 551, Guide for the Evaluation of Fire Risk Assessment, 2004 Edition, 2004/2005 National Fire Code, National Fire Protection Association, Quincy, MA (2004).
- [94] Peacock, R.D. And W. W. Jones, W.W., "Consolidated Model of Fire Growth and Smoke Transport, User's Guide (Version 5)," National Institute of Standards and Technology, Special Publication (in press).
- [95] Barnett, J. R. and C.L.Beyler, C.L., "Development of an Instructional Program for Practicing Engineers HAZARD I Users," National Institute of Standards and Technology, GCR 90-580 (1990).
- [96] Brenan, K. E., Campbell, S.L., and Petzold, L.R., "Numerical Solution of Initial-Value Problems in Differential-Algebraic Equations," Elsevier Science Publishing, New York (1989).
- [97] Iman, R. L. and J.C. Helton, "An Investigation of Uncertainty and Sensitivity Analysis Techniques for Computer Models," *Risk Analysis* **8**, No. 1, 71-90 (1988).
- [98] Peacock, R. D., Reneke, P. A., Forney, C. L., and Kostreva, M. M., "Issues in Evaluation of Complex Fire Models," *Fire Safety Journal* **30**, 103-136 (1998).
- [99] Beard, A., "Evaluation of Fire Models: Part I – Introduction," *Fire Safety Journal* **19**, 295-306 (1992).
- [100] Notarianni, K. A., "The Role of Uncertainty in Improving Fire Protection Regulation," PhD Thesis, Carnegie Mellon University, Pittsburgh, PA (2000).
- [101] Khoudja, N., "Procedures for Quantitative Sensitivity and Performance Validation of a Deterministic Fire Safety Model," Ph.D. Dissertation, Texas A&M University, National Bureau of Standards, GCR-88-544 (1988)
- [102] Box, G. E. P., Hunter, W. G., and Hunter, J. S., "Statistics for Experimenters, An Introduction to Design, Data Analysis and Model Building," John Wiley & Sons (1978).
- [103] Daniel, C., "Applications of Statistics to Industrial Experimentation," John Wiley & Sons (1976).
- [104] Walker, A. M., "Uncertainty Analysis of Zone Fire Models," University of Canterbury, New Zealand, Fire Engineering Research Report 97/8 (1997).
- [105] Emmons, H.W., "Why Fire Model? The MGM Fire and Toxicity Testing," *Fire Safety Journal* **13**, 77 (1988).

- [106] Duong, D. Q., "The Accuracy of Computer Fire Models: Some Comparisons with Experimental Data from Australia," *Fire Safety Journal* **16**, 415 (1990).
- [107] Beard, A., "Evaluation of Fire Models: Overview," Unit of Fire Safety Engineering, University of Edinburgh, Edinburgh, UK (1990).
- [108] NFPA 72, National Fire Alarm Code, National Fire Protection Association, Quincy, Massachusetts (2003).
- [109] Babrauskas, V. and Krasny J. F., "Fire Behavior of Upholstered Furniture," National Bureau of Standards (U. S.), Monograph 173 (1985).
- [110] Peacock, R. D., Davis, S. and Babrauskas, V., "Data for Room Fire Model Comparisons," *Journal of Research* **96**, 411 (1991).
- [111] Drysdale, D., "An Introduction to Fire Dynamics," John Wiley and Sons, pp. 310 (1985).
- [112] Babrauskas, V., "Upholstered Furniture Room Fires – Measurements, Comparisons with Furniture Calorimeter Data, and Flashover Predictions," *Journal of Fire Sciences* **2**, 5 (1984).
- [113] Dembsey, N.A, Pagni, P.J and Williamson, R.B., "Compartment Fire Experiments: Comparison With Models," *Fire Safety Journal* **25**(3), 187 (1995).
- [114] 1997 Uniform Building Code, International Conference of Building Officials, Whittier, California (1997).
- [115] Pitts, W.M., Braun, E., Peacock, R.D., Mitler, H.E., Johnsson, E.L., Reneke, P.A., and Blevins, L.G., "Temperature Uncertainties for Bare-Bead and Aspirated Thermocouple Measurements in Fire Environments," Proceedings of *Thermal Measurements: The Foundation of Fire Standards. American Society for Testing and Materials*, Special Technical Publication 1427 (2001).
- [116] He, Y. and Beck, V., "Smoke Spread Experiment in a Multi-Storey Building and Computer Modeling," *Fire Safety Journal* **28**(2), 139 (1997).
- [117] Luo, M., He, Y. and Beck, V., "Comparison of Existing Fire Model Predictions With Experimental Results From Real Fire Scenarios," *Journal of Applied Fire Science* **6**(4), 357- (1996/1997).
- [118] Poole, G.M., Weckman, E.J. and Strong, A.B., "Fire Growth Rates in Structural Fires," National Institute of Standards and Technology NISTIR 5499 (1994).
- [119] Bailey, J. and Tatem, P., Validation of Fire/Smoke Spread Model (CFAST) Using Ex-USS SHADWELL Internal Ship Conflagration Control (ISCC) Fire Tests," NRL/MR/6180-95-7781 (1995).
- [120] Bailey, J.L., Tatem, P.A., Jones, W.W., and Forney, G.P., "Development of an Algorithm to Predict Vertical Heat Transfer Through Ceiling/Floor Conduction," *Fire Technology* **34**(2), 139 (1998).

- [121] Peacock, R.D., Jones, W.W., and Bukowski, R.W., "Verification of a Model of Fire and Smoke Transport," *Fire Safety Journal* **21**, 89-129 (1993).
- [122] Babrauskas, V., "Upholstered Furniture Room Fires -- Measurements, Comparison with Furniture Calorimeter Data, and Flashover Predictions," *Journal of Fire Sciences*, **4**, 5-19 (1984).
- [123] Lee, B. T., Effect of Wall and Room Surfaces on the Rates of Heat, Smoke, and Carbon Monoxide Production in a Park Lodging Bedroom Fire, *Natl. Bur. Stand. (U. S.), NBSIR 85-2998*, 78 p. (1985).
- [124] Heskestad, G., and Hill, J. P., "Propagation of Fire and Smoke in a Corridor," *Proceedings of the 1987 ASME:JSME Thermal Engineering Joint Conference, Honolulu, HI*, 371-379 (1987).
- [125] Cooper, L. Y., Harkleroad, M., Quintiere, J. G., and Rinkinen, W. J., "An Experimental Study of Upper Hot Layer Stratification in Full-Scale Multiroom Fire Scenarios," *Journal of Heat Transfer* **104**, 741 (1982).
- [126] Quintiere, J.G., and McCaffrey, B.J., "The Burning of Wood and Plastic Cribs in an Enclosure," National Bureau of Standards (U. S.) NBS IR 80-2954, 2 vols (1980).
- [127] Delichatsios, M. A., "Fire Growth Rate in Wood Cribs," *Combustion and Flame* **27**, 267-278 (1976).
- [128] Peacock, R. D., Reneke, P.A., Davis, W.D., and Jones, W. W., "Quantifying Fire Model Evaluation Using Functional Analysis," *Fire Safety Journal* **33**, 167 (1999).
- [129] Davis, W., "Comparison of Algorithms to Calculate Plume Centerline Temperature and Ceiling Jet Temperature With Experiments." *Journal of Fire Protection Engineering* **12**, 9-29 (2002).
- [130] Jones, W. W. And Peacock, R. D., "Refinement and Experimental Verification of a Model for Fire Growth and Smoke Transport," International Association for Fire Safety Science. Fire Safety Science. Proceedings. 2nd International Symposium. June 13-17, 1988, Tokyo, Japan, Hemisphere Publishing Corp., New York, Wakamatsu, T., Hasemi, Y., Sekizawa, A., Seeger, P. G., Pagni, P. J. and Grant, C. E., Editor, 897-906, (1989).
- [131] Levine, R. S. and Nelson, H. E., "Full Scale Simulation of a Fatal Fire and Comparison of Results with Two Multiroom Models," National Institute of Standards and Technology, NISTIR 90-4268, 105 p. (1990).
- [132] Deal, S. "A Review of Four Compartment Fires with Four Compartment Fire Models," Fire Safety Developments and Testing, *Proceedings of the Annual Meeting of the Fire Retardant Chemicals Association* October 21-24, 1990, Ponte Verde Beach, Florida, 33-51.
- [133] Nelson, H. E., "FPETOOL: Fire Protection Engineering Tools for Hazard Estimation," National Institute of Standards and Technology, NISTIR 4380, (1990).

- [134] Duong, D. Q., "The Accuracy of Computer Fire Models: Some Comparisons with Experimental Data from Australia," *Fire Safety Journal* **16**, 415 (1990).
- [135] Chow, W., "Predictability of Flashover by Zone Models," *Journal of Fire Sciences* **16**, 335 (September/October 1998).
- [136] Luo, M., He, Y. and Beck, V., "Application of Field Model and Two-Zone Model to Flashover Fires in a Full-Scale Multi-Room Single Level Building," *Fire Safety Journal* **29**, 1 (1997).
- [137] Collier, P., "Fire in a Residential Building: Comparisons Between Experimental Data and a Fire Zone Model," *Fire Technology* **32**, 195 (August/September 1996).
- [138] White, D., Beyler, C., Scheffey, J., and Williams, F., "Modeling the Impact of Post-Flashover shipboard fires on adjacent spaces," *Journal of Fire Protection Engineering* **10** (2000).
- [139] Peacock, R. D., Reneke, P. A., Bukowski, R. W., and Babrauskas, V., "Defining Flashover for Fire Hazard Calculations," *Fire Safety Journal* **32**, 4 331-345 (1999).
- [140] Babrauskas, V., Peacock, R. D., and Reneke, P. A., "Defining Flashover for Fire Hazard Calculations: Part II," *Fire Safety Journal* **38**, 613-622 (2003).
- [141] Babrauskas, V., "COMPF2-A Program for Calculating Post-Flashover Fire Temperatures," National Bureau of Standards (US), TN 991 (1979).
- [142] Deal, S. and Beyler, C., "Correlating Preflashover Room Fire Temperatures," *Journal of Fire Protection Engineering* **2** (2), 33-48 (1990).
- [143] Thomas, P. H., "Testing Products and Materials for Their Contribution to Flashover in Rooms," *Fire and Materials* **5**, 103-111 (1981).
- [144] McCaffrey, B. J., Quintiere, J. G., and Harkleroad, M. F., "Estimating Room Temperatures and the Likelihood of Flashover Using Fire Test Data Correlations," *Fire Technology* **17** (2), 98-119 (1981).
- [145] Hägglund, B., "Estimating Flashover Potential in Residential Rooms. Forsvarets Forskningsanstalt, Stockholm, FOA Rapport C 20369-A3 (1980).
- [146] Rockett, J. A., and Morita, M., "The NBS Harvard VI Multi-room Fire Simulation," *Fire Science and Technology* **5(2)**, 159-164 1985.
- [147] Bukowski, R., "Modeling a Backdraft Incident: The 62 Watts Street (New York) Fire," *Fire Engineers Journal* **56**, No. 185, 14-17, (1996).
- [148] Chow, W., "Preliminary Studies of a Large Fire in Hong Kong," *Journal of Applied Fire Science*, **6**, No. 3, 243-268 (1996/1997).
- [149] Bukowski, R.W., "Analysis of the Happyland Social Club Fire with HAZARD I," *Fire and Arson Investigator* **42**, 36 (1992).

- [150] Floyd, J., "Comparison of CFAST and FDS for Fire Simulation With the HDR T51 and T52 Tests," National Institute of Standards and Technology, NISTIR 6866 (2002).
- [151] Lui, G., and Chow, W., "A Short Note on Experimental Verification of Zone Models with an Electric Heater," *International Journal on Engineering Performance-Based Fire Codes* **5**, 30 (2003).
- [152] Chow, W., "Studies on Closed Chamber Fires," *Journal of Fire Sciences* **13**, 89 (1995).
- [153] Chow, W., "Experimental Evaluation of the Zone Models CFAST, FAST and CCFM.VENTS," *Journal of Applied Fire Science* **2**, 307 (1992-1993).
- [154] Altinakar, M., Weatherill, A., and Nasch, P., "Use of a Zone Model in Predicting Fire and Smoke Propagation in Tunnels," BHR Group Vehicle Tunnels, Proceedings, 623-639 (1997).
- [155] Peacock, R. D., Averill, J. D., Madrzykowski, D., Stroup D. W., Reneke, P. A., and Bukowski, R. W., "Fire Safety of Passenger Trains; Phase III: Evaluation of Fire Hazard Analysis Using Full-Scale Passenger Rail Car Tests," National Institute of Standards and Technology, NISTIR 6563 (2004).
- [156] Hoover, J., Tatem, P., "Application of CFAST to Shipboard Fire Modeling. Part 3. Guidelines for Users," Naval Research Laboratory NRL/MR/6180-01-8550 (2001).
- [157] Bailey, J., Forney, G., Tatem, P., and Jones, W., "Development and Validation of Corridor Flow Submodel for CFAST," *Journal of Fire Protection Engineering* **12**, 139 (2002).
- [158] Chow, W., "Use of Zone Models on Simulating Compartmental Fires With Forced Ventilation," *Fire and Materials* **19**, 101 (1995).
- [159] Luo, M., "One Zone or Two Zones in the Room of Fire Origin During Fires? The Effects of the Air-Handling System," *Journal of Fire Sciences* **15**, 240 (1997).
- [160] Chow, W., "Performance of Sprinkler in Atria," *Journal of Fire Sciences* **14**, 466 (1996).
- [161] Matsuyama, K., Wakamatsu, T., and Harada, K., "Systematic Experiments of Room and Corridor Smoke Filling for Use in Calibration of Zone and CFD Fire Models," National Institute of Standards and Technology, NISTIR 6588 (2000).